Sensitivity of Ambient NO_2 Concentration to Upstream Oil and Gas and Transportation Emissions in Alberta

by

Erfan Hajiparvaneh

A thesis submitted in partial fulfillment of the requirements for the degree of

Master of Science

Department of Mechanical Engineering
University of Alberta

Abstract

Ambient exposure to nitrogen dioxide (NO_2) and ozone (O_3) is associated with severe health problems and health-related economic burdens. The levels of NO_2 concentration in the province of Alberta show that they will exceed the updated Canadian Ambient Air Quality Standards (CAAQS) in Edmonton and Calgary. This research aims to identify the sensitivity of NO_2 concentration to changes in emissions from two primary sources of transportation and upstream oil and gas for populated areas in Alberta. It also investigates the O_3 concentration differences in the summer and winter due to variations of NO_2. Understanding primary sources of criteria air contaminants (CACs), including NO_2 and O_3 in Alberta, using a detailed atmospheric air pollution model is the focus of this work.

Meteorological parameters of temperature and wind were captured using the open-source Weather Forecasting and Research (WRF) model. The most recent comprehensive Alberta emission inventory data for 2013 was used as the base year emission input. The emission data were processed using the US EPA Sparse Matrix Object Kernel (SMOKE) to generate gridded outputs of temporal, spatial, and chemical profiles of emission sources. WRF and SMOKE outputs were combined with the Community Multiscale Air Quality (CMAQ) chemical transport model. A nested domain with the finest spatial resolution of 4 km$\times$4 km was used in the model domain of the province of Alberta.

The air pollution model output was validated using data from 40 air quality ground observation stations provided by the National Air Pollution Surveillance (NAPS) program. Validation was performed using two periods: January 2019 (10th-20th)

and July 2019 (15th-25th). Hourly averaged simulation results were compared to ground station measurements. The model performance adequately replicated the spatiotemporal profiles of hourly averages of NO_2 and O_3 measurements. The effect of winter and summer temperatures on both temporal and spatial emission concentration was evaluated. Analyzing the diurnal simulation data shows that the average daily NO_2 concentration in winter is $18 \leq NO_2 \leq 24$ ppb in Calgary and Edmonton, the major cities of Alberta, which is approximately three times higher than the average of $6 \leq NO_2 \leq 8$ ppb for summer. Industries and oilsands areas also experience the same trend from $3 \leq NO_2 \leq 5$ ppb in summer to $9 \leq NO_2 \leq 13$ ppb in winter.

A sensitivity analysis was carried out to determine the effect of primary anthropogenic emission sources, namely mobile sources and upstream oil and gas (UOG), on the concentration of NO_2. Approximately 48% and 15% of NO_x emissions in Alberta come from UOG and mobile sources, respectively. The sensitivity analysis results at monitoring stations located in the cities of Edmonton and Calgary showed that mobile sources contributed to significantly higher fractions of 54% and 46% of NO_2 in cold and warm modeling periods, respectively. In these stations, the impact of UOG sources was found to be less than 10% for each modeling period. The UOG sources effect is more pronounced at a regional background station and outside urban areas. Analyzing O_3 concentration variation due to perturbed emission reveals that the cities of Edmonton and Calgary, are NO_x-saturated regimes. Furthermore, sensitivity analysis showed that the NO_2 concentration almost linearly responded to emission changes. The linear response of NO_2 to emission perturbation indicates in Alberta's two large cities, emissions from mobile sources should be reduced by 20% to meet 2025 CAAQS limits.

The research air pollution simulation tool developed in this thesis has been validated with ground-level concentration measurements. It can be used to examine scenarios to analyze the interactions of CACs concentrations with weather-related incidents, climate change, and technologies and policy changes.

Table of Contents

List of Tables

List of Figures

List of Symbols

Quantitative variables

CO	Carbon monoxide	ppm
HO_x	Hydrogen oxide radicals	ppb
NO_x	Nitrogen oxides	ppb
O_3	Ozone	ppb
OH	Hydroxyl radicals	ppb
PM_{10}	Particulate matter 10 micrometers or less in diameter	$\mu g/m3$
$PM_{2.5}$	Fine particulate matter	$\mu g/m3$
RH	Reactive volatile organic compounds	ppb
RO_2	Alkyl peroxy radicals	ppb

Latin

C	Concentration
C_b	Base case concentration
C_n	Modelling concentration after applying perturbations
D	Molecular Diffusion
E	Rate of Emission
FB	Fractional bias
K_H	Horizontal turbulent diffusion coefficient

K_Z Vertical turbulent diffusion coefficient

$NMSE$ Normalized mean square error

R Chemical Reaction

r Correlation coefficient

T Temperature

t Time

u, v, w Velocity

x, y, z Eulerian coordinates

Greek

ϵ Perturbation in emission

Abbreviations

AAAQO Alberta Ambient Air Quality Objectives.

AQHI air quality health index.

AQM Air Quality Model.

AQMS Air Quality Management System.

CAAQS Canadian Ambient Air Quality Standards.

CCME Canadian Council of Ministers of Environment.

CMAQ Cummunity Multiscale Air Quality.

ECCC Environment Canada and Climate Change.

EGUs Electrical Generating Units.

EPEA Alberta Environmental Protection and Enhancement Act.

NAPS National Air Pollution Surveillance.

NCAR National Center for Atmospheric Research.

NPRI National Pollutant Release Inventory.

PE Population Exposure.

PS Point Source.

RB Regional Backgroud.

SMOKE Sparse Matrix Operator Kernel Emissions.

T Traffic.

UOG Upstream Oil and Gas.

US EPA United States Environmental Protection Agency.

VOC Volatile Organic Compounds.

WRF Weather Researh Forecast model.

ZOC zero-out case.

Chapter 1

Introduction

1.1 Motiviation and Objectives

Industrialization, the growth of population, and as a result the growing need for transportation have motivated many studies on air pollution and its adverse effects [1–3]. Canada's latest health report reveals that, in 2021, air pollution contributed to the 15,300 premature death around Canada [4]. Recently, Nitrogen dioxide (NO_2), as one of the criteria for air contaminants, has received particular attention from the government of Alberta [5, 6]. Exposure to NO_2 (above the background level) is attributed to adverse health issues such as asthma, irritation, and infection of the respiratory system [7]. The majority of NO_2 concentration is formed through the combustion process of fossil fuel, which happens at power plants, on-road and off-road vehicles [8]. In Alberta, the trends of NO_2 concentrations show that although the NO_2 emission have been decreasing, it still exceeds the new Canadian Ambient Air Quality Standards (CAAQS) [6]. Therefore, new policies and management plans for NO_2 emission abatement are needed in Alberta Province [9]. To help Alberta's decision-makers to define informed policies, an air quality model (AQM) for the province of Alberta has been developed in this study. By incorporating the AQM, the effectiveness of proposed plans for emission reduction can be evaluated.

Air Quality Models are computational tools to simulate the physicochemical processes in the atmosphere [10]. AQM helps us to better understand the origin, trans-

portation, and fate of different pollutants in the atmosphere [11]. The AQM is a tool to analyze the impact and effectiveness of emission control strategies, and as such is a key tool for helping air pollution stakeholders to define science-based policies for emission abatement. The AQM, used in this study, consists of three complex numerical models for a domain consisting of 4km $\times$ 4km cells covering the entire Alberta province. Firstly, the weather research forecast (WRF) model to determine and predict 3-dimensional meteorological fields. Secondly, the sparse matrix operator kernel emissions (SMOKE) model which provides a spatiotemporal profile for emission inventory data. And the last model is community multiscale air quality (CMAQ). CMAQ is a chemical transport model that provides an hourly map of the concentration of different species. The main objective of this research is to develop and validate an integrated AQM for the whole Alberta province in order to allow the analysis of NO_2 emissions in Alberta. The COVID-19 pandemic significantly altered human activities and resulted in an unusual trend for emissions after the COVID [12]. To avoid this bias, the model is validated for a pre-COVID period in 2019. A second objective is to analyze the contribution of major NO_2 sources and their impact on the NO_2 spatial and temporal distribution over the entire province of Alberta. The AQM, once validated, can be used to explore emission scenarios where NO_2 emissions are changed.

Providing guidance for strategies to comply with future CAAQS' regulations is performed by providing a better understanding of the spatiotemporal distribution of NO_2 concentration. Two major NO_2 sources in Alberta are the Upstream oil and gas (UOG) industry and mobile sources (transportation). In this study, the impact of these two sources are compared using sensitivity analysis. UOG is responsible for emitting almost half of the total NO_x emission in Alberta (322,712 tons/year) [13], and mobile sources emitting almost 98,357 tons/year are among the high NO_x emitters in Alberta [13]. The effect of these sources on the air quality health index (AQHI), which is used as a known standard to inform the health risk associated with

exposure to pollution [14], is studied in detail. It is important to note that in order to generalize (extrapolate) the results for the whole year, data from time periods without extreme events, like a forest fire, are considered.

The most recent Canadian Ambient Air Quality Standards (CAAQS) define more stringent thresholds for NO_2 and O_3 concentrations starting in 2025, compared to the previous standards for 2020 [15]. For example, the NO_2 threshold is an annual average of 17 ppb in 2020 but this threshold is reduced by 30% to 12 ppb in 2025 [15]. In Alberta, the actual trends of NO_2 concentration show the exceedance of 2025 CAAQS [6]. To quantify and understand the emission trends, detailed and up-to-date emission files are needed to parametrize and execute the AQM. To understand the capabilities and limitations of the AQM, validation on measured NO_2 concentrations is performed. Observation data from 40 monitoring stations in Alberta from the National Air Pollution Surveillance (NAPS) program are used for ground-level pollution concentration validation. Stationary and mobile emission sources are obtained from Alberta Environment and protected areas [16].

The effect of each UOG or mobile source emissions is examined by zeroing out each source individually. In the zero-out case (ZOC), the emission from one specific source will be eliminated and the model's response will be re-calculated. The difference between the base case and ZOC shows the influence of the respective source. Variation of NO_2 concentration by applying a perturbation to the emission sources allows an emission sensitivity to be performed for small perturbations. To gain insight into possible emission abatement strategies, hypothetical scenarios of emission change of mobile sources and UOG sources are performed.

1.2 Thesis Contribution

The previous atmospheric modeling studies for Alberta province focused on some parts of the province and the model was validated for $PM_{2.5}$ and Ozone contaminants. In this study, the model was developed and validated for the entire province

considering the most updated emission inventory available. The focus of this study was addressing the NO_2 exceedance from CAAQS. Therefore, the model results were validated for replicating the NO_2 concentration.

Alberta has a continental climate. In warm seasons, the temperature normally varies between 16 to 30°C with a mean value of around 22°C. Although a number of researchers have analyzed NO_2 concentrations around the world, a limited number of studies consider the effect of considerable temperature variation and cold climate impact on NO_2 concentration. Analyzing a case study for the province of Alberta, this study addresses the impacts of large temperature variations and cold climate on NO_2 concentration.

Adopting a sensitivity analysis approach, different emission scenarios considering both minor and major perturbations on emission sources were evaluated for the first time for the province of Alberta. The major perturbation provided details on major sources' contribution to NO_2 concentration. And minor perturbation was used to evaluate the response of NO_2 concentration to emission changes and to determine the NO_2 regime for Alberta. Using the sensitivity results, observed data, and 2025 CAAQS thresholds, the required emission change for realizing the new CAAQS standard was calculated.

1.3 Thesis Outline

This thesis is organized into 5 chapters. The problem statement, motivation, and thesis contribution are summarized in chapter 1. In the second chapter, the background and literature review of NO_2 modeling using an atmospheric model is described. Details regarding the emission files, sensitivity analysis, and tropospheric chemistry are also provided. Chapter 3 describes the meteorological model and the atmospheric chemistry model used in the simulation of the transportation of chemical species. Details of the model including assumption and numerical method are described. The benchmark data used for model validation are also described in chapter 3. In chapter

4, the results of the model validation are presented first. The model is compared to the ground measurements and the accuracy and validity of the model are discussed. Using the validated model, a zero-out study and sensitivity analysis are performed and the impact of different scenarios is described. Finally, the effect of emission sources on the air quality health index is investigated to start making a connection between air quality and human health.

Chapter 2

Background and Literature Review

2.1 Alberta Air Quality Objectives and Standards

Alberta Environmental Protection and Enhancement Act (EPEA) is the primary legislation in Alberta to promote and support the protection and enhancement of the environment as well as define regulations to control activities that affect the environment [17]. Under this act, the Alberta Ambient Air Quality Objectives (AAAQO) were developed considering scientific, social, technical, and economic factors for improving air quality [18]. AAAQO is used to manage and orient the activities and construction of major emission industries and sources, to inform Albertans regarding the state of the atmospheric environment and air quality index [18]. These objectives, shown in table 2.1 for pollutants of concern in this study, can be evaluated for different averaging periods of either 1-hr, 24-hr, or annual, where applicable.

Table 2.1: Alberta Ambient Air Quality Objectives [18]

Substance	Averaging Period	Concentration (ppb)	Effective Date	Last review
Nitrogen dioxide	1-hr Annual	159 24	1975	2009
Ozone (ground level)	1-hr daily maximum	76	1975	2019

AAAQO is an Alberta provincial act. The Canadian Council of Ministers of Environment (CCME) have established the Canadian Ambient Air Quality Standards

(CAAQS) on a national scale [19]. CCAQS, as a part of the Air Quality Management System (AQMS), was developed to assess the realization of the actions for improving the air quality across Canada. To help protect human health and reduce the emission of various pollutants, the CAAQS have been defined for several chemical substances. A summary of CAAQS for the pollutants of concern in this study is provided in table 2.2.

Table 2.2: Canadian Ambient Air Quality Standards [19]

Management Level	NO_2 1-hour (ppb)		NO_2 annual (ppb)		O_3 8-hour (ppb)	
	2020	**2025**	**2020**	**2025**	**2020**	**2025**
Red	>60	>42	>17.0	>12.0	>62	>60
Orange	32 to 60	32 to 42	7.1 to 17.0	7.1 to 12.0	57 to 62	57 to 60
Yellow	21 to 31	21 to 31	2.1 to 7.0	2.1 to 7.0	51 to 56	51 to 56
Green	≤ 20	≤ 20	≤ 2.0	≤ 2.0	≤ 50	≤ 60

The calculation procedures of the thresholds, presented in table 2.2 are different. NO_2 1-hour threshold is the 3-year average of the annual 98th percentile of the NO_2 daily maximum 1-hour average concentrations [20]. 98th percentile is considered to eliminate the effects of occasionally observed maximums due to exceptional events like forest fires. NO_2 annual is the average over a single calendar year of all NO_2 1-hour average concentrations in the year [20]. O_3 8-hour is the 3-year average of the annual 4th highest daily maximum 8-hour average concentrations [21]. In this study to analyze the CAAQS achievement the NO_2 annual was considered and calculated.

CAAQS divides the concentration level of intended pollutants at a certain location into four categories corresponding to air quality objectives as [22]:

- **Red**: To reduce pollutant levels below the CAAQS through advanced air management actions.
- **Orange**: To improve air quality through active air management and prevent exceedance of the CAAQS.

- **Yellow**: To improve air quality using early and ongoing actions for continuous improvement.

- **Green**: Air quality stakeholders should apply management measures to maintain clean air levels.

Compared with 2020, more stringent CAAQS for NO_2 and O_3 have been established for 2025. The status of different monitoring stations in Alberta is compared with the NO_2 CAAQS standards based on the annual averages of measured NO_2. To do this, observation data from the year 2019 for forty stations are averaged and compared to CAAQS standards for 2020 and 2025. The year 2019 was chosen as it was before the COVID pandemic and was judged to be more representative of a "typical" situation. The more stringent CAAQS for the year 2025 is included to investigate how the future standard will impact the CAAQS management level of these stations across Alberta. The results are shown in table 2.3.

Table 2.3: CAAQS Management Level for 40 stations in Alberta based on an annual average of measured NO_2 values in 2019

Station Name	NO_2-measured	CAAQS 2020	CAAQS 2025
Beaverlodge	4.7	Y	Y
Grande Prairie-Henry Pirker	11	O	O
Anzac	2.3	Y	Y
Cold Lake South	3.5	Y	Y
Conklin	1.3	G	G
Fort Chipewyan	2.1	Y	Y
Fort McKay-Bertha Ganter	8.3	O	O
Fort McKay South	7.3	O	O
Fort McMurray-Athabasca Valley	7.7	O	O
Fort McMurray-Patricia McInnes	5.4	Y	Y
Carrot Creek	4.7	Y	Y
Edson	8.1	O	O
Hinton	7	Y	Y
Steeper	2.1	Y	Y
Ardrossan	7.1	O	O
Breton	4.2	Y	Y
Bruderheim	5.8	Y	Y

Caroline	2.6	Y	Y
Edmonton Central	14.9	O	R
Edmonton East	12.1	O	R
Edmonton South	10.4	O	O
Edmonton-Woodcroft	12.4	O	R
Elk Island	3.5	Y	Y
Fort Saskatchewan	7.9	O	O
Genesee	6.9	Y	Y
Gibbons	7	Y	Y
Lamont County	4.1	Y	Y
Redwater	5.3	Y	Y
Sherwood Park	10.1	O	O
St. Albert	10.4	O	O
St. Lina	2.1	Y	Y
Tomahawk	3.9	Y	Y
Violet Grove	4.4	Y	Y
Red Deer-Lancaster	8.8	O	O
Red Deer-Riverside	9.8	O	O
Airdrie	6.5	Y	Y
Calgary Central-Inglewood	15.5	O	R
Calgary Southeast	13.3	O	R
Lethbridge	5.5	Y	Y
Medicine Hat-Crescent Heights	6.9	Y	Y

For the CAAQS management level for 2020, 43% and 55% of stations are orange and yellow levels respectively, one station, Conklin, is green and there is no station in the red level. If the emission levels based on 2019 remain constant the CAAQS management levels will get worse in 2025 due to the more stringent requirement in this year. Considering 2025 CAAQS at 2019 emission levels, 13% of stations will be red, 30% stations will be orange, 55% will be yellow and one station will be green. At 2019 emission levels, all the major cities of Edmonton and Calgary will be in red management level. Although this is only around 12% of the total NAPS stations in Alberta, these cities have nearly 55% of the total population of the province. The NO_2 exceedance of the CAAQS is a crucial and pressing issue that requires targeted actions and new policies to prevent exceeding CAAQS. Because of this important and pressing problem, NO_2 concentration is the focus of this study. Due to the bidirectional reaction between NO_2 and O_3 in the atmosphere, the O_3 also must also

be analyzed. Further, since meteorological parameters such as ambient temperature and sunlight affect NO_2 and O_3 concentration considerably, both summer, and winter conditions are analyzed in Alberta.

Developing an integrated air quality model to address the NO_2 exceedance of the CAAQS and corresponding issues, is the main goal of this study. The contribution of different anthropogenic emission sources to the NO_2 and O_3 concentration are determined using the validated model. Then different emission scenarios are analyzed to help decision-makers understand impacts of different sources and their sensitivities. The results can then provide Alberta policy makers a scientific basis to implement new emission policies to meet CAAQS regulations and provide Albertants with clean air. The AQM is a useful tool to evaluate the effectiveness of new policies for improving air quality and will be described in detail.

2.2 Air Quality Modeling

Air Quality Models (AQMs), also called chemical transport models are computational 3-D models to reproduce or predict the physical and chemical behavior of pollutants in the atmosphere. AQMs are an important tool providing government and policy-makers guidance on the effectiveness of a new policy for emission abatement [23]. Recently, AQMs have been extensively used in global, regional, and local scales for scientific research and environmental assessment plans [24]. AQMs are typically used to assess the impact of emission and climate scenarios, assess the long-term air quality and atmospheric behavior, and to forecast short-term periods of air quality [25]. In this research, the impact of emission and climate scenarios are assessed. The effect of emission sources and emission scenarios on NO_2 and O_3 concentration for Alberta is the focus of this work.

Air quality studies within Alberta province to address the regional or local air quality concerns using AQMs have been performed in the past. Most of these studies have focused on the northern part of Alberta, the Athabasca oil sands region. They

introduced and evaluated AQMs [26, 27], and performed source apportionment study [28] for Ozone and $PM_{2.5}$. The most recent Alberta government modeling report, which developed an AQM for the whole province, the source apportionment study was carried out to facilitate planning the management actions for controlling $PM_{2.5}$ [13]. These modeling studies did not analyze the NO_2 concentration exclusively. In contrast, in this study the model results for the NO_2 pollutants and emission scenarios and sensitivity analysis for NO_2 concentration are performed while considering the emission sources for the entire province of Alberta. Review of the relevant AQM studies worldwide that either analyzed NO_2 or O_3 is described next.

2.2.1 Nitrogen Dioxide in Literature

Due to the rapid growth of population, urbanization, and therefore need for transportation, anthropogenic emissions have increased significantly [1–3]. NO_2 is one of the most important anthropogenic emissions which adversely affect human health and the atmosphere [29, 30]. NO_2 major anthropogenic sources are the combustion of fossil fuel in vehicles, power plants, and industrial sources [31]. Worldwide, there has been a growing number of air quality modeling studies to address the NO_2 issues [30, 32, 33]. In a case study of two major urban traffic sites in Italy, it was shown that traffic sources' contribution to the NO_2 level is much higher than the domestic heating or industrial sources [34]. For Turin, Italy, a modeling study suggest that the NO_2 and O_3 concentrations have an inverse relationship, when one increases the other decreases[30]. Using a hybrid models by fusing observation data to improves the resolution of the AQM for analyzing NO_2 concentration. The hybrid model's high-resolution results for the winter period, show a high sensitivity of NO_2 concentration to mobile emission sources (traffic) [35]. The most recent Alberta photochemical modeling performed a source apportionment study and show that although the up-stream oil and gas (UOG) industry emitted more than half of the total NO_2 emission in Alberta, the NO_2 concentration in urban areas is also affected considerably by

traffic and mobile sources [13].

A long-term AQM simulation of NO_2 concentration changes in China, is used to understand the effect of meteorology and emission changes[36]. For an inter-annual period, they found that although the meteorological conditions affect the NO_2 concentration, the impact of emission changes is more dominant [36]. In another long-term analysis, the ground-level NO_2 concentration is evaluated along coastal areas in China, over a long term [37]. The effectiveness of the emission reduction policies for these regions is demonstrated using an AQM [37].

In this study, an AQM to evaluate ground-level NO_2 and O_3 concentration is developed for the province of Alberta. Using AQM, sensitivity analysis is performed to determine the effect of emission sources. Since NO_2 concentration is sensitive to both mobile sources and UOG in Alberta, the sources are categorized as the mobile source, UOG source, and other sources. To analyze the impact of meteorology changes in winter and summer on NO_2 and O_3, the simulation is performed for two two-week periods, one in the summer and one in the winter.

2.3 Alberta Emission Inventory

To have an accurate AQM it is essential to account for all the sources of emission in an emission inventory. Emission Inventory is the most important and, at the same time, most uncertain input of AQMs [23]. The quality and accuracy of the emission inventory files directly affect the performance of the modeling system [38]. There are several different emission inventory databases available for province of Alberta including National Pollutant Release Inventory (NPRI) [39], Environment Canada and Climate Change (ECCC) modelers' air pollution emission inventory [13]. In this study, the latest emission inventory comprised of a combination of available inventories is used. This emission inventory was compiled by the Ramboll company and NOVUS Environmental [13] and is currently the most complete emission inventory available for air quality modeling purposes. This emission inventory has also been

used in the latest Alberta photochemical modeling report [13]. This database, developed for the year 2013, categorizes the emission sources into seven sectors [13].

- Agriculture
- Coal-fired Electrical Generating Units (EGUs)
- Forestry, wood products, pulp, and paper production
- On-road mobile sources
- Industrial sources
- Non-industrial sources
- Upstream Oil and Gas (UOG)

The total emission from these major sources is shown in the fig. 2.1.

Highlighting significant data in fig. 2.1, NO_x, which is a total concentration of Nitrogen oxides (NO and NO_2), after PM10 and CO is the third highest anthropogenic emission in Alberta. As shown in fig. 2.1, the total NO_x emission in Alberta is more than 600,000 tons/year and when comparing the contribution of different NO_x emission sources, UOG emission is almost three times higher than any other NO_x sources with approximately 48% of total NO_x in Alberta. The second and third highest NO_x sources are non-industrial point and non-point sources and on-road mobile sources, respectively. The contribution of these sectors to the production of NO_x emission is almost 20% for the former and 15% for the latter.

The large contribution of the UOG sector to the production of NO_x, and the sensitivity of NO_x to mobile sources in large cities [34, 35], is the motivation to evaluate the impact of these two sources on the NO_2 exceedance of CAAQS.

The United States Environmental Protection Agency (US EPA), divides emission sources into two broad groups: point sources and non-point sources [40]. Point sources refer to any sources that emit from an easily identifiable and confined place. Examples

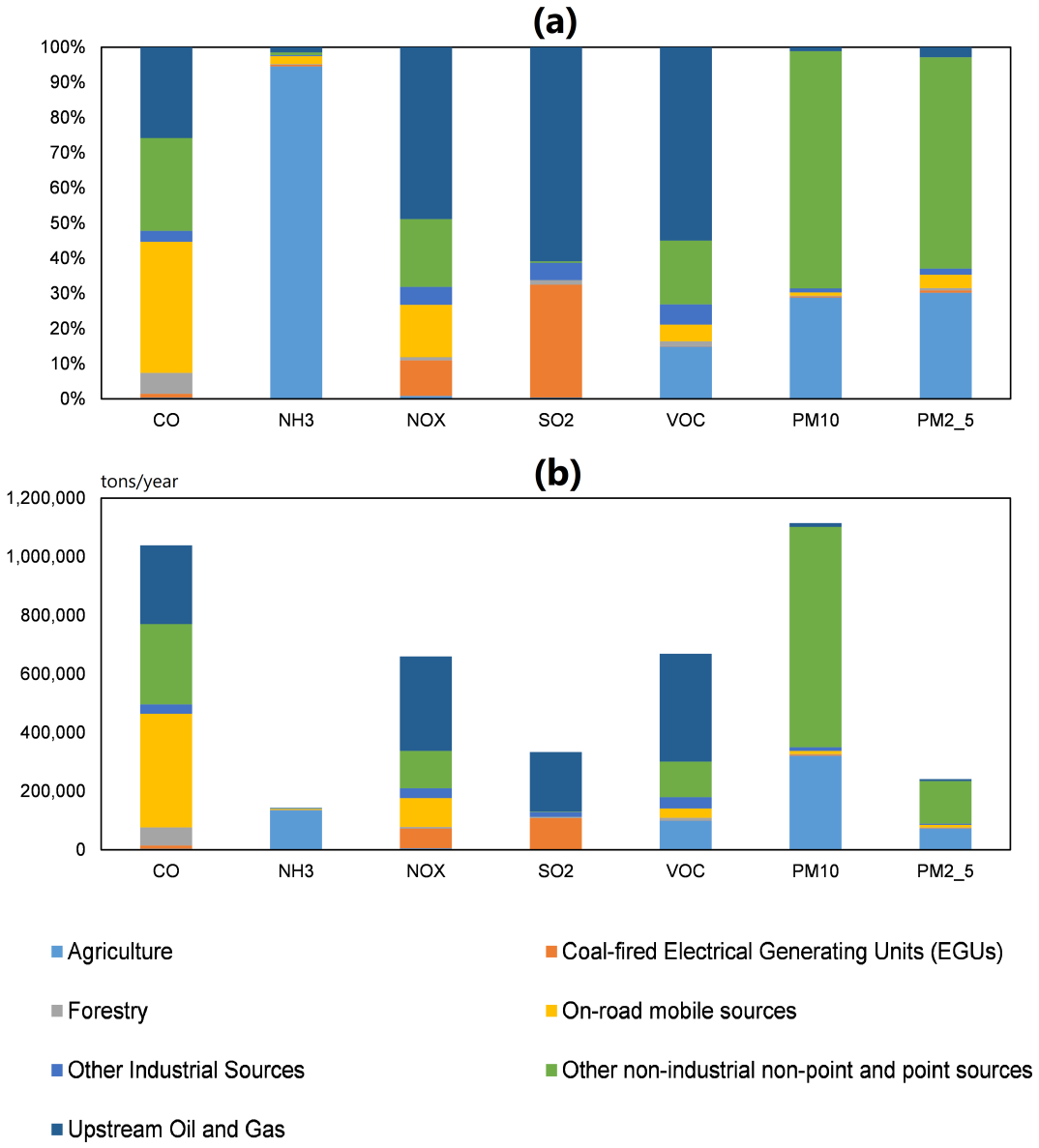

Figure 2.1: Alberta anthropogenic emissions summary for 2013 by sector; a)percentage of total emission by sector, b)Emission by pollutants by sector in tons/year

of these types of sources are UOG, industrial sources, power plants, etc. Non-point sources refer to sources where the total emission comes from many distributed (in space) sources. A good example of a non-point source is on-road mobile sources of many vehicle.

2.4 Tropospheric Chemistry

The Earth's atmosphere has been divided into five layers from the earth's surface to space (>500km altitude) [41]. The lower layer, which we live in, extends from the ground to approximately 12 km in height and is called the troposphere. Nearly 80% of the total mass of the atmosphere exists within the troposphere layer. Almost all the emissions emitted from anthropogenic sources and natural activities enter this layer. It is important to note that within this layer, most emissions are trapped in the lower 1 km of the troposphere. This 1km height layer is called the planetary boundary layer[41]. The high concentration of emissions in the troposphere layer necessitates understanding the chemistry of common air pollutants in this layer for air quality modeling.

NO_2 and ground-level Ozone are two common air pollutants denoted "Criteria Air pollutants" [42]. They are the focus of this study since NO_2 levels exceed the 2020 CAAQS yellow management level for almost the entire province of Alberta as shown in table 2.3. The Ozone level is also relatively high [43]. These two pollutants are crucial species in atmospheric chemistry especially in the tropospheric layer since they affect adversely human health and the environment [44, 45]. Long and short exposure to these chemical compounds could lead to severe health issues such as asthma, hypertension, heart disease, chronic respiratory and lung disease, and premature death [4, 46, 47]. Understanding the chemical behavior of these substances, and how they interact with other species and transport through the troposphere is the focus of the rest of this chapter.

2.4.1 Nitrogen Dioxide Chemistry

Nitrogen dioxide (NO_2), which is one of the US EPA criteria air contaminants[42], is a highly reactive chemical compound and temperature dependent in the troposphere. NO_2 lifetime varies from a few seconds at high temperatures to several days at lower

temperatures. Nitrogen oxides (NO_x), which are comprised of NO and NO_2, can highly affect the troposphere chemistry through the formation of Ozone, smog, and acid rain. Nitrogen oxides sources are Both natural and anthropogenic sources. Natural sources of NO_2 include forest fires and lightning strikes. However, the majority of NO_2 emissions are the product of the oxidization of the NO generated through the combustion process of fossil fuels [48]. This combustion occurs in on-road and off-road vehicles, industrial sources, power plants, construction equipment, etc. In combustion reactions, the temperature is high enough so nitrogen and oxygen react and produce nitrogen monoxide [41]. Then this nitrogen monoxide combines with oxygen and produces NO_2 [41].

$$N_2 + O_2 \longrightarrow 2NO \tag{2.1}$$

$$2NO + O_2 \longrightarrow 2NO_2 \tag{2.2}$$

NO_2 can participate in the formation of ground-level Ozone. As NO_2 is highly reactive, this formation can occur in the presence of sunlight in a process called photo-dissociation.

$$NO_2 + hv \longrightarrow NO + O \tag{2.3}$$

$$O + O_2 \longrightarrow O_3 \tag{2.4}$$

$$NO + O_3 \longrightarrow NO_2 + O_2 \tag{2.5}$$

First, the sunlight energy, which is depicted by hv, breaks NO_2 into nitric oxide and a free oxygen atom. Then, the free oxygen atom reacts with oxygen molecules and produces Ozone. The NO generated in reaction 2.3 quickly reacts with Ozone generated in reaction 2.4 and reproduces the NO_2 molecules. These series of reactions could take place in a time scale of minutes depending on the temperature and concentrations. In a clean atmosphere, this whole process establishes an equilibrium between NO, NO_2 and Ozone concentration and is called the null cycle between NO_2 and O_3 in atmospheric chemistry. The null cycle is a diurnal steady-state cycle that affects

steady-state O_3 concentration. The removal process of NO2 from the atmosphere happens through the solvation of NO_2 in water particles and generating acid rains or through absorption by larger particles like ammonia and generating particulate matter.

As said earlier, the null cycle happens during the daytime and in the presence of sunlight. However, at night, NO_2 chemistry is different. Almost all the NO_x in the form of NO reacts rapidly with O_3 and converts into NO_2 (reaction 2.5). Then NO_2 through reaction with O_3 generated nitrate radical (NO_3).

$$NO_2 + O_3 \longrightarrow NO_3 + O_2 \tag{2.6}$$

The conversion of NO, NO_2, O_3 to NO_3 at night decreases the O_3 concentration. However, NO_3 in the presence of sunlight rapidly photolyze to NO and NO_2 in a matter of seconds.

$$NO_2 + NO_3 \longrightarrow N_2O_5 \tag{2.7}$$

$$N_2O_5 + H_2O_{(s)} \longrightarrow 2HNO_3 \tag{2.8}$$

At night, through some reactions involving water particles (H_2O), NO_2 and NO_3 produce HNO_3 and remove from the atmosphere (reactions 2.7 and 2.8). Reaction 2.8 is one of the major removal paths of NO_x from the atmosphere.

2.4.2 Ozone Chemistry

Ozone is a reactive oxidant that plays two completely different roles in the atmosphere [41]. In the upper layer of the atmosphere, the Ozone presence is vitally important cause it absorbs the ultraviolet radiation of sunlight [41]. However, in the troposphere layer, Ozone is known as a criteria pollutant, which can affect adversely human health [49]. The adverse effects of Ozone in the troposphere are not limited to human health [50]. Ozone is one of the main ingredients of the "smog", which disturb the regional weather substantially [50].

Ozone is a secondary air pollutant, which means that it is a production of the chemical reactions of another species. Nitrogen oxides (NO_x), volatile organic compounds (VOCs), and carbon monoxide (CO) are the major species from which Ozone is formed and called precursors of the Ozone.

$$CO + 2O_2 + hv \longrightarrow CO_2 + O_3 \tag{2.9}$$

Reaction 2.9 is the net effect of the series of reactions involving CO that result in O_3 production. The major sources of Ozone chemical precursors compounds are vehicle exhaust, industrial sources, and chemical solvent [51]. The chemical reactions that generate Ozone, like the null cycle, are highly dependent on energy and radiation from sunlight [52]. The peak periods of Ozone typically happen in the summertime [52].

One of the key reactive species in atmospheric chemistry that affect O_3 significantly is hydroxyl radical (OH). Prior to directly affecting the O_3 production, hydroxyl and hydroperoxyl (HO2) radicals react with VOCs, and NO_x to initiate the process.

$$RH + OH + O_2 \longrightarrow RO_2 + H_2O \tag{2.10}$$

$$RO_2 + NO \longrightarrow RO + NO_2 \tag{2.11}$$

$$HO_2 + NO \longrightarrow OH + NO_2 \tag{2.12}$$

Consider a reactive VOC (denoted RH), the reaction of this substance with the hydroxyl radical generates alkyl peroxy radicals (denoted RO_2) and H_2O [53]. Then the resulting RO_2 reacts with nitric oxide and produces nitrogen dioxide, which goes through a null cycle [53]. The propagation and termination of these series of reactions are affected by the availability of hydroxyl and hydroperoxyl radicals [54]. The availability of these radicals is dependent on the VOC and NO_x concentration level. Therefore the ratio of VOCs to NO_x is important to determine Ozone production. At low NO_x concentration, which is called a NO_x-limited regime, these radicals have a tendency to react with VOCs. However, when the NO_x concentration level is higher,

called the NO_x-saturated regime, these radicals have a tendency to react with NO_x rather than VOCs. Generally, in NO_x-limited regime, the O_3 rate of production varies linearly with NO_x, and VOCs do not affect the Ozone level [41]. In NO_x-saturated regimes, Ozone concentration varies inversely with NO_x concentration and linearly with VOC concentration [41]. In this case, NO_x is a sink for HO_x radicals [41, 55].

Considering the null cycle, at NO_x-limited regimes, reactions 2.3 and 2.4 are dominant direction and will lead to higher O_3 concentration. While, at NO_3-saturated regimes, reaction 2.5 is dominant and O_3 destroy.

2.4.3 Atmospheric Stability

stability is one of the essential concepts in atmospheric chemistry. To evaluate stability, consider a parcel of air containing emitted pollutants. The tendency of this air parcel to displace vertically from its position determines the level of stability [41]. In a stable atmosphere, the displaced parcel returns to its initial position; in an unstable atmosphere, the displaced parcel accelerates and moves to a new place [41]. The level of atmospheric stability near the surface affects the pollutant concentration [56]. Atmospheric stability generally leads to pollutant builds up, and unstability helps pollution dispersion. The degree of stability can be derived from the idea of turbulent flow in the atmosphere. The atmospheric turbulence is affected mainly by buoyancy forces and mechanical shears (like wind) [56]. The proportion of these two effects determines the level of stability. For example, in an unstable atmosphere, buoyant forces dominate the mechanical shears and the air parcel accelerates upward, resulting in emission dilution near the surface [56]. The Monin-Obukhov similarity is a method to parametrize the turbulence fluxes near the surface. Using this method, the height at which the effect of buoyancy dominates the mechanical shear for the first time can be derived mathematically [56]. This length is called Monin-Obukhov length (L) in meters and is proportional to the actual height above the surface. The table 2.4 categorizes the level of stability based on the L [57]. Generally, if L is

positive atmosphere is stable and if L is negative, the atmosphere is unstable.

Table 2.4: Class of atmospheric stability based on Monin-Obukhov length [57]

Class of Stability	L (m)
Extremely unstable	$-100 < L < 0$
Slightly unstable	$-10^5 \leq L \leq -100$
Neutral	$\|L\| > 10^5$
Slightly stable	$10 < L < 10^5$
Extremely stable	$0 < L < 10$

Chapter 3

Model deployment and Validation

Each component of the Air Quality Model (AQM) and their interconnections are described in this chapter. The AQM comprises three major models. The first model is WRF which calculates the spatiotemporal pattern of the meteorological fields including temperature, wind speed and etc. Then the SMOKE model which prepares the emission data is described. Next, the CMAQ model which determines the chemical reactions is described. The modeling results are then validated by observation data from NAPS monitoring stations.

3.1 Weather Research Forecast (WRF)

Meteorological fields, such as temperature, wind speed, direction, pressure, etc are the critical inputs of the atmospheric modeling system. A community mesoscale weather research forecast (WRF) model is used to calculate the spatial and temporal variation of the meteorological fields. WRF model, an approved model by the U.S. Environmental Protection Agency (EPA), is a fully compressible non-hydrostatic model, which implements Reynolds averaged primitive equations coupled with conservation equation of scalar quantities. In the WRF model, Time-dependent derivatives are resolved using Runge-Kutta 2nd and 3rd order. Advection terms are approximated by different 2nd to 6th-order advection schemes.

3.1.1 Model Configuration

Physics	**Micro-physics**	**Long-wave radiation**	**Short-wave radiation**	**Surface layer**	**Land surface**	**Boundary Layer**
Scheme	WSM6	RRTMG	RRTMG	Monin-Obukhov	Noah	MYJ
Reference	Hong and Lim (2006)	Iacono-et-al. (2008)	Iacono-et-al. (2008)	-	-	Janjic (1994)

Table 3.1: WRF Physics Configuration

3.1.2 Computational Domain

The WRF computational domain comprises three nested domains with 32 vertical layers going to a height of approximately 2000m. Figure 3.1 shows the course domain with a resolution of 36x36km covering the northern part of America, the medium domain with a resolution of 12x12km includes Alberta province and its contiguous provinces, and the finer domain, which is a region of interest, covers whole Alberta province with the 4x4km cells. The computational domain is a one-way nested domain which means that the information is only carried from the coarser domain to the finer domain. In WRF nested domain, the results, captured from the coarse domain, are used as initial and boundary conditions for the finer domain.

Regarding the vertical structure of the model, WRF uses a train-following approach to define the vertical layer. Each layer in the WRF model represents a surface with constant pressure. In the air quality modeling in most cases, only planetary boundary layer (around 2000 meters from the surface) is considered. Increasing the number of vertical layers directly causes an increase in computational time to evaluate the meteorological fields. In this study, 32 vertical layers are considered as suggested by National Center for Atmospheric Research (NCAR). The resolution of the coarse domain is large enough to capture the large-scale (1000 km) low-pressure atmospheric conditions called “Extratropical Cyclone”. These atmospheric waves are responsible for producing atmospheric events like mild showers, thunderstorms, tornadoes and etc. The 12km domain takes into account the effect of the mid-scale atmospheric

phenomena such as turbulent potential vorticity. The 4km domain is a relatively fine domain to capture the required inputs for the chemical model. The computational domain chosen in this study is consistent with the latest air quality modeling report published by the Alberta Government [13].

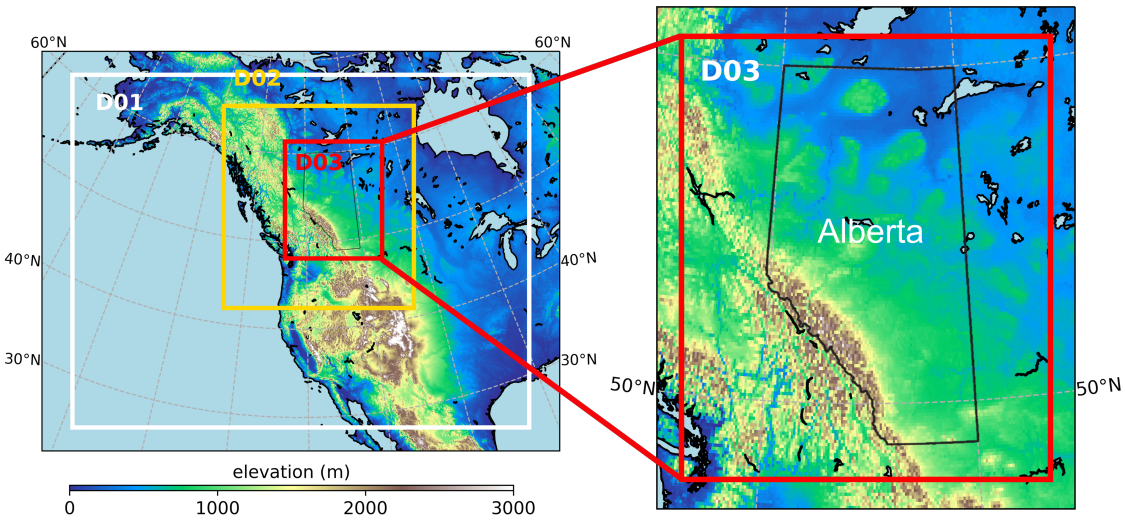

Figure 3.1: WRF Domain

3.1.3 Model Validation on Standard Benchmarks

Validation of the meteorological model is a necessary step to develop an integrated air quality dispersion model. The reason is that the error in the meteorological field could propagate through the chemical dispersion model and leads to the wrong results [58]. To analyze how well the meteorological model can capture real data, a number of studies have introduced performance benchmarks. First, in 2001, Emery et. al introduced a series of benchmarks for evaluating the model performance. Emery focused on the limited number of stations where the majority of them were in simple terrain regions [59]. Then in year 2009, McNally introduced a new set of benchmarks trying to consider the complex terrain regions as well [60]. Finally, in 2015, Bowden et. al. combined these two approaches and introduced a series of benchmarks for both complex and simple terrain [61]. The statistical metrics that are used in Bowden study are presented in equations 3.1, 3.2, and 3.3.

$$MB = \frac{1}{N}\sum_{i=1}^{N}(P_i - O_i) \tag{3.1}$$

$$ME = \frac{1}{N}\sum_{i=1}^{N}|P_i - O_i| \tag{3.2}$$

$$RMSE = \sqrt{\frac{1}{N}\sum_{i=1}^{N}(P_i - O_i)^2} \tag{3.3}$$

Where MB, ME, and RMSE represent mean bias, mean error, and root mean square error respectively. In the above equation, P_i and O_i represent simulation and observation data respectively and i is time in hours of simulation. The total number of available observation data for a specific station is N. The Index of Agreement (IOA) criteria, which was introduced by Emery et. al. 2001, is also calculated [59].

$$IOA = 1 - \frac{\sum(P_i - O_i)^2}{\sum(\left|P_i - \bar{O}\right| + \left|O_i - \bar{O}\right|)^2} \tag{3.4}$$

In equation 3.4 the $\overline{O}$ represents the average of available observation data for a specific station. All the statistical metrics are calculated only considering the hours that observation data were available. Using these statistical metrics and performance benchmark data, the meteorological model performance was analyzed to evaluate the model's capability to replicate the trend and real values of the meteorological field.

To validate the results of the WRF model, temporal variation of simulation outputs, including temperature at 2m altitude and wind speed at 10m altitude, were quantitatively compared to the surface observation data for the 40 air quality monitoring stations across Alberta. The summary of the benchmark proposed by Bowden and Emery for the statistical metrics introduced above is presented in table 3.2.

Table 3.2: Meteorological model performance benchmarks

Parameter	Mean Bias(MB)		Mean Error(ME)		RMSE		IOA
	Simple	Complex	Simple	Complex	Simple	Complex	
1-hr 2m temperature (°C)	$\leq \pm 0.5$	$\leq \pm 1.0$	≤ 2.0	≤ 3.0			≤ 0.8
1-hr 10m wind speed (m/s)	$\leq \pm 0.5$	$\leq \pm 1.0$			≤ 2.0	≤ 3.0	≤ 0.6

Both the simulation and observation data are 1-hour averaged parameters. The meteorological parameters temperature and wind speed have the most effect on the emission concentration, so these parameters were chosen to evaluate the model performance. The validation results are presented in section 3.6.

3.2 Observation Data

The air quality monitoring network across Alberta consists of 110 monitoring stations [62]. Among these stations, 54 are part of the National Air Pollution Surveillance (NAPS) program network. NAPS is a governmental program, managed by Environmental and Climate Change Canada (ECCC), which serves as the main source of continuous ambient air quality data across Canada [63]. Based on the Alberta Air Zones 2017-2019 report, which provides the status of the province to realizing the CAAQS, 47 stations from NAPS programs are subjected to CAAQS reporting [64]. In this study, based on the availability of the observation data, including temperature, wind speed, NO_2, and Ozone, 40 stations were chosen to validate the output of both meteorological and dispersion models. Table 3.3 provides the details of these stations and Figure 3.2 shows geographical distribution of these stations.

The NAPS program divides stations into 4 different classes; Urbanization, Neighbourhood Population, Local Land Use, and Site Type. In each class, stations are categorized based on different criteria. For example, the Site Type criterion categorizes the stations into 4 groups, in terms of source influences [65]. This criterion is chosen to understand the impact of different sources on NO_2 concentration at monitoring stations.

- **General Population Exposure (PE)**: representative of urban background conditions, Normally in these regions concentration gradients are small.

- **Regional Background (RB)**: representative of outside of the urban area. Networks of these stations are useful for providing good spatial coverage which is needed for mapping, modeling, remote sensing and etc.

- **Transportation Source-influenced (T)**: emission in this station is highly affected by transportation. Normally these sites are located within the 100m distance of a major roadway.

- **Point Source-influenced (PS)**: these sites are located in a populated area in the proximity of the major stationary emission sources of VOC and SO2.

The observation data needed for validation of meteorological fields were obtained from the open accessed governmental website, Alberta Air Data Warehouse[1]. In this database, the historical weather data are available for all the monitoring sites across Alberta. Furthermore, the observation data needed for evaluation of the chemical model was retrived from NAPS online open accessed database[2]. This database, provides the hourly concentration data for all NAPS monitoring stations across Canada.

Table 3.3: 40 Monitoring stations used for model validation

Air Zones	Station Name	Elevation	Latitude	Longitude	NAPS ID	Site Type
Peace	Beaverlodge	762	55.19	-119.39	91501	RB
	Grande Prairie-Henry Pirker	658	55.17	-118.80	92001	PE
Lower Athabasca	Anzac	495	56.44	-111.03	94601	RB
	Cold Lake South	556	54.41	-110.23	94301	PE
	Conklin	562	55.63	-111.07	none	
	Fort Chipewyan	238	58.70	-111.17	91801	RB
	Fort McKay-Bertha Ganter	268	57.18	-111.64	90801	RB
	Fort McKay South	342	57.14	-111.64	90806	PS
	Fort McMurray-Athabasca Valley	260	56.73	-111.39	90701	PE

[1]Accessed on 24 Oct 2022. https://airdata.alberta.ca/reporting/Download/MultipleParameters

[2]Accessed on 24 Oct 2022. https://data.ec.gc.ca/data/air/monitor/national-air-pollution-surveillance-naps-program/Data-Donnees/2019/ContinuousData-DonneesContinu/HourlyData-DonneesHoraires/?lang=en

	Fort McMurray-Patricia McInnes	255	56.75	-111.47	90702	PE
	Janvier	741	55.90	-110.74	none	
	Stony Mountain	673	55.62	-111.17	90808	RB
Upper Athabasca	Carrot Creek	800	53.62	-115.86	91601	RB
	Edson	894	53.59	-116.39	92901	PE
	Hinton	1215	53.42	-117.54	93202	RB
	Steeper	1400	53.13	-117.09	91701	RB
North Saskatchewan	Ardrossan	708	53.55	-113.14	90135	PE
	Breton	900	53.09	-114.46	92601	RB
	Bruderheim	632	53.80	-112.92	90609	PE
	Caroline	1140	51.94	-114.69	91901	RB
	Edmonton Central	663	53.54	-113.49	90130	PE
	Edmonton East	670	53.54	-113.36	90121	PS
	Edmonton South	675	53.50	-113.52	90120	PE
	Edmonton-Woodcroft	670	53.56	-113.56	90133	PE
	Elk Island	714	53.68	-112.86	91101	RB
	Fort Saskatchewan	628	53.69	-113.22	90601	T
	Genesee	772	53.30	-114.22	93101	RB
	Gibbons	673	53.82	-113.32	90607	PE
	Lamont County	767	53.76	-112.88	92201	RB
	Redwater	627	53.95	-113.10	90608	PE
	Sherwood Park	710	53.53	-113.32	90134	T
	St. Albert	681	53.62	-113.61	90136	PE
	St. Lina	679	54.21	-111.50	94401	RB
	Tomahawk	789	53.37	-114.76	91301	RB
	Violet Grove	1000	53.14	-115.13	91401	RB
Red Deer	Red Deer-Lancaster	907	52.24	-113.76	90304	T
	Red Deer-Riverside	858	52.29	-113.79	90302	PE
South Saskatchewan	Airdrie	1090	51.26	-114.03	90250	PE
	Calgary Central-Inglewood	1034	51.03	-114.00	90230	PE
	Calgary Southeast	1032	50.95	-113.96	90229	PE
	Lethbridge	918	49.71	-112.80	90502	PE
	Medicine Hat-Crescent Heights	709	50.04	-110.68	90402	PE

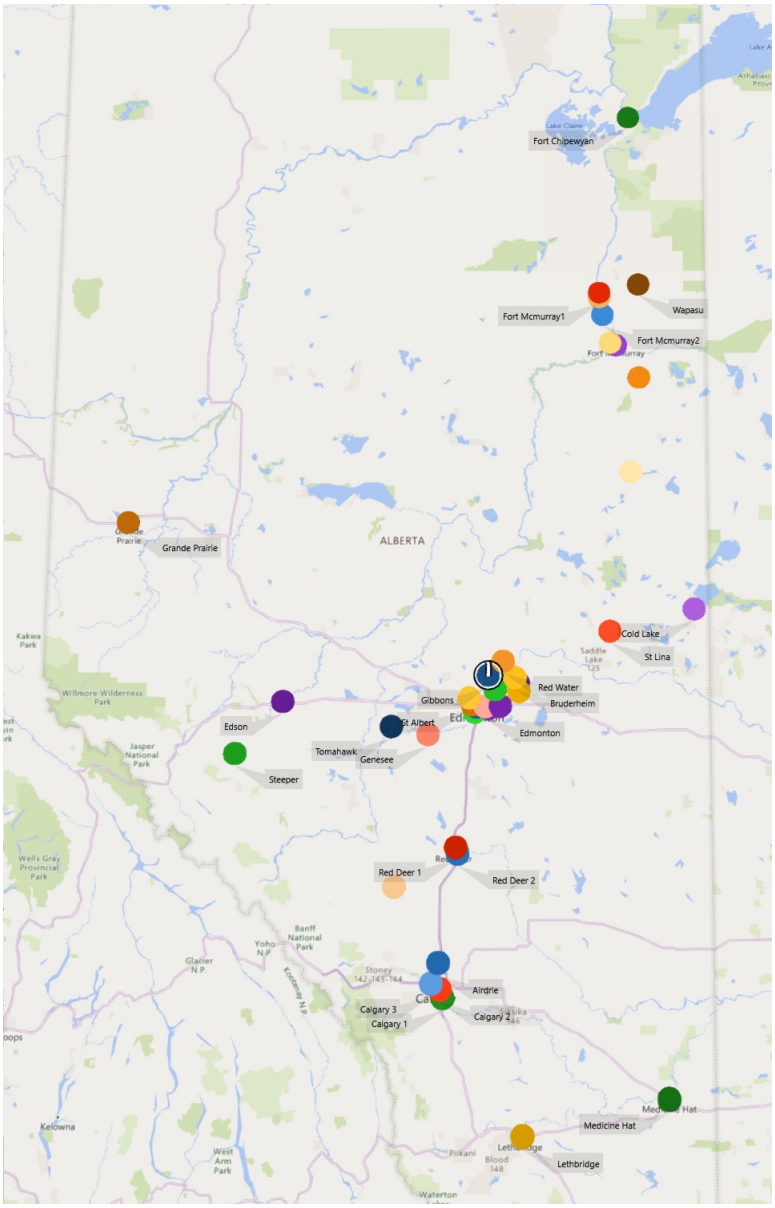

Figure 3.2: 40 Air Quality Monitoring Stations location

3.3 SMOKE

Emission inventory data are vital input of air quality modeling systems since they provide the emission input to the model. To prepare emission data, Sparse Matrix Operator Kernel Emissions (SMOKE) is used which is both flexible and user-friendly. The SMOKE modeling System which is developed by The MCNC Environmental Modeling Center (EMC), is an emission data processing tool [66]. By integrating

high-performance computing methods, SMOKE allows users to prepare specialized emission data for air quality modeling studies. SMOKE converts the available resolution of the emission data to the required resolution needed for the modeling process. Moreover, SMOKE provides a spatiotemporal profile along with a chemical speciation profile for the available set of emission data.

3.4 Community Multiscale Air Quality (CMAQ)

Photochemical models are the principal elements of the air quality modeling process, which simulate the transport and chemical interaction of pollutants in the atmosphere [67]. The photochemical models have been widely employed by governments and decision-makers to address the source of pollution and evaluate the effectiveness of emission control strategies [68]. Furthermore, the photochemical models are employed by academia for a wide range of applications such as understanding the effects of meteorology on air pollution, understanding chemical reactions that happen in the tropospheric layer, and determining the effect of emissions on climate change.

The Community Multiscale Air Quality (CMAQ) is a state-of-the-art photochemical grid model with the capability of analyzing and simulating the behavior of multiple primary and secondary pollutants. CMAQ model developed and maintained by the US. Environment Protection Agency has the capability to simulate the pollutant's behavior on continental, regional, and urban scales. Furthermore, the model's temporal features allow the user to model both short-term events like haze events [69] and long-term phenomena like climate change [70].

CMAQ is a three-dimensional Eulerian grid-based model. Eulerian models employ a fixed coordinate system with respect to the ground. The computational domain is divided into cells where the summation of inflow, outflow, generation, and loss processes are represented by coupled differential equations. The variation of emission within each grid cell could be affected by diffusion and advection in either horizontal or vertical directions, chemical reactions, and deposition or loss processes. These

processes are mathematically related by the continuity equation for concentration in each grid cell as:

$$\frac{\partial C}{\partial t} + \nabla.(\vec{v}C) = D\nabla^2 C + R + E - S \tag{3.5}$$

In eq. (3.5), C represents the concentration, which is a function of location and time, $\vec{v}$ is the velocity vector, and D depicts the molecular diffusion coefficient. Finally, R, E, and S represent rates of concentration change in chemical reactions, rate of emission from sources, and rate of removal processes, respectively. If eq. (3.5) is extended for each specie i, the mass balance of that specie is called Atmospheric Diffusion Equation (ADE) and is represented as:

$$\frac{\partial C_i}{\partial t} + \frac{\partial (uC_i)}{\partial x} + \frac{\partial (vC_i)}{\partial y} + \frac{\partial (wC_i)}{\partial z} = \frac{\partial}{\partial x}\left(K_H \frac{\partial C_i}{\partial x}\right) + \frac{\partial}{\partial y}\left(K_H \frac{\partial C_i}{\partial y}\right) + \frac{\partial}{\partial z}\left(K_Z \frac{\partial C_i}{\partial z}\right) + R_i + E_i - S_i \tag{3.6}$$

where, K_H and K_Z depict the horizontal and vertical turbulent diffusion coefficients respectively. The ADE equation is solved to determine the concentration of chemical species as a function of time and space. The module Chemical Transport Model (CTM), within the modular platform of the CMAQ model, is responsible for solving ADE equations.

To run the CTM module of CMAQ model several input files that include meteorological fields, initial and boundary conditions, and emission inventory files are needed. The Meteorology-Chemistry Interface Processor (MCIP) module of CMAQ reconfigures the WRF output data to provide CMAQ-ready meteorological files. The BCON and ICON modules of CMAQ are used to generate the boundary and initial conditions. Finally, to prepare the emission inventory files SMOKE is utilized. SMOKE provides temporal, spatial, and speciation profiles which are readable for CMAQ model.

3.4.1 Model Configuration

The time history of pollutant concentrations in the atmosphere are affected by many physical and chemical processes. These include advection and diffusion in either horizontal or vertical direction, wet or dry deposition, gas-phase chemistry, aerosol chemistry, and secondary organic aerosol chemistry. CMAQ includes a large library of up-to-date physical and chemical atmospheric processes. Previous Air Quality studies carried out for the whole or part of Alberta provided a basis for setting up the CMAQ model. The following options presented in table 3.4 are chosen for setting up the CMAQ model.

Table 3.4: CMAQ Model Configuration

Science	**Option**	**Description**
Gas-phase Chemistry	cb6r3_ae7_aq	Carbon Bond 6 version r3 with aero7 treatment of Secondary Organic Aerosol
Aerosol Chemistry	Aero6	The 6th generation CMAQ aerosol module which expanded the chemical speciation of PM
Horizontal Advection	piecewise parabolic method (PPM)	This algorithm is based on the finite-volume sub-grid definition of the advected scalar
Horizontal Diffusion	multiscale	horizontal diffusion fluxes for transported pollutants are parameterized using eddy diffusion theory
Vertical Advection	Local_cons	use the layer-by-layer integrated mass-conserving scheme to calculate vertical advection
Vertical Eddy diffusivity	Asymmetrical Convective Model Version 2 (ACM2)	combined local and non-local PBL scheme for consistency of meteorology and chemistry
Deposition	M3Dry	Dry deposition is computed by electrical resistance analogy

The initial and boundary conditions are generated using ICON and BCON modules of CMAQ. The effect of the initial condition (IC) on the model performance is limited to from a few hours to a few days at the start of the simulation. To eliminate the effect of IC, many studies remove a few days of results from the start of the simulation. Here, the first day of each modeling scenario was removed. It is important to choose the correct source for obtaining the base data for boundary condition (BC) as this influences the results. In this study, the northern hemisphere modeling results

of CMAQ, which are available online through CMASCenter, were used. Using a CMAQ model, these data are generated on a monthly and seasonal basis for the whole northern hemisphere on a three-dimensional domain consisting of elements with the size of 108km × 108km [71].

3.4.2 Computational Domain

CMAQ's domain is a sub-domain of the finest WRF computational domain introduced in section 3.1.2. The only modification is that some elements in the horizontal directions are removed from the domain to reduce the effects of the boundary conditions of the meteorological model. The specifications of the domain are presented in table 3.5. Although the domain shown in fig. 3.1, covers some regions in contiguous provinces, the province of Alberta is the primary focus. Since the emission input is for the inside of Alberta, the simulation is only useful for the inside of Alberta. The domain has been chosen slightly larger than the actual Alberta's borderline to reduce the effect of boundary conditions.

Table 3.5: Specification of the CMAQ domain projection and size

Projection	Central Latitude	Central Longitude	1st Sta. Parallel	2nd Sta. Parallel	Ellement # (x*y)	SW of domain	Element Size
Lambert Conformal Conic	49.0	-121.0	30.0	60.0	201*306	-12km, -24km	4km*4km

3.4.3 Model Validation

To use CMAQ results for different emission abatement scenarios, a comprehensive evaluation of the photo-chemical model performance is needed. Model performance evaluation (MPE) is the process of using statistical metrics to quantitatively analyze and compare the model outputs with the observational data. Generally, there are four different MPE approaches for air quality models [72][73] which are:

- **Operational Evaluation**: In this approach, typical observation data, like temperature, wind speed, and pollutant concentration which are normally mea-

sured at monitoring stations, are compared to the modeled data using statistical metrics and graphical tools.

- **Diagnostic Evaluation**: This approach, refers to the evaluation of the interactions and processes involved within the model. In other words, are the correct data resulting from the correct interaction and process? This approach requires extensive oriented field study.

- **Dynamic Evaluation**: This approach is a comprehensive evaluation of the model response to the known emission change or meteorological change. Is the model capable to replicate the effect of the determined changes.

- **Uncertainty Analysis**: In this approach, the level of uncertainties is analyzed and the impact of each uncertainty or source of error on the model prediction is quantified.

The capability of the model to reproduce the actual observation data was the focus of this study, so an operational approach was chosen to evaluate the model performance. This approach, compared to the other methods, is less complex and due to the availability of routine weather data is computationally feasible.

The evaluation of the model to reproduce NO_2 and Ozone concentration was the main focus of this study. In particular, 1-hr averaged NO_2 and 1-hr averaged Ozone were both compared both at ground level, to observations at the monitoring stations (see table 3.3). Since NO_2 and Ozone have different chemistry, different performance metrics were used to evaluate them with the modeling results.

For NO_2, a set of metrics are first proposed by Chang et. al in 2004 [74], for rural areas. Then in 2012, Hanna et, al, [75], modified these metrics and also suggest a set of benchmarks for the urban areas as well. The statistical metrics used in Hanna's study, are:

$$FB = 2\frac{\frac{1}{N}\sum_{i=1}^{N}(P_i - O_i)}{\bar{P} + \bar{O}} \tag{3.7}$$

$$NMSE = \frac{1}{N}\frac{\sum_{i=1}^{N}(P_i - O_i)^2}{\bar{P} * \bar{O}} \tag{3.8}$$

$$NAD = \frac{\frac{1}{N}\sum_{i=1}^{N}|P_i - O_i|}{\bar{P} + \bar{O}} \tag{3.9}$$

$$FAC2 = Fraction\ where\ 0.5 < \frac{P_i}{O_i} < 2 \tag{3.10}$$

These equations are Fractional Bias (FB) in equation 3.7, Normalized Mean-Square Error (NMSE) in equation 3.8, Normalized Absolute Difference (NAD) equation 3.9, and the last one is FAC2 which point to the fraction of data where the ratio of simulation results to the observation data is greater than 0.5 and less than 2 (equation 3.10). In these equations, P_i and O_i depict the modeled concentration and observed concentration respectively. The benchmark data for this set of statistical metrics are shown in table 3.6.

Table 3.6: NO_2 performance benchmark [75]

	$\|FB\|$	NMSE	NAD	FAC2
Rural	≤ 0.30	≤ 3	≤ 0.30	≥ 0.50
Urban	≤ 0.67	≤ 6	≤ 0.50	≥ 0.30

The metrics and criteria for O_3 are different than NO_2. Metrics and performance benchmarks, that were presented by Emery et. al. [76] in 2017, were used. The intention of Emery was to recommend a set of statistical metrics and performance benchmarks for MPE process in different applications.

$$NMB = \frac{\sum(P_i - O_i)}{\sum O_i} * 100 \tag{3.11}$$

$$NME = \frac{\sum|P_i - O_i|}{\sum O_i} * 100 \tag{3.12}$$

$$r = \frac{\sum\left[(P_i - \bar{P}) * (O_i - \bar{O})\right]}{\sqrt{\sum(P_i - \bar{P})^2 * \sum(O_i - \bar{O})^2}} \tag{3.13}$$

Normalized Mean Bias (NMB), Normalized Mean Error (NME), and Correlation Coefficient (r) are the metrics that Emery recommended. Equations 3.11 to 3.13 show how to calculate these metrics with table 3.7 showing the performance benchmark for these metrics.

Table 3.7: O_3 performance benchmark

Parameter	NMB	NME	r
1-hr Averaged O_3	$\leq \pm 15\%$	$\leq 25\%$	≥ 0.50

3.5 Alberta air quality dispersion model Platform

Each module of the air quality dispersion model for Alberta has been individually introduced. How these modules are connected is the subject of this section. These three categories of data are required for running the whole model: (1) Meteorological input data, (2) Hemispheric CMAQ data, and (3) Emission inventory data. Meteorological input data including: terrestrial data, land-use data, and NCEP FNL forecast data, are fed to the WRF model to calculate meteorological fields. At this step, the outputs of the WRF model are verified using observation data. Then, the MCIP module creates a CMAQ-ready meteorological input from WRF outputs.

The Hemispheric CMAQ data are fed to ICON and BCON modules of CMAQ to generate initial and boundary conditions. The third category of input data is emission inventory files. Emission files classified as mobile sources and stationary sources are fed to the SMOKE module. The SMOKE module creates CMAQ-ready emission files that have temporal, spatial, and speciation profiles. For different simulation scenarios, the input of the SMOKE module is changed. Then, the outputs of the modules are fed to the CTM module of the CMAQ model to calculate the hourly concentration profiles over Alberta. Then, to verify the output of the simulation, the concentration values and profiles are compared to the ground-level observation data. A schematic of the simulation modules and how they are connected is shown in fig. 3.3.

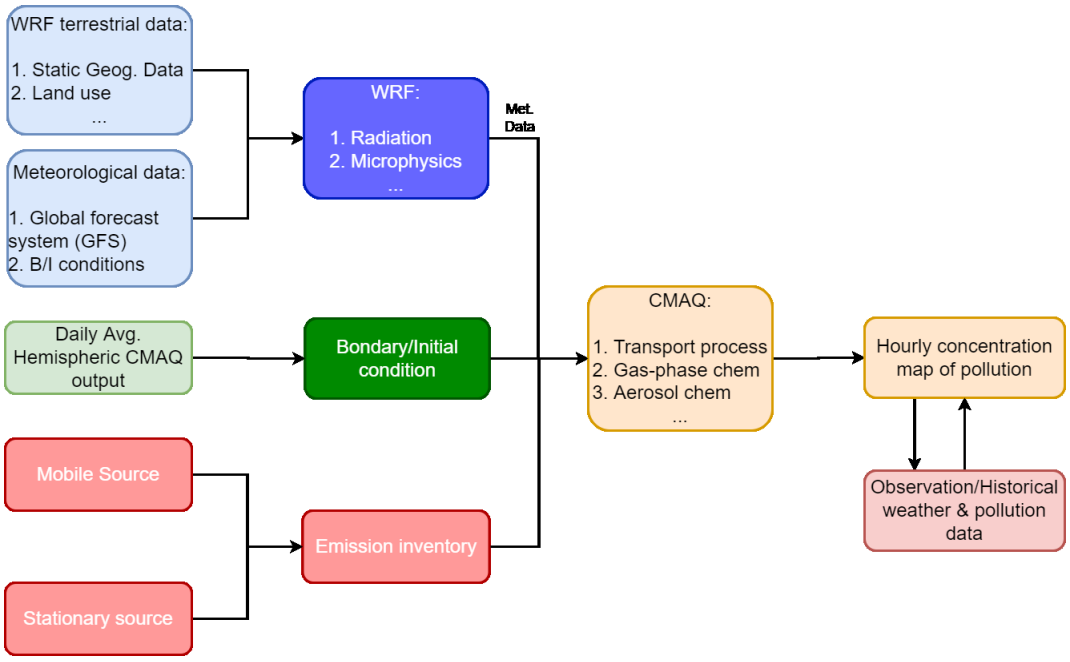

Figure 3.3: Schematic of Integrated Model

3.6 Model Performance and Validation

Next an evaluation process of model performance for both the meteorological model (WRF) and the chemical transport model (CMAQ) is described and a comprehensive analysis of the different modeling scenarios is provided. Table 3.8 provides a description of different scenarios which are evaluated in this section. First, to validate the model, a comparison between the simulation results of base case and observation data from NAPS program monitoring stations was performed to see how well the model can capture the real trend of meteorological field, NO_2 concentration, and O_3 concentration. Then, scenarios to analyze the impact of each Mobile and UOG sector are performed. In particular, the results of the zero-out study and sensitivity analysis to perturbation of the emissions in Mobile and UOG will be presented.

All the simulation results are generated for these two periods: (1) In the warm season (July 15-25, 2019) and (2) In the cold season (January 10-20, 2019). The whole period is used for the base cases, While the remaining emission scenarios were analyzed using only the first 3 days of each period. Then, the AQHI parameter was

calculated to analyze the effects of emission scenarios on the air quality of the two largest cities in Alberta. The results could be useful for decision-makers for evidence-informed policymaking toward future NO_2 compliance with upcoming CAAQS. A summary of the modeling scenarios is given in table 3.8, where Mobile sources and UOG are systematically varied.

Table 3.8: Description of modelling scenarios

Sc. Name.	Description
Base	Considering all emission sources
M1-	Assuming 1% reduction in Mobile emission
M5-	Assuming 5% reduction in Mobile emission
M25-	Assuming 25% reduction in Mobile emission
M50-	Assuming 50% reduction in Mobile emission
M75-	Assuming 75% reduction in Mobile emission
MZ	Eliminating all Mobile sources emission
UOG-1	Assuming 1% reduction in UOG emission
UOG-5	Assuming 5% reduction in UOG emission
UOG-25	Assuming 25% reduction in UOG emission
UOG-50	Assuming 50% reduction in UOG emission
UOG-75	Assuming 75% reduction in UOG emission
UOGZ	Eliminating all UOG sources emission

3.7 Validation for the Base Case Scenario

Prior to analyzing different scenarios, it is necessary to evaluate the capability of the model to reproduce the real trend of ground-level meteorological fields and emission concentration profiles. To achieve this goal, an operational evaluation of the model results was performed. Statistical metrics, recommended by the US EPA[3] including Mean Bias (MB), Mean Error (ME), Root Mean Square Error (RMSE), and Index of Agreement (IOA), were used to examine the correlation between modeling results and observation. In addition to these metrics, which are extensively used in air

[3]More details are available in sections 3.1.3 and 3.4.3

quality model evaluation studies [72], some other metrics like FB, NMBE, FAC2, and NAD are also analyzed. These former metrics are presented by Hanna et. al.[75] as acceptance criteria to evaluate model agreement with observation data for NO_2.

Table 3.9: Selected monitoring stations specifications

County	Station Name	Latitude	Longitude	Site Type
Peace	Beaverlodge	55.196	-119.397	RB
	Grande Prairie-Henry Pirker	55.177	-118.808	PE
Lower Athabasca	Conklin	55.632	-111.079	
	Fort McMurray-Athabasca Valley	56.733	-111.390	PE
Upper Athabasca	Carrot Creek	53.621	-115.869	RB
	Edson	53.594	-116.396	PE
	Steeper	53.133	-117.091	RB
North Saskatchewan	Ardrossan	53.555	-113.145	PE
	Edmonton East	53.548	-113.368	PS
	Fort Saskatchewan	53.699	-113.223	T
	St. Lina	54.217	-111.503	RB
	Violet Grove	53.142	-115.138	RB
Red Deer	Red Deer-Riverside	52.299	-113.794	PE
South Saskatchewan	Airdrie	51.268	-114.038	PE
	Calgary Central-Inglewood	51.031	-114.009	PE
	Lethbridge	49.716	-112.801	PE

To compares simulation results against ground-level observation, the latter data has been collected from monitoring stations that are part of the National Air Pollution Surveillance (NAPS) program. Generally, 40 NAPS stations are located within Alberta. Considering the model performance and stations' geographical distribution, 16 stations were chosen to analyze the model results. Selected stations are chosen in a way that they provide good geographical coverage and also an insight into the model results over the whole province. Table 3.9 provides a detailed specification of these stations, including geographic information and station categorizations. Furthermore, fig. 3.4 shows how these stations are distributed over the Alberta province.

To validate the simulation results and compares them with observation data, some important limitations should be considered. These limitations could be a source of inconsistency between the simulation and observation. As mentioned in section 3.1.2, the computational domain consists of 4km*4km cells. The value of each cell rep-

resents the volume-averaged ensemble mean concentration for three-dimensional regions. However, the observation data at each station is a point measurement that only reflects the small area around the station. This problem which is called "incommensurability" or "change of support"[77], could be one of the main reasons for the inconsistency of the modeling results and observation data, especially for the wind speed. Another limitation is that the observation data itself contains measurement errors while the source of error for modeling results is different. The model errors and limitations could be due to inadequacies of input data or due to inaccuracy of the chemical models which represent the atmospheric process[72].

3.7.1 WRF Meteorological Model Validation

Meteorological fields are one of the most important inputs of the air quality dispersion models, and their level of accuracy highly affects the performance of the air quality model. In order to validate WRF results, the temporal variation of 1-hr average temperature at 2m altitude, and wind speed at 10m altitude, were compared against

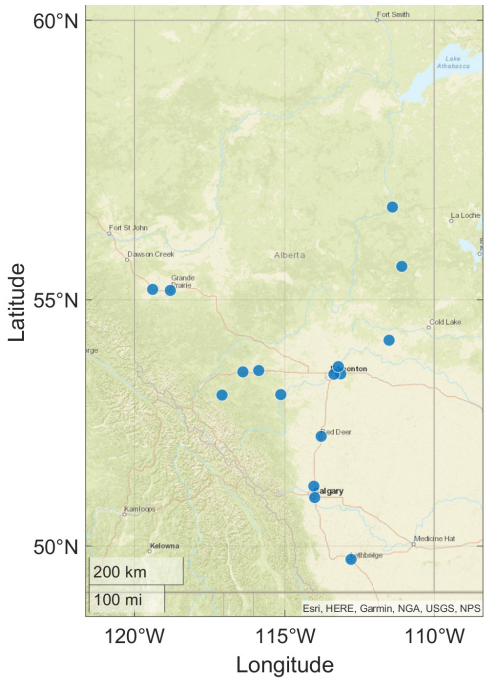

Figure 3.4: Location of selected monitoring stations

ground-level observation. The reliability of mentioned parameters was assessed using the performance benchmark presented by Bowden et. al. 2015 [61]. The Index of Agreement (IOA) criteria, which was proposed by Emery et. al. 2001, is also calculated [59].

The wind speed simulation results at 10m altitude were compared with the observation since the standard elevation for a wind speed detector at monitoring stations is 10-m above the ground [78]. However, this height might be changed depending on each station's surrounding area. The important point to consider is that the wind speed varies significantly with the change of elevation within the planetary boundary layer [79]. The sensitivity of the wind speed on the elevation could affect the level of agreement between the modeling results and observation and lead to a bias.

The result of the statistical comparison between WRF output (meteorological parameters) and ground-level observation data are presented in table 3.10. In this table MB, ME, RMSE, and IOA are calculated based on hourly averaged data for the whole period of the 10-day simulation in both July and January 2019. For the July period, the simulation results show a slight underestimation of temperature. Nevertheless, almost all the mean bias, mean error, and IOA values are within the benchmark recommendations. In contrast, positive mean bias values for wind speed show a slight overestimation. As Huang et. al. mentioned in their work, the positive bias of wind speed has also been seen in earlier WRF versions [80]. Among all stations, Fort Chipewyan and Elk Island have the highest bias. The reason could be the proximity of these stations to the open water [81], Lake Athabasca, and Astotin Lake. Using a more detailed land-use model which provides a better resolution of water surfaces could improve the modeling results on these stations. In the July period, overall the average of metrics of the monitoring stations meet the benchmark criteria for both temperature and wind speed. The overall results are listed as the average values at the end of table 3.10.

Table 3.10: Comparison of meteorological parameters

Station Name	July						January					
	Temperature(°C)			Wind Speed(m/s)			Temperature(°C)			Wind Speed(m/s)		
Metrics	MB	ME	IOA	MB	RMSE	IOA	MB	ME	IOA	MB	RMSE	IOA
Criteria	$\leq \pm 1$	≤ 3	$0.8 \leq$	$\leq \pm 1$	≤ 3	$0.6 \leq$	$\leq \pm 1$	$\leq \pm 3$	$0.8 \leq$	$\leq \pm 1$	≤ 3	$0.6 \leq$
BEVE	-0.63	1.64	0.94	0.99	1.97	0.75	**-5.62**	**5.88**	0.82	1.47	3.31	**0.18**
GPHP	-1.51	1.89	0.94	1.77	2.34	0.69	-3.62	5.13	0.82	**3.38**	**4.18**	**0.23**
ANZA	-0.66	2.06	0.93	0.47	1.38	0.55	-4.45	6.17	0.84	1.14	1.94	0.59
CLSO	-1.61	2.27	0.89	1.86	2.55	0.37	-3.87	5.69	0.84	2.55	3.22	0.32
CONK	-0.26	2.24	0.92	1.46	2.05	0.37	-3.38	5.84	0.88	0.65	1.77	0.46
FOCH	**-8.87**	**8.87**	**0.48**	-0.73	2.32	0.72	-1.27	4.23	0.83	1.91	2.92	0.55
FMBG	-0.68	2.16	0.93	0.09	1.33	0.69	-4.53	5.69	0.87	0.59	1.59	0.46
FMSO	-0.34	2.20	0.94	0.30	1.47	0.65	-4.10	5.39	0.87	0.71	1.84	0.48
FMAV	-0.93	2.38	0.92	0.52	1.27	0.67	-4.23	5.86	0.86	0.61	1.73	0.65
FMPM	-0.96	2.16	0.92	0.38	1.31	0.68	-4.90	6.11	0.85	0.66	1.78	0.66
JANV	-0.83	2.03	0.93	1.29	1.71	0.40	-4.17	6.22	0.87	0.93	1.73	0.49
STMO	-0.88	1.98	0.92	1.53	1.98	0.36	**-5.09**	**7.20**	0.81	0.29	1.50	0.66
CACR	-1.23	1.91	0.89	1.13	1.81	0.78	-2.65	5.77	0.79	1.09	1.86	0.53
EDSO	-1.84	2.52	0.88	1.25	2.18	0.46	-3.25	5.66	0.81	1.07	1.93	0.39
HINT	-0.68	2.07	0.93	**2.36**	**2.96**	**0.25**	-1.84	5.33	0.84	**2.98**	**3.60**	**0.17**
STEP	-1.62	2.46	0.89	1.95	2.79	0.44	**-5.85**	**6.18**	0.84	1.24	**3.46**	**0.17**
ARDR	-1.63	2.19	0.90	1.92	2.76	0.60	-1.78	5.23	0.82	2.46	3.07	0.47
BRET	-1.34	2.27	0.90	1.81	2.82	0.54	-2.09	5.22	0.81	**2.49**	**3.14**	**0.24**
CARO	-1.92	3.00	0.85	1.02	2.39	0.46	-4.12	5.22	0.88	0.93	2.25	0.41
EDEA	-1.14	2.21	0.90	1.01	2.21	0.70	-3.37	5.00	0.82	0.71	1.51	0.42
ESOU	-0.19	1.65	0.93	1.74	2.62	0.55	-3.69	5.29	0.77	0.59	1.29	0.58
ELIS	**-3.94**	**4.07**	**0.75**	**3.12**	**3.87**	**0.23**	-1.06	5.51	0.81	2.37	2.90	0.67
FSAS	-1.69	2.17	0.90	1.41	2.34	0.65	**-3.81**	**6.11**	**0.71**	1.10	1.95	0.54
GENE	-1.50	2.10	0.92	0.62	2.33	0.71	-3.48	5.74	0.77	1.39	2.44	0.49
GIBB	-1.93	2.30	0.90	**2.47**	**3.01**	**0.53**	-2.19	**6.29**	0.76	2.27	3.02	**0.36**
LACO	-1.20	2.09	0.91	0.92	2.35	0.61	-2.46	5.05	0.86	0.92	2.32	0.60
REDW	-1.39	2.07	0.91	1.57	2.43	0.65	-2.15	5.83	0.78	1.53	2.28	0.60
SHEP	-0.68	1.83	0.92	1.86	2.57	0.59	-2.50	4.67	0.86	1.42	1.95	0.47
STAL	-0.25	1.41	0.95	0.82	2.00	0.73	-2.67	5.16	0.81	1.05	1.77	0.34
STLI	-1.67	2.36	0.87	1.38	2.47	0.52	-2.89	5.67	0.83	1.42	2.44	0.53
TOMA	-0.83	1.98	0.93	0.74	2.32	0.69	-2.95	5.11	0.81	0.90	1.76	0.67
VIGO	-0.14	2.12	0.89	0.83	2.14	0.70	-3.36	4.91	0.87	1.31	2.15	0.42
RDLA	-1.87	2.81	0.87	1.56	2.47	0.54	-1.51	4.36	0.82	2.15	2.69	0.48
RDRI	-1.62	2.60	0.88	2.10	2.80	0.54	-0.74	4.80	0.77	2.48	3.04	0.32
AIRD	-1.61	2.44	0.90	0.94	2.60	0.55	-3.56	4.44	0.90	1.48	2.65	0.69
CACE	-0.58	2.07	0.91	1.37	2.34	0.64	**n/a**	**n/a**	**n/a**	0.75	1.51	0.43
CASE	-1.69	2.58	0.89	1.14	2.33	0.62	**n/a**	**n/a**	**n/a**	1.07	1.90	0.35
LETH	-1.44	2.15	0.93	1.47	2.49	0.72	-3.15	3.98	0.90	0.96	1.79	0.62
MHCH	-1.04	2.47	0.92	0.79	1.98	0.73	1.15	4.32	0.83	0.73	2.25	0.46
Average	**-1.4**	**2.4**	**0.9**	**1.3**	**2.3**	**0.6**	**-3.1**	**5.4**	**0.8**	**1.4**	**2.3**	**0.5**

The WRF simulation results for the January period compared to the July period are poorer. For January, MB is 3.1 °C and ME is 5.4 °C for temperature, which is higher than the benchmark criteria. Nevertheless, the IOA of temperature satisfies the benchmark recommendation, which shows that the model in January could capture the temporal variation of temperature. However, there are negative biases in modeling results compared to the actual values of temperature. The reason could

be the overprediction of surface albedo by the WRF model which results in the underestimation of actual values of temperature near surfaces [82]. In contrast, wind speed simulation results did satisfy the MB=1.4 and RSME=2.3 criteria with some overestimation but the value of IOA=0.5 is slightly lower than the benchmark. In summary, the model successfully replicates the meteorological fields for both summer and winter simulation periods.

To further understand the strong correlation between modeling results and observation data, time series, box plots, and scatter plots were provided for the temperature at the selected stations, listed in table 3.9. To visually compare how well the model can capture the temporal variation of temperature, the time series of modeled results and observed data are presented in fig. 3.5. From these figures, it is apparent that the modeled temperature in the July period has accurately captured both the observed trend and actual values with minor under-prediction of maximums and slight overprediction of minimums. However, for the January period, the simulations and measurements have larger discrepancies. The model did replicate the trend of temperature variations in January, but the actual values are underestimated (see fig. 3.5b). This is attributed to the overestimation of the WRF model for surface albedo in snow-covered surfaces. Unfortunately, the observation data for the January period was not available for the Calgary Central-Inglewood monitoring station. In the July period, temperature varies between 10°C and 30°C at most stations, while in the January period, a minimum of -35°C to a maximum of 10°C was reported at the monitoring stations. A noticeable diurnal change in temperature creates a sinusoidal pattern in July, while in the January period, these changes are less pronounced due to the winter in Alberta.

The model's capability to reproduce the diurnal variation of temperature observed at monitoring stations is evaluated using Box-plots. The agreement between the interquartile range of simulation results and observation data is plotted in fig. 3.6. Where a comparison between the observed data and simulated 2m-temperature is

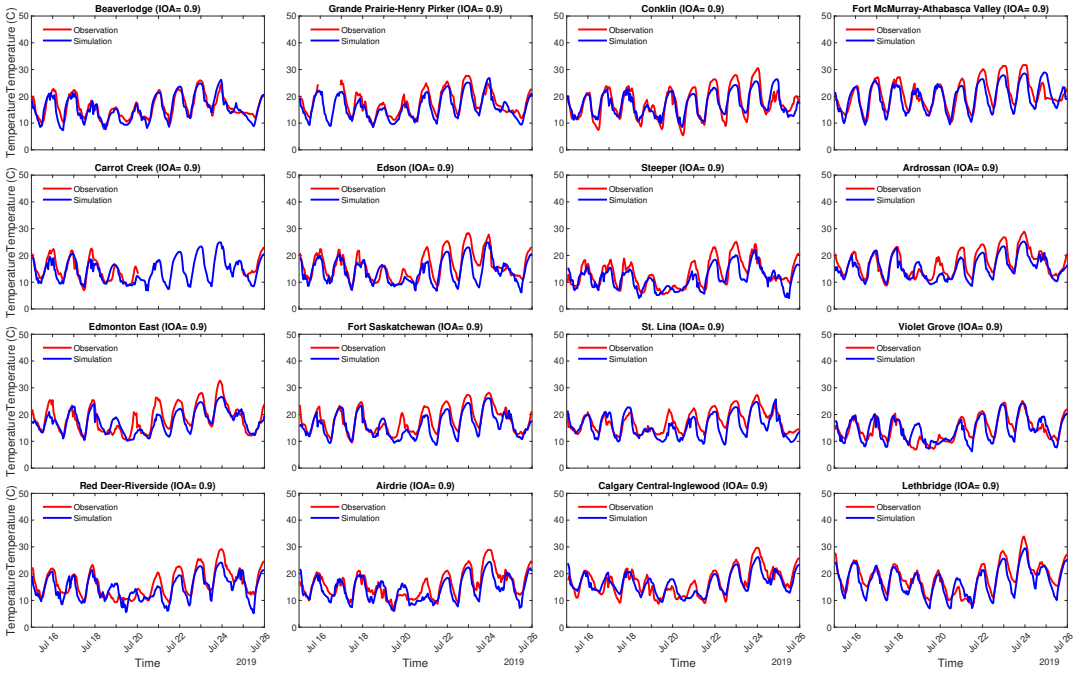

(a) July

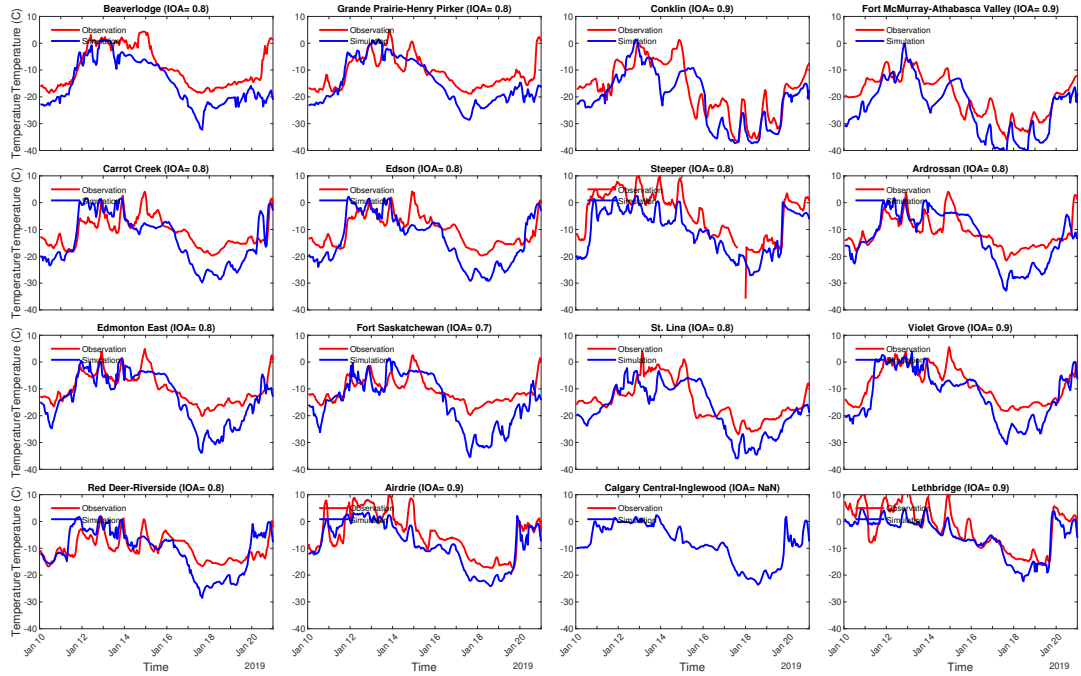

(b) Jan

Figure 3.5: Model Validation: Ground level temperatures model vs experimental. Hourly time series of observed (red line) and modeled (blue) temperature (°C) at selected monitoring stations in July period (a) and January period.

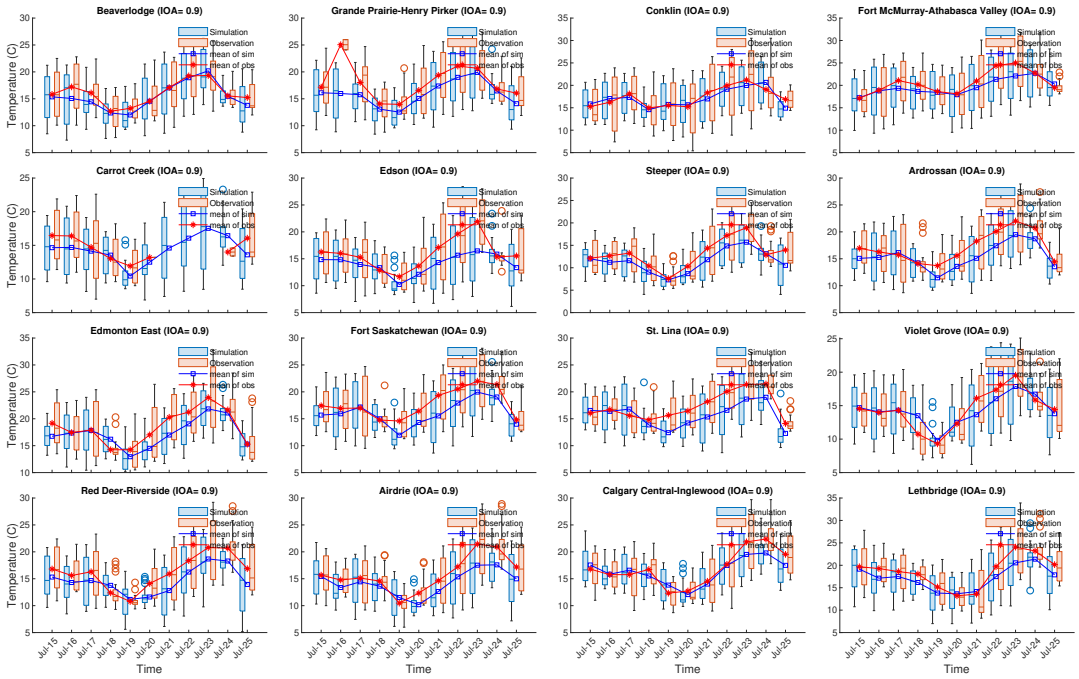

(a) July

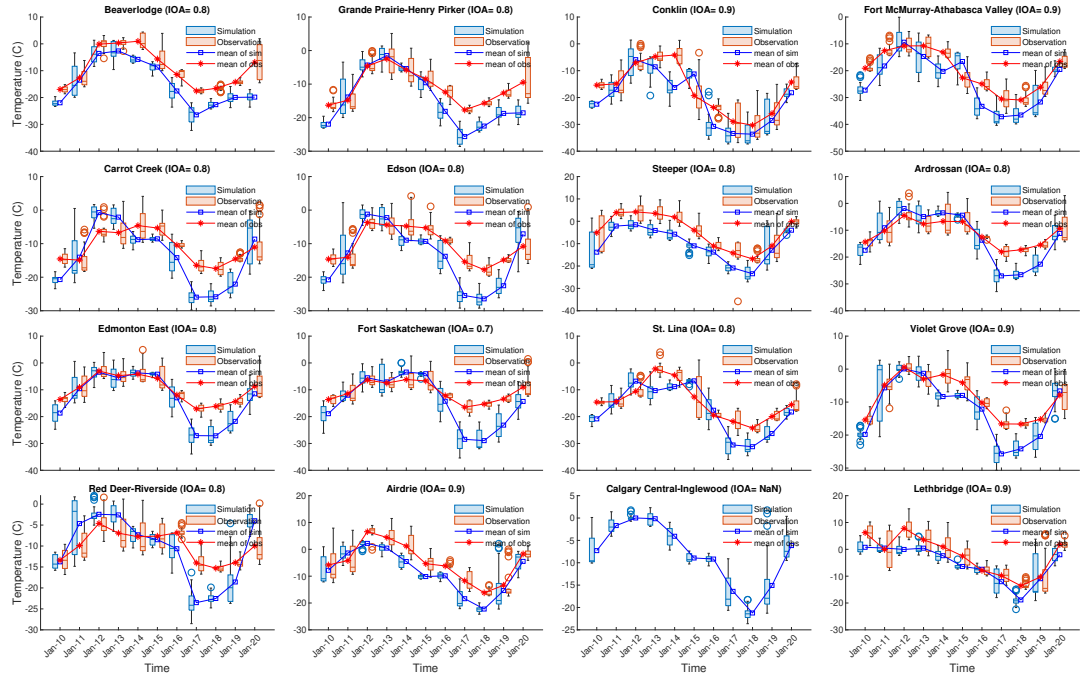

(b) Jan

Figure 3.6: Boxplot to show diurnal temperature variation at selected stations and compare the simulation results (Blue) with observation data (red). The lines show the mean value of the respective colors. The edge of the boxes shows the 25th and 75th percentiles. The circle points show outrange data.

shown for each modeling day. The boxes represent the range of 25th to 75th percentiles of 1-hr averaged temperature. This shows that the daily temperature variation in July is much higher than that for the January period as described in fig. 3.5. The model captures this variation for each day with sufficient accuracy. However, there are some minor underestimations in the modeling results and particularly in the January period the underestimation is higher compared to the July period.

To further understand the level of underestimation or overestimation of simulation results for 2-m temperature, the hourly modeling results versus observation are shown in fig. 3.7 for the selected stations. Each data point shows the averaged 2m modeled temperature on the y-axis and its corresponding observation value on the x-axis. The majority of the data points in these plots are either located near the unity line of slope one (simulation=observation) or within the $\pm 20\%$ of this unity line. Fig. 3.7 shows that, despite the overestimation and underestimation mentioned earlier, the cloud of points is around the unity line for all the stations which is another way to visualize the model's capability to successfully replicate the temperature measurement data.

So far the performance of the meteorological model (WRF) has been analyzed at monitoring stations and has been evaluated by the benchmark metrics. The model results have a strong correlation with observation data at monitoring stations. To evaluate how the model performs over the whole of Alberta, Bubble geographic maps are presented in fig. 3.8. This plot compares the IOA for all 40 monitoring stations introduced in section 3.2 for the two simulation periods in January and July 2019. Each bubble represents a station and its size indicates the IOA level. Generally, the stations over the whole of Alberta have high IOA for temperature (except the northeast at Fort Chipewyan station. The poor performance of the model at this location could be a local effect of the open water, i.e. Lake Athabasca. As mentioned earlier the meteorological statistics for Fort Chipewyan are lower than that for other stations). Considering Bubble maps for wind speed, overall the model has approximately the same performance over the whole province with a tendency for a better

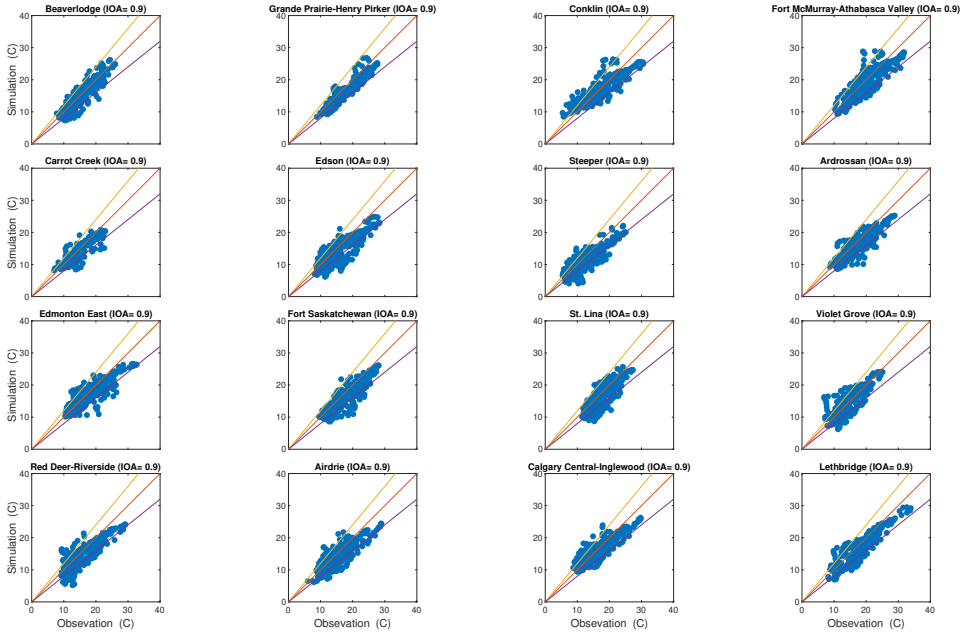

(a) July

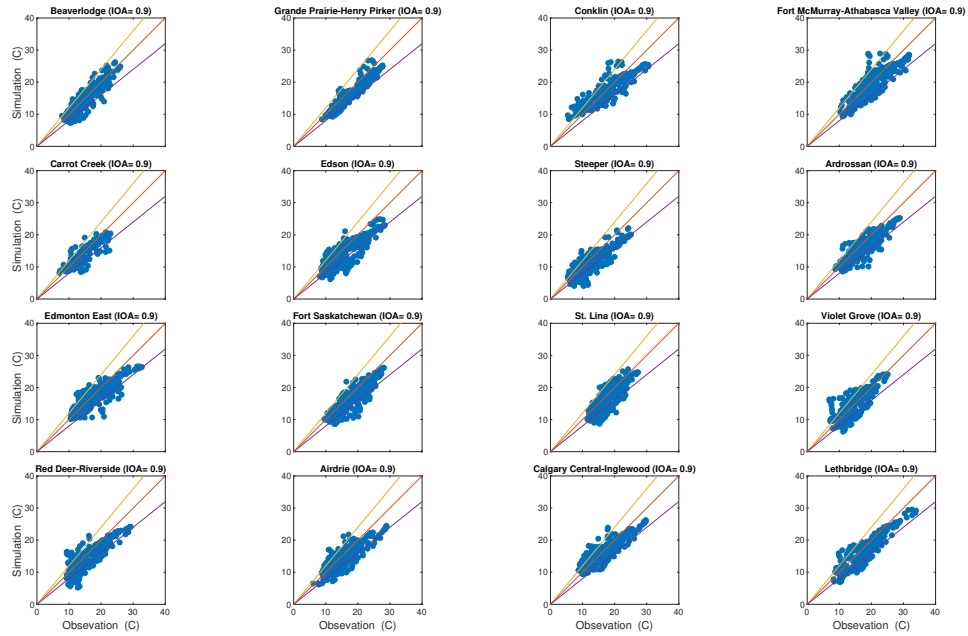

(b) Jan

Figure 3.7: Scatter plot comparing simulated temperature with observation. The red line shows the identity line (simulation=observation). The yellow and purple lines show ±20% of the line of equality.

performance near the central regions of the province and major cities. The slightly poorer performance of the model at the southwest of the domain could be linked to

the effects of the Rocky Mountains topography.

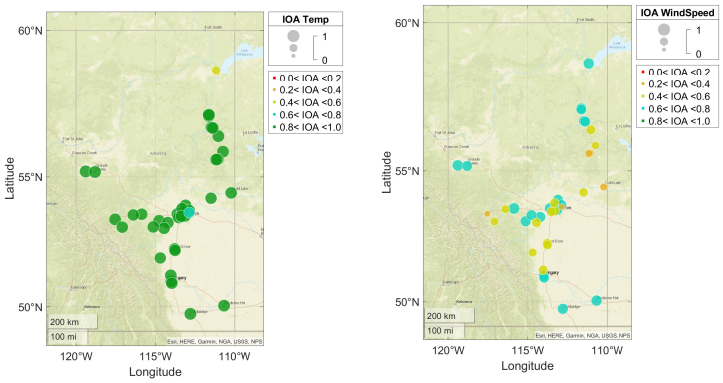

(a) July

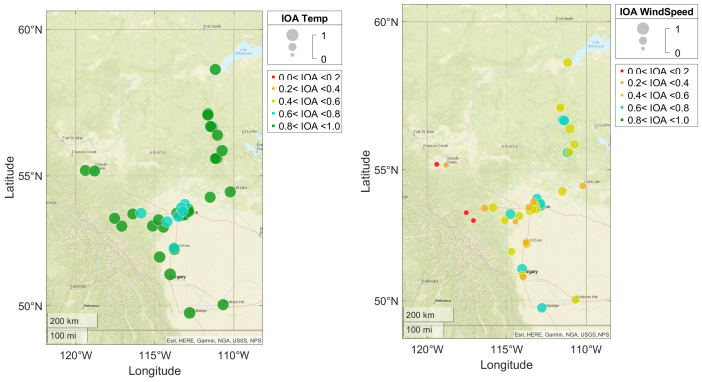

(b) Jan

Figure 3.8: Model Validation: Bubble geographic map indicates the IOA level of each monitoring station. First row(a) shows the averaged IOA in January, second row shows averaged IOA in July. Left, middle and right columns represent IOA for temperature, wind speed and wind direction respectively.

Next, a color map of temperature over the whole province for the July and January periods is shown in fig. 3.9. The average temperature over the whole monitoring region is 16.2°C and -14.7°C for the July and January period respectively. The Rocky Mountain topography in the southwest of Alberta affected the average temperature considerably. In this region, the July period is cooler with an average near 7 (°C) and the average temperature for January temperature is near -15 (°C). In contrast to the Rocky Mountains, the northeast of Alberta which is topographically a flat region experienced warmer July, and colder January with an average temperature

of around 22 (°C) and -30 (°C) respectively. The 2m temperature is also highly affected by the open water. For example, the boundaries of Athabasca Lake at the northeast of Alberta or Lesser Slave Lake at the center of Alberta are apparent in fig. 3.9. Focusing on major cities, i.e. Edmonton and Calgary, the average modeling temperatures for the simulation period in July are -17 and -16 respectively. These values for the January period are -13 and -8 for Edmonton and Calgary.

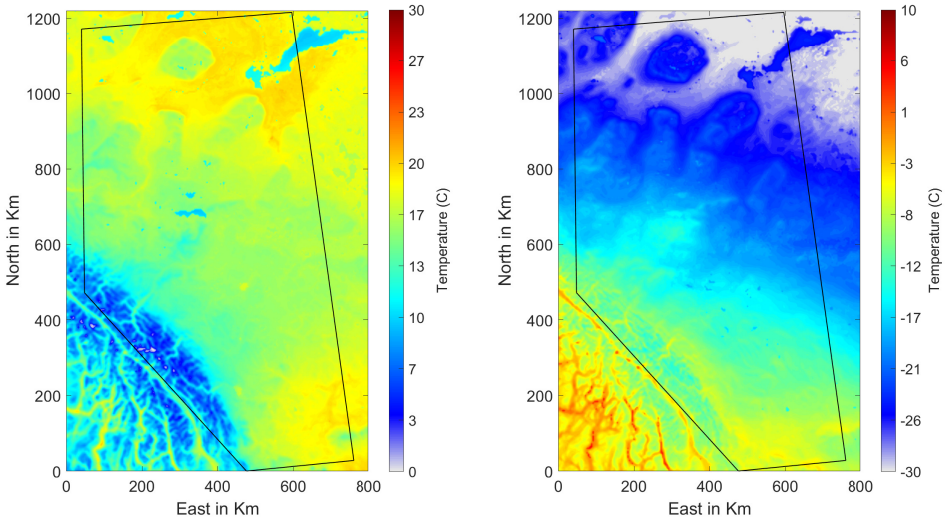

(a) July (b) Jan

Figure 3.9: Averaged Temperature over the simulation period.

3.7.2 Chemical Transport Model Validation

The results of the evaluation of the CMAQ model are presented to assess the chemical transport model. The purpose of this evaluation is to see how well the simulation results replicate the real values and trends of observation [72]. Statistical metrics from eqs. (3.7) to (3.10) and performance benchmarks from tables 3.6 and 3.7, are calculated at monitoring stations to examine the CMAQ model performance for capturing 1-hr average Ozone and 1-hr average NO_2 emission concentration. First, NO_2 validation results are presented, and then Ozone.

3.7.2.1 Nitrogen Dioxide: Validation

To judge the model performance for capturing NO_2 concentration, benchmark metrics and criteria, presented by Hanna et. al. 2012[75], were employed. Fractional bias (FB) eq. (3.7), Normalised mean square error (NMSE) eq. (3.8), Normalised absolute difference (NAD) eq. (3.9), and Fraction of prediction that are within a factor two of observation (FAC2) eq. (3.10) are the metrics to evaluate NO_2 performance. The benchmark values of these metrics are presented in table 3.6. The simulation is able to capture the hourly NO_2 concentration with acceptable accuracy according to the metrics in table 3.6. The overall average of metrics for all monitoring stations is within the acceptance range. Considering the metrics values for each station individually, for Fort Chipewyan the metrics values did not meet the criteria. One reason could be the deficiency of the WRF model to reproduce meteorological fields like the temperature at this station. Two other stations at Fort McKay show poor agreement with the criteria. This is attributed to the proximity of these stations to the emission sources, especially Kearl Oil Sands. Perhaps improving the emission inventory near this region could improve model outputs. Airdrie station also did not meet the criteria for NMSE metric. An unusual trend of observation data at this station, which is shown in fig. 3.10, is a possible reason.

Table 3.11: CMAQ model performance statistics for Nitrogen Dioxide

Station Name	**July**					**Jan**				
	FB	**NMSE**	**NAD**	**FAC2**	**IOA**	**FB**	**NMSE**	**NAD**	**FAC2**	**IOA**
Criteria	**$\leq$ 0.67**	**$\leq$ 6**	**$\leq$ 0.5**	**0.3 $\leq$**		**$\leq$ 0.67**	**$\leq$ 6**	**$\leq$ 0.5**	0.3 $\leq$	
BEVE	-0.16	0.71	0.31	0.49	0.65	-0.28	1.70	0.42	0.43	0.49
GPHP	0.13	0.84	0.29	0.65	0.55	-0.29	1.42	0.41	0.48	0.58
ANZA	0.01	2.64	0.48	0.35	0.38	0.03	1.89	0.44	0.40	0.35
CLSO	0.25	2.47	0.45	0.54	**0.23**	-0.13	1.49	0.38	0.52	0.52
CONK	-0.10	0.93	0.37	0.41	0.48	-0.03	0.61	0.27	0.70	0.48
FOCH	**-0.63**	**9.32**	**0.78**	**0.02**	0.41	-0.44	4.72	**0.63**	**0.11**	0.46
FMBG	**-0.61**	**11.43**	**0.78**	**0.10**	0.42	-0.45	2.92	**0.61**	**0.17**	0.43
FMSO	-0.48	5.75	**0.69**	**0.14**	0.43	-0.37	2.03	**0.55**	**0.23**	0.41
FMAV	-0.16	1.11	0.34	0.55	0.48	-0.21	0.88	0.35	0.46	0.49

FMPM	-0.33	2.55	0.51	**0.21**	0.56	-0.22	1.13	0.36	0.58	0.50
JANV	-0.13	1.02	0.39	0.38	0.44	-0.14	1.20	0.35	0.54	0.40
STMO	0.01	0.83	0.34	0.48	0.58	-0.02	0.54	0.27	0.70	0.50
CACR	-0.13	0.66	0.31	0.48	0.67	-0.18	0.86	0.33	0.57	0.50
EDSO	-0.09	0.98	0.35	0.49	0.56	-0.20	0.76	0.32	0.61	0.53
HINT	0.07	0.87	0.34	0.55	0.40	-0.21	0.77	0.33	0.55	0.49
STEP	-0.35	2.52	0.54	**0.16**	0.48	-0.12	0.56	0.26	0.45	0.87
ARDR	0.10	1.55	0.41	0.37	0.51	-0.24	1.34	0.37	0.57	0.68
BRET	-0.31	1.40	0.48	**0.22**	**0.25**	0.03	1.53	0.45	0.44	**0.25**
BRUD	0.17	1.86	0.40	0.45	0.47	-0.26	2.24	0.43	0.56	0.53
CARO	0.25	1.68	0.41	0.50	0.35	0.32	1.99	0.48	0.34	**0.30**
EDCE	0.23	0.86	0.34	0.58	0.48	0.00	0.14	0.14	0.92	0.67
EDEA	0.31	1.33	0.43	0.35	0.49	0.06	0.33	0.23	0.60	0.69
ESOU	0.45	1.84	0.48	**0.23**	0.40	0.13	0.31	0.23	0.67	0.61
EDWO	0.28	1.19	0.39	0.47	0.52	0.06	0.28	0.22	0.68	0.57
ELIS	0.10	2.13	0.42	0.39	0.44	-0.17	2.61	0.44	0.57	0.41
FSAS	0.30	2.93	0.50	0.38	0.30	-0.09	0.76	0.31	0.63	0.66
GENE	-0.30	1.69	0.48	0.34	0.35	0.03	1.47	0.44	0.45	**0.32**
GIBB	0.09	1.62	0.36	0.48	0.61	-0.20	1.38	0.41	0.48	0.56
LACO	0.28	3.07	0.47	0.48	0.33	-0.05	1.60	0.38	0.54	0.63
REDW	0.30	2.61	0.48	0.46	0.37	0.03	1.10	0.38	0.40	0.54
SHEP	0.34	1.62	0.44	0.37	0.42	0.07	0.40	0.24	0.66	0.72
STAL	0.29	1.50	0.40	0.41	0.57	0.04	0.54	0.30	0.50	0.54
STLI	-0.19	0.79	0.36	0.39	0.63	-0.08	0.98	0.32	0.63	0.53
TOMA	-0.14	1.29	0.39	0.42	0.54	-0.08	1.16	0.41	0.46	0.34
VIGO	-0.21	1.36	0.43	0.37	0.52	-0.13	0.94	0.36	0.54	0.38
RDLA	0.14	1.47	0.34	0.67	0.37	-0.20	1.15	0.40	0.48	0.55
RDRI	0.07	1.35	0.37	0.48	0.46	-0.20	0.86	0.36	0.51	0.58
AIRD	-0.26	**8.42**	**0.56**	0.44	0.40	0.24	1.93	0.46	0.47	0.34
CACE	0.22	0.98	0.34	0.56	0.54	0.05	0.33	0.23	0.71	0.56
CASE	0.26	1.44	0.39	0.47	0.45	-0.03	0.45	0.25	0.70	0.49
LETH	0.26	2.04	0.42	0.43	0.51	0.09	0.86	0.35	0.55	0.52
MHCH	0.18	1.17	0.34	0.59	0.43	0.04	1.08	0.37	0.58	**0.27**
Average	**0.23**	**2.23**	**0.43**	**0.41**	**0.46**	**0.14**	**1.22**	**0.36**	**0.53**	**0.51**

The time series of NO_2 concentration in fig. 3.10, reveals that the simulation shows a good performance for capturing the NO_2 trend at selected monitoring stations. Most of the monitoring stations in the July period did not experience NO_2 concentration greater than 20 ppb with a total average of less than 10 ppb. The model captures this trend well with only minor overprediction in the middle of the day and during rush hour. This could be related to the temporal profile and overprediction of emission

sources nearby the monitoring stations. Among all monitoring stations, the major differences between observed and modeled data can be seen at Airdrie station. During the modeling period, this station experienced two episodes of high NO_2 concentration, one between July 17-19 and one on July 21. Historical weather data show that there were thunderstorms during that period. While thunderstorms could affect the ambient NO_2 concentration, their uncertainty affects the model results due to the inability of the current 4km×4km grid to accurately resolve these meteorological events. The observation data shows an unusual NO_2 concentration over 60 ppb which might be an error of the measuring equipment during the thunderstorm. In January, the differences between the simulation and measurement data are larger. Almost all stations experienced a higher level of NO_2 concentration. In the January period, the average NO_2 concentration for most of the stations is equal to or greater than 10 ppb. Some of the stations show a maximum of 55 ppb for the January period which is almost three times higher than that value for the July period. For some stations like Fort Saskatchewan and Steeper, the IOA changed considerably, when comparing the July and January results. In January, in contrast to July, most of the stations underpredict NO_2 peaks. For model validation of NO_2 concentration, the "incommensurability" problem and the quality of the emission inventory must be considered.

Box plots shown in fig. 3.11 compare the daily variation of modeled and observed NO_2 concentration at selected monitoring stations. Each box shows the interquartile range of data for one calendar day. While the lines connect the mean value of each calendar day in the simulation periods. In the July period, modeled results compared to the observation, show a larger variation on each day. The mean values show a good agreement between the simulation and observation. However, there is a deviation between the median value of simulation and observation for each day. This trend also exists in the January period. Some deviations in modeled results are apparent. Nevertheless, the model has captured the diurnal variation and also the daily trend

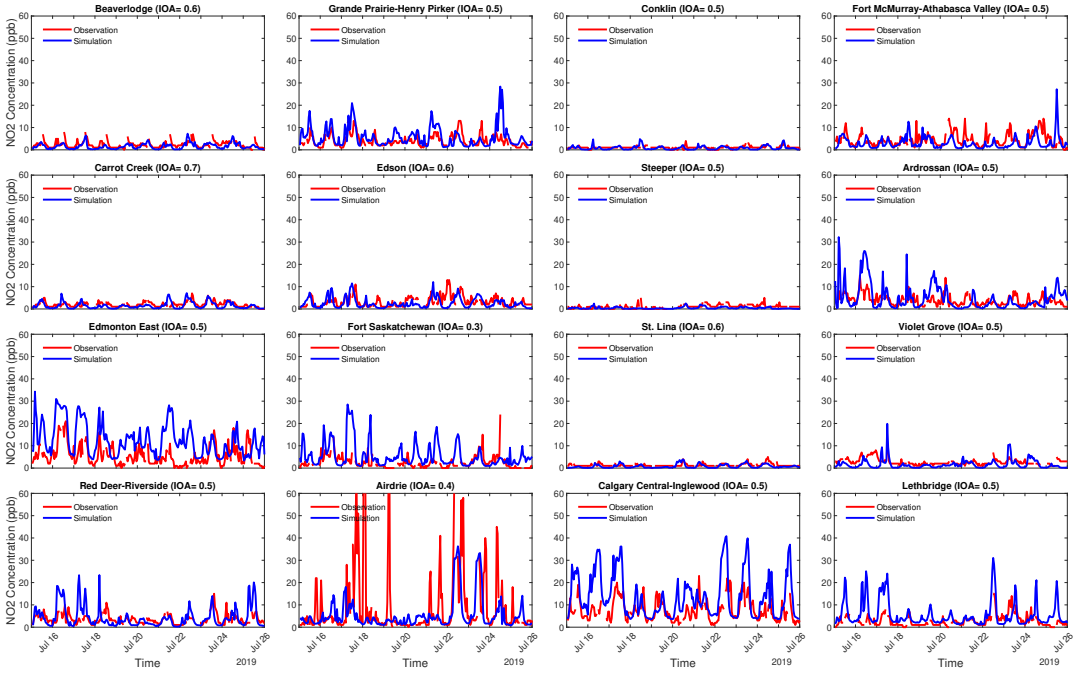

(a) July

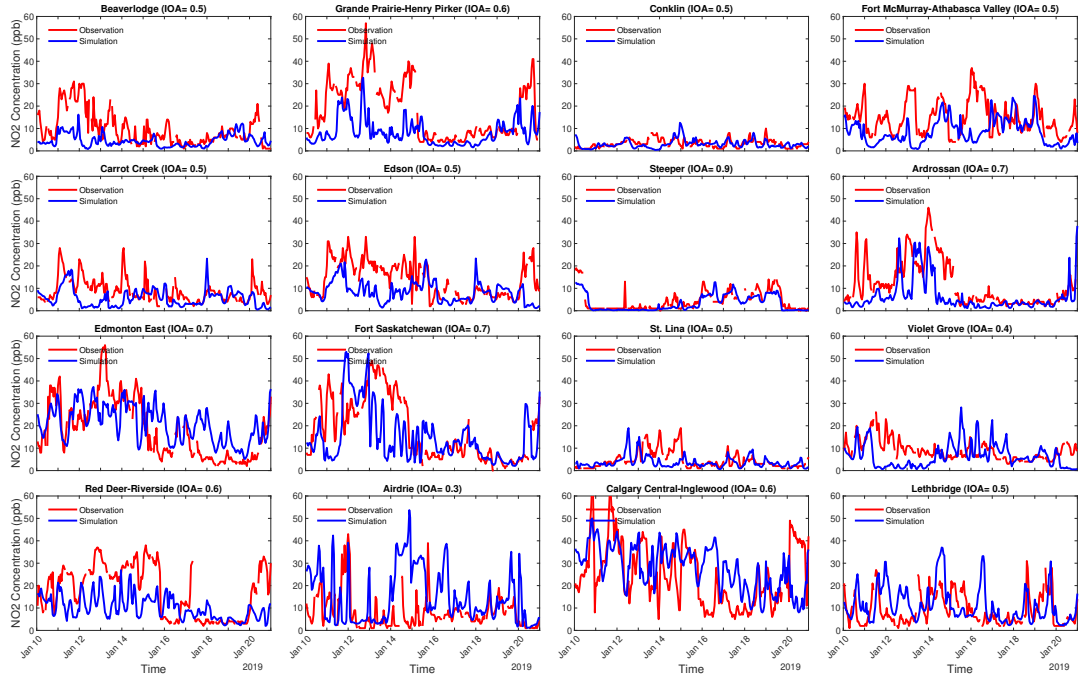

(b) Jan

Figure 3.10: Model Validation: Time series of Observed (red line) and modeled (blue line) hourly averaged NO_2 at selected monitoring stations for July period (a) and January period (b).

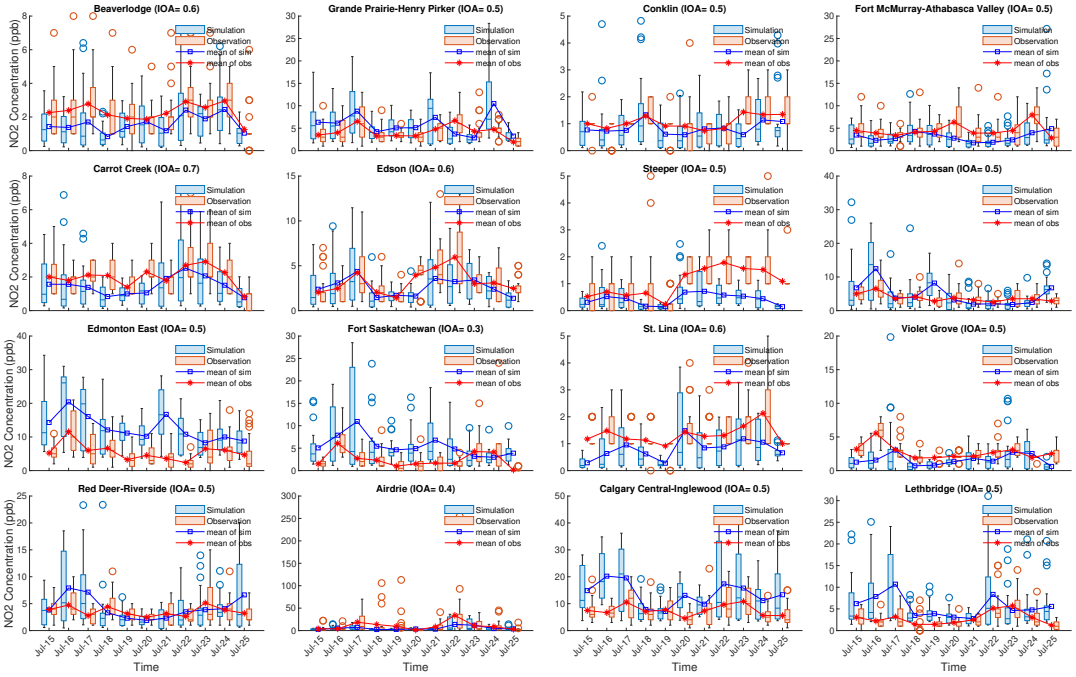

(a) July

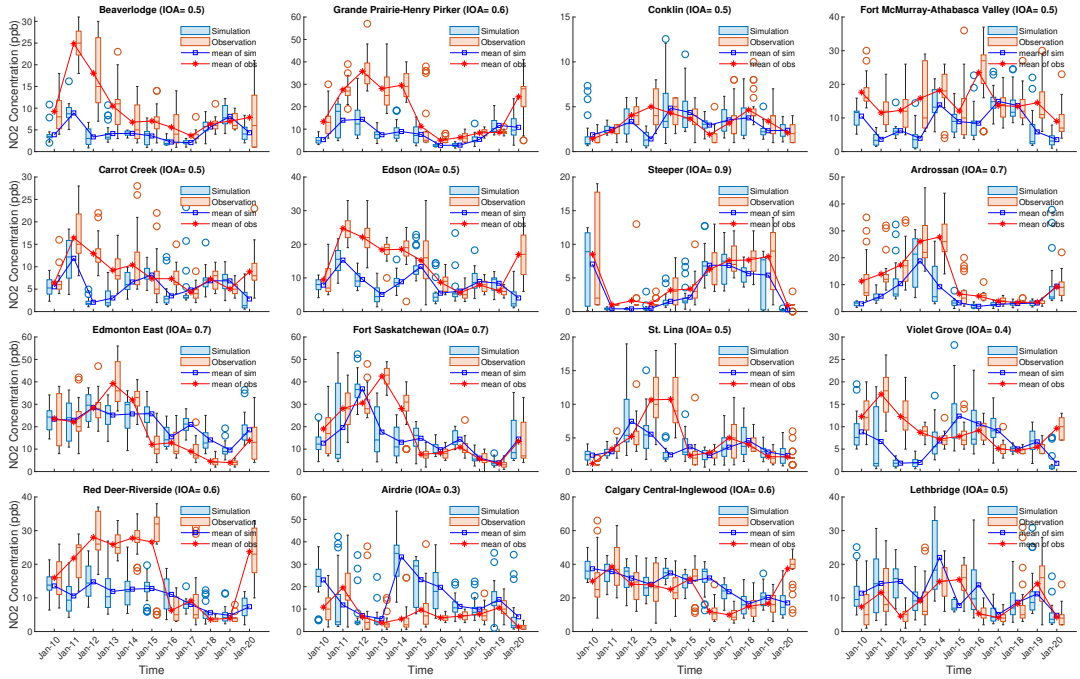

(b) Jan

Figure 3.11: Model Validation: Boxplot to show NO_2 variation at selected stations and compare the simulation results (Blue) with observation data (red). The lines show the mean value of the respective colors. The edges of the boxes show the interquartile range of data (25th to 75th percentile) and circle points show outrange data.

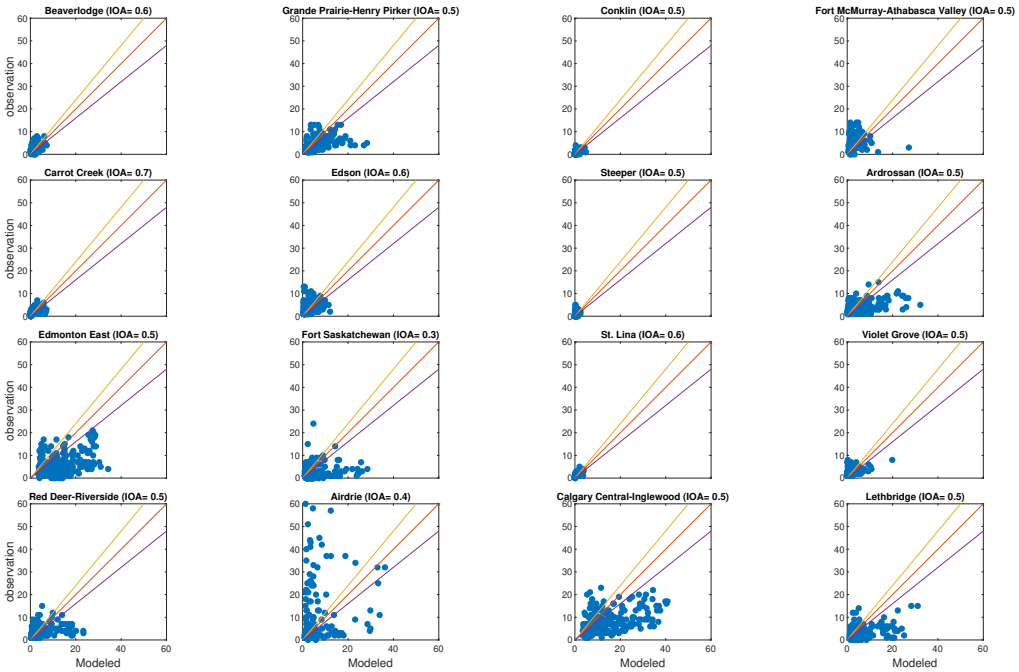

(a) July

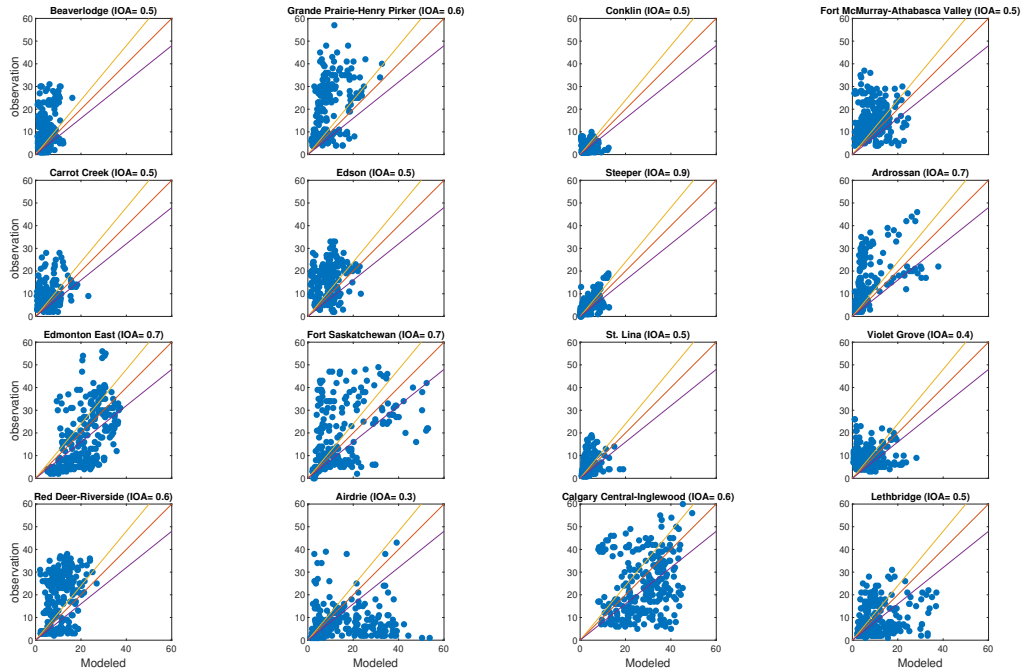

(b) Jan

Figure 3.12: Model Validation: Scatter Plot NO_2 for the selected station, comparison of observed and modeled results. The red line shows the identity line (simulation=observation). The yellow and purple lines show ±20% of the line of equality.

of the NO_2 concentration.

In fig. 3.12, each data point shows the averaged 1-hr modeled NO_2 and its respective observation value on the horizontal and vertical axis respectively. From this plot, it is apparent that the model provides a better estimation for the low-level NO_2 concentration of less than 20 ppb. For the higher NO_2 values of 20 ppb, there is an underestimation for almost all the stations. This underestimation could be linked to the positive bias in modeled wind speed. Since the simulation wind speed is higher than the actual wind speed, this could lead to a lower concentration at the monitoring stations.

As mentioned before and as shown in fig. 3.10, in the July period most of the stations experienced NO_2 less than 20 ppb, which indicates a lower level of NO_2 in the July period. The average value of NO_2 concentration over the whole 10 days of simulation for two periods in January and July is shown in fig. 3.13 using color maps. In the July period, the average NO_2 level is lower compared to the January period. Also, the area of the regions that are polluted by NO_2 is much lower in the July period. This could be related to the NO_2 reactions resulting in a short life cycle in warmer temperatures (less than a few hours). A longer NO_2 life cycle in winter (nearly 1 day) and atmosphere stability can result in NO_2 spreading spatially. It is also evident that the major cities (Edmonton and Calgary) experienced a higher averaged NO_2 concentration compared to the other areas. From the color maps in fig. 3.13 other hotspots can be identified especially in the center of Alberta province between Edmonton and Calgary. These average hot spot values of NO_2 concentration are lower than that in the major cities.

3.7.2.2 Ozone: Validation

The metrics and criteria for O_3 are different. The Ozone criteria were proposed by Emery et. al. 2017[76]. Table 3.12 provides the statistical values for evaluation of the 1-hr average O_3 modeling results at the monitoring stations. The benchmark

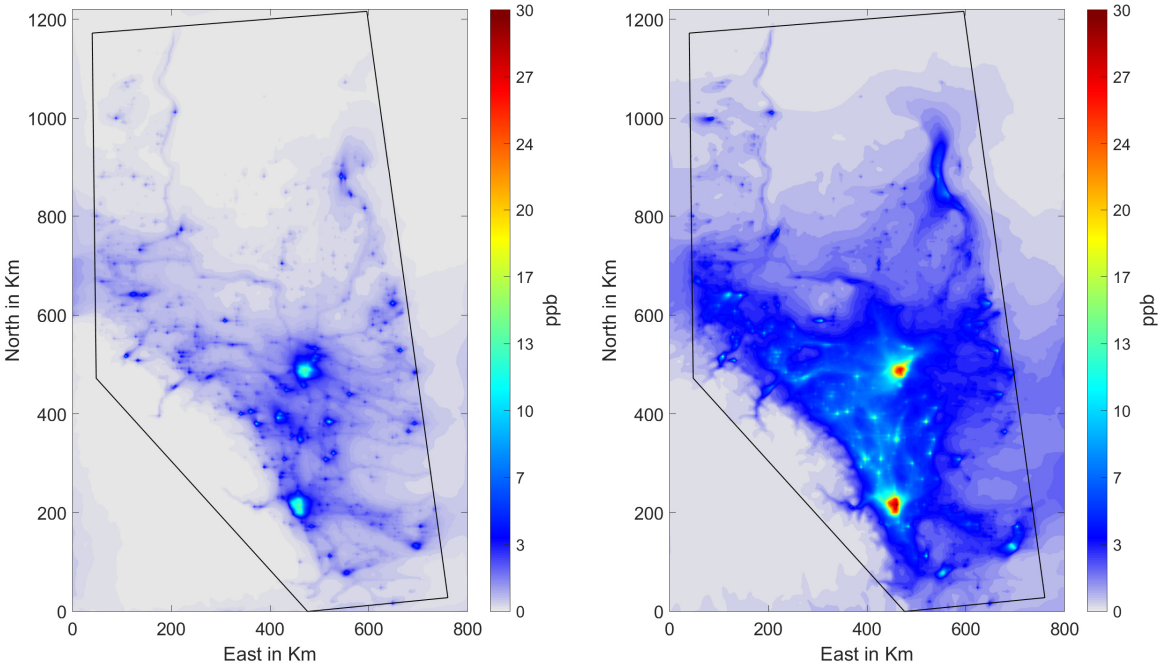

(a) July (b) Jan

Figure 3.13: Average NO_2 concentration over the 10-day simulation period.

recommended criteria are based on Emery et. al. 2017 studies [76]. Overall, in the July period, the average values of metrics met the benchmark criteria except for the NME, which its value is slightly higher than the benchmark results. NMB values for the monitoring stations indicate an underprediction of O_3 at most of the monitoring stations. The reason could be both the negative bias of modeled temperature and the positive bias of modeled wind speed. The O_3 concentration is highly dependent on chemical reactions which are affected by temperature, so the negative bias (underestimation) of temperature can lead to the underprediction of O_3. Furthermore, an overprediction of modeled wind speed also reduces the ground level of modeled O_3 concentration. In January the metrics show opposite results. Some of the stations satisfy the benchmark criteria while most of the stations did not. Since the O_3 formation is highly dependent on sunlight and temperature, the poor model results could be linked to the uncertainty of the WRF model for capturing the sunlight and snow-cover effect. This leads to biases between modeled and observed temperature

and as a consequence a discrepancy in O_3 modeled results. For the January period, there is also an overprediction of wind speed which affects the O_3 concentration. Nevertheless, the IOA values in January show that the model could capture the trend of O_3 variation.

Table 3.12: CMAQ model performance statistics for Ozone

Station Name	**July**				**Jan**			
	NMB	**NME**	**r**	**IOA**	**NMB**	**NME**	**r**	**IOA**
Criteria	$\leq \pm$**15**	$\leq$ **25**	**0.5** $\leq$		$\leq \pm$**15**	$\leq$ **25**	**0.5** $\leq$	
BEVE	4.07	24.04	0.60	0.65	16.13	39.29	0.16	0.48
GPHP	-13.39	28.99	0.64	0.55	52.30	75.18	0.21	0.54
ANZA	-4.18	24.71	0.57	0.38	-25.33	36.23	0.26	0.48
CLSO	12.07	30.49	0.72	0.23	-17.25	32.87	0.47	0.58
CONK	-21.75	24.19	0.70	0.48	-25.35	32.33	0.24	0.44
FOCH	-28.07	30.40	0.33	0.41	-26.50	27.15	0.17	0.41
FMBG	5.94	36.65	0.63	0.42	59.78	93.51	0.15	0.51
FMSO	-7.68	36.60	0.69	0.43	42.48	92.19	0.02	0.45
FMAV	-21.46	28.22	0.72	0.48	-6.72	47.21	0.28	0.58
FMPM	-37.66	39.11	0.68	0.56	-26.89	40.53	0.32	0.52
JANV	-36.88	37.44	0.75	0.44	-34.69	37.35	0.18	0.42
STMO	-21.26	23.90	0.69	0.58	-24.53	31.43	0.23	0.44
CACR	2.31	25.99	0.80	0.67	4.48	52.32	0.00	0.43
EDSO	4.48	29.70	0.70	0.56	28.31	79.21	0.02	0.42
HINT	29.43	47.26	0.60	0.40	42.90	58.24	0.43	0.64
STEP	-1.34	20.45	0.47	0.48	-14.28	21.47	0.87	0.88
ARDR	-7.37	27.88	0.64	0.51	4.03	36.27	0.54	0.66
BRET	-1.71	23.73	0.64	0.25	-8.20	39.77	-0.02	0.36
BRUD	-22.61	26.63	0.70	0.47	1.62	38.24	0.39	0.62
CARO	-3.85	23.25	0.63	0.35	-22.93	38.29	0.33	0.58
EDCE	-34.28	44.57	0.48	0.48	-46.41	73.02	0.27	0.55
EDEA	-25.33	37.60	0.55	0.49	-40.22	58.23	0.49	0.62
ESOU	-26.03	36.34	0.62	0.40	-53.74	70.18	0.33	0.54
EDWO	-21.01	34.94	0.64	0.52	-49.95	77.53	0.12	0.48
ELIS	-1.76	20.21	0.72	0.44	-5.41	31.36	0.43	0.59
FSAS	-11.85	27.44	0.63	0.30	-10.47	51.49	0.52	0.71
GENE	28.00	41.92	0.53	0.35	9.72	59.58	-0.04	0.39
GIBB	-1.62	26.95	0.65	0.61	-3.30	57.28	0.11	0.46
LACO	-11.72	21.58	0.66	0.33	-23.12	34.57	0.38	0.57
REDW	-11.25	24.94	0.66	0.37	-28.74	54.15	0.14	0.47
SHEP	-28.09	36.47	0.60	0.42	-35.68	47.90	0.55	0.64
STAL	-18.09	29.24	0.67	0.57	-32.62	84.84	-0.16	0.37
STLI	-5.01	16.53	0.70	0.63	-22.23	29.05	0.32	0.50
TOMA	0.27	21.05	0.70	0.54	3.98	56.14	-0.22	0.26

VIGO	3.78	22.77	0.68	0.52	-2.56	37.63	0.10	0.45
RDLA	-8.84	25.96	0.54	0.37	13.93	62.21	0.12	0.48
RDRI	-2.59	29.11	0.58	0.46	47.58	90.67	0.16	0.49
AIRD	-7.29	22.88	0.56	0.40	-18.37	43.42	0.37	0.63
CACE	-22.56	34.73	0.63	0.54	-26.33	86.46	0.13	0.50
CASE	-25.83	35.35	0.61	0.45	16.10	75.63	0.21	0.54
LETH	-11.96	23.64	0.52	0.51	-0.49	40.52	0.35	0.59
MHCH	-26.34	29.66	0.69	0.43	19.66	60.91	0.22	0.55
Average	**14.79**	**29.37**	**0.63**	**0.46**	**23.70**	**53.14**	**0.24**	**0.52**

Time series of hourly averaged modeled and observed O_3 are shown in fig. 3.14. For the July period, the index of the agreement for all the stations is $\geq$0.7, which indicates a strong agreement between simulation and observation. For the time series in July, the model captures the Ozone trends and values accurately, but there is a slight underestimation of peak hours and a small overestimation of minimum values. The underestimation of Ozone occurs at peak hours in midday, which is attributed to the tendency of the model to underestimate the NO_2 concentration (one of the main Ozone precursors). The slight underestimation of temperature in the July period and also uncertainty in the emission inventory files for Ozone precursors can also lead to Ozone underestimation[83–85]. The overestimation of Ozone at midnight can be linked to the following three factors: (1) bias in temperature and wind speed[86]; (2) uncertainty in the temporal profile of emissions; (3) model performance for representing the physicochemical process during the night[83]. For the January period, the deviation between simulation and observation is larger compared to the July period. As a result, almost all the stations have a lower IOA in the January period. One reason could be the larger bias of the meteorological model for temperature and wind speed in the winter period. In the January period, Steeper has the highest IOA (0.9) of all stations. The bias of temperature and NO_2 concentration for this station is lower than that for other selected stations.

Fig. 3.15 provides a comparison of daily variation of Ozone concentration between the observed and modeled data. Each box represents the interquartile range of data

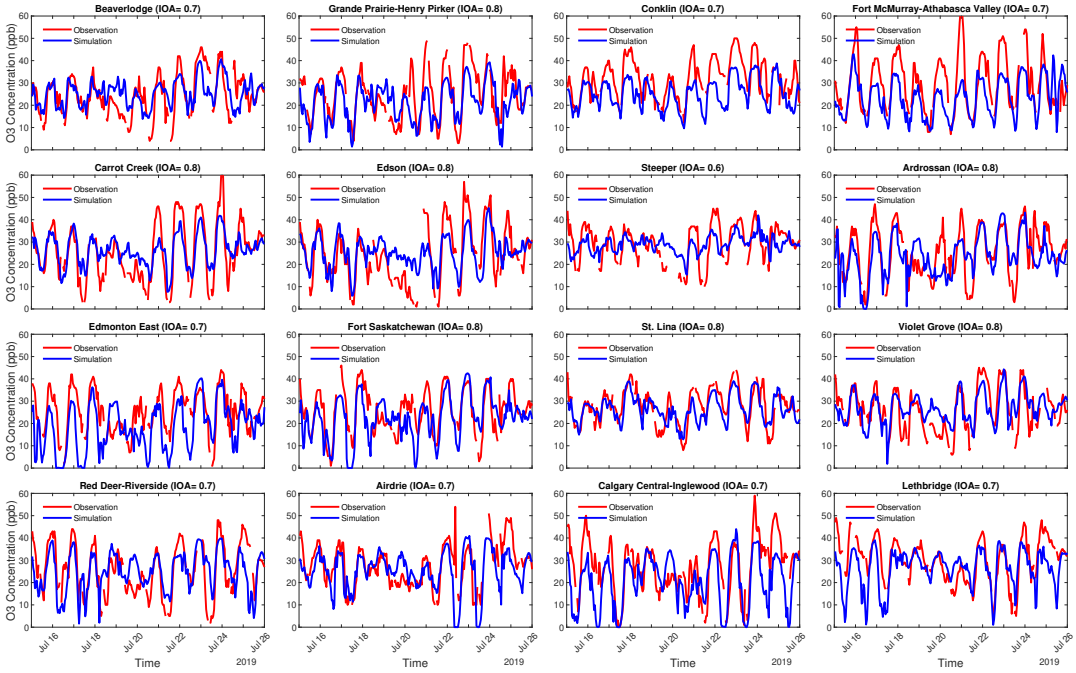

(a) July

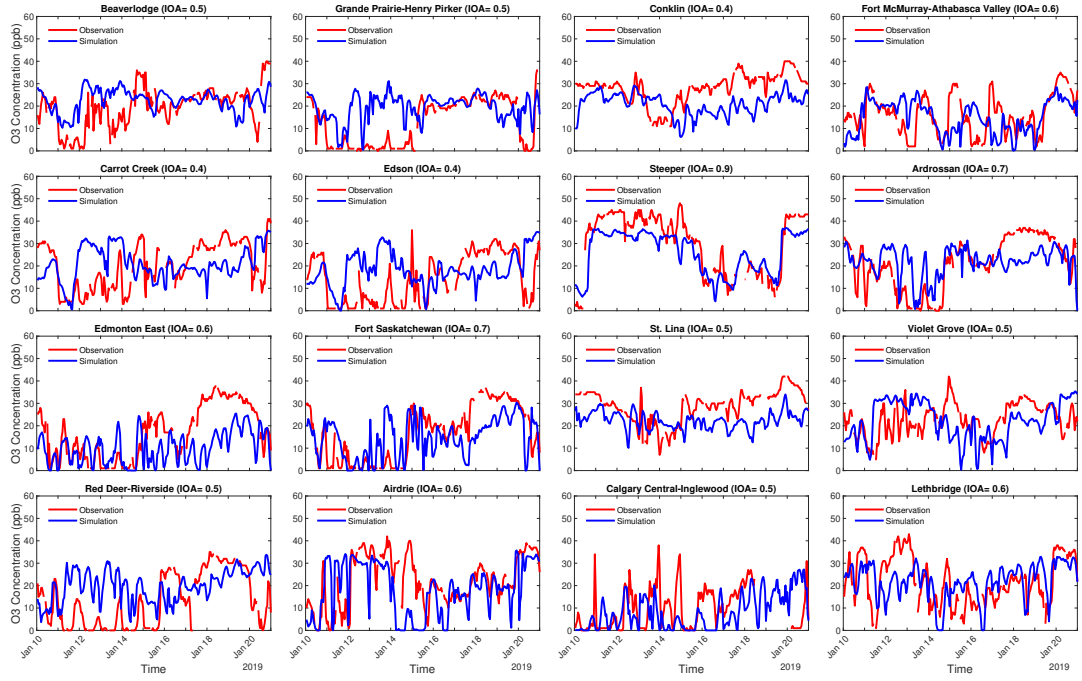

(b) Jan

Figure 3.14: Time series of Observed (red line) and modeled (blue line) hourly averaged O_3 at selected monitoring stations for July period (a) and January period (b).

for one calendar day. The lines connect the mean value of each day. Similar to NO_2, the daily variation of O_3 in the July period is larger than that of the January period.

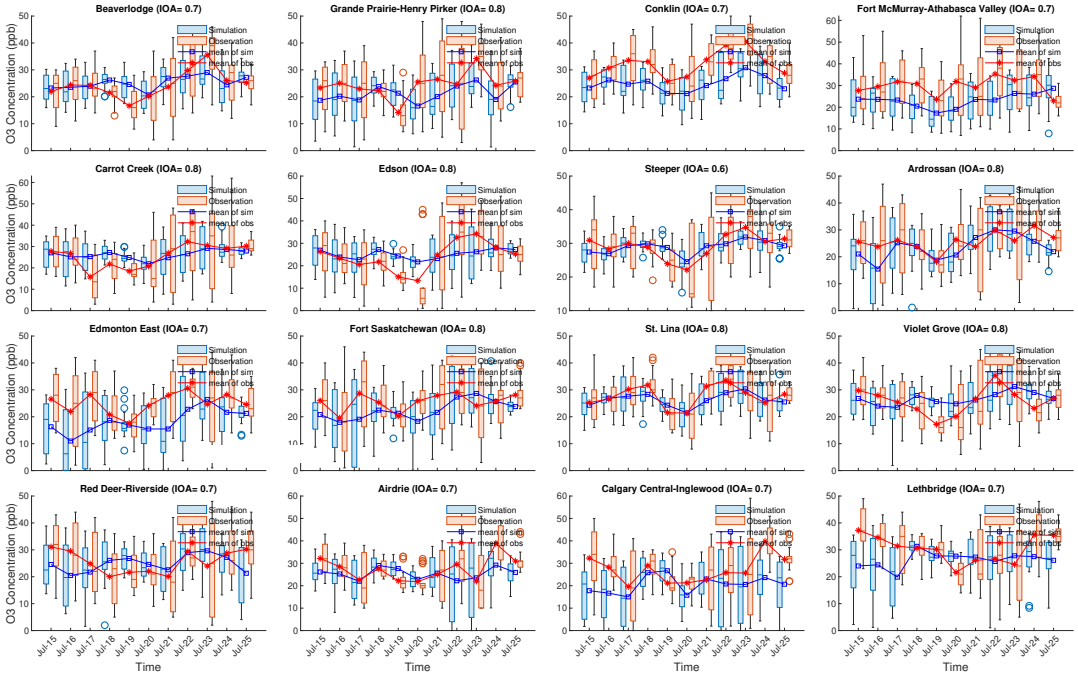

(a) July

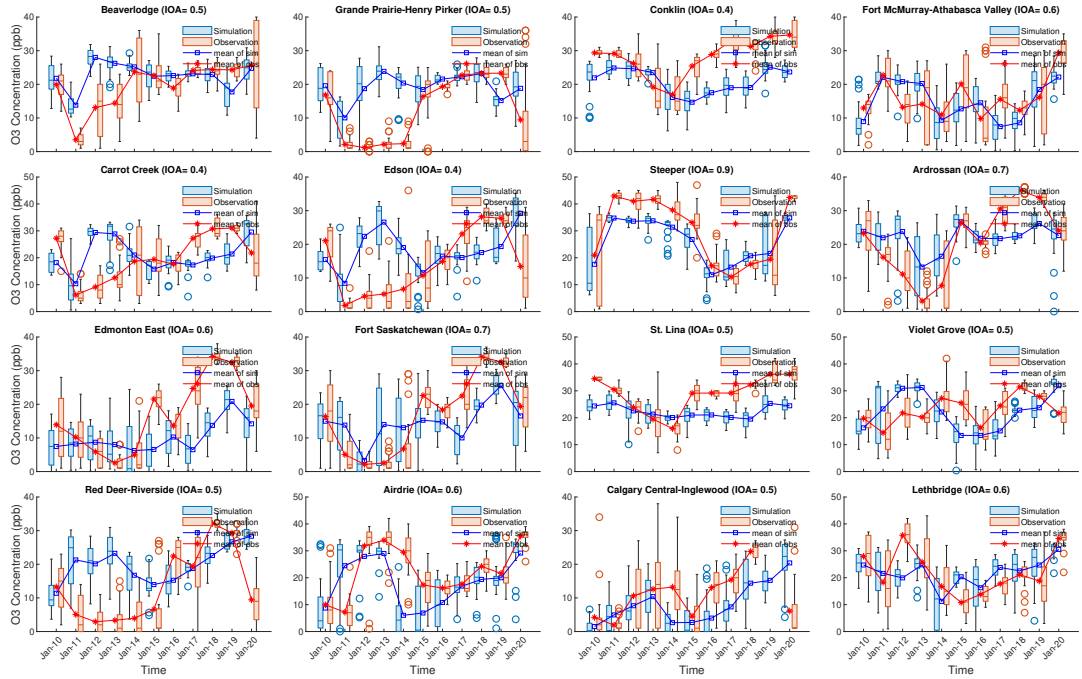

(b) Jan

Figure 3.15: Boxplot to show O_3 variation at selected stations and compare the simulation results (Blue) with observation data (red). The lines show the mean value of the respective colors. The edge of the boxes shows the 25th and 75th percentiles. The circle points show outrange data.

Since the temperature variation is higher in the summer period and O_3 concentration is highly dependent on temperature[85]. Overall, the July period shows a strong correlation between observed and modeled data. For the January period, although the interquartile range and median values of simulation and observation show a slight deviation, the mean values show that the model captures the trend of Ozone variation. Now comparing figs. 3.11 and 3.15, it is apparent that an underestimation of NO_2 concentration resulted in an overestimation of O_3 concentration in the monitoring sites.

An overview of the model performance for capturing O_3 concentration in the July and January periods is shown in fig. 3.16. Each data point is the averaged 1-hr modeled O_3 and its respective observation value on the horizontal and vertical axis respectively. For the July period, although some underestimation and overestimation can be seen (as mentioned earlier), for the majority of the stations, the cloud of points lies around the $\pm 20\%$ of the identity line. The trend in the January period is worse. For both July and January periods, the model shows a good performance for capturing Ozone concentrations higher than 30 ppb. However, there is a considerable underestimation for lower Ozone concentration ($\leq$ 10 ppb).

Average O_3 concentration over 10-day modeling periods for both January and July are shown in fig. 3.17. Unexpectedly, results indicate that the maximum level of O_3 concentration happened in southern Alberta over the Rocky Mountains and near the province boundary with British Columbia, particularly high elevated regions near the Rocky Mountains. Analyzing the results and comparing them with the monitoring stations in British Columbia showed that the boundary condition affects the Ozone concentration in that area considerably. The model is validated for inside Alberta and the modeling results within the province show a good correlation with observation data. Therefore, the effect of these high Ozone areas in the southwest of the domain can be neglected. However, further studies, where the boundary conditions are modified, are needed. Neglecting the high Ozone concentration outside of the province

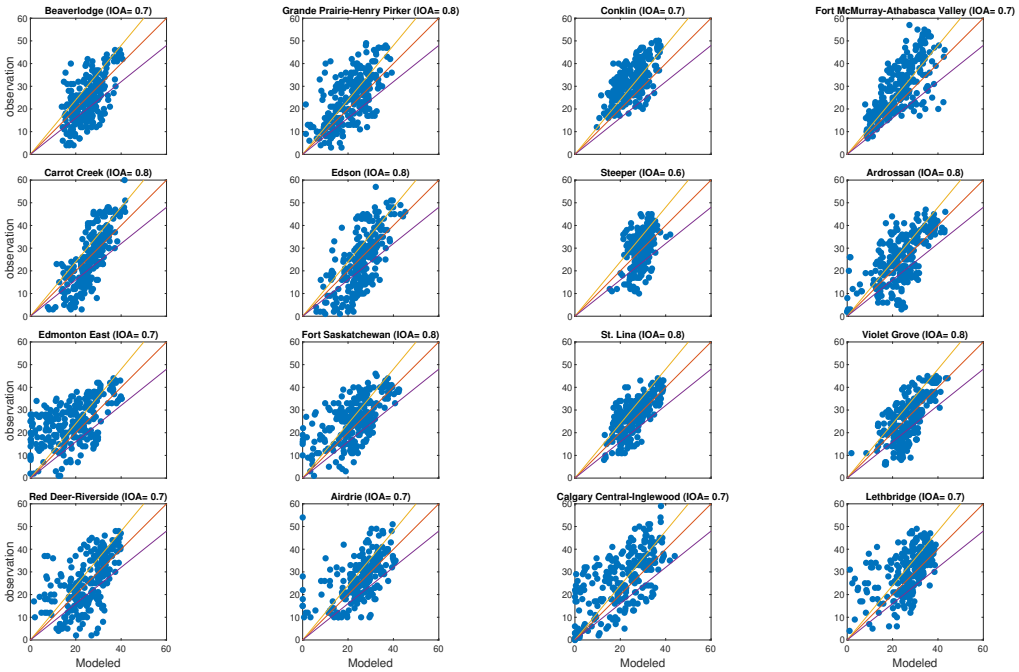

(a) July

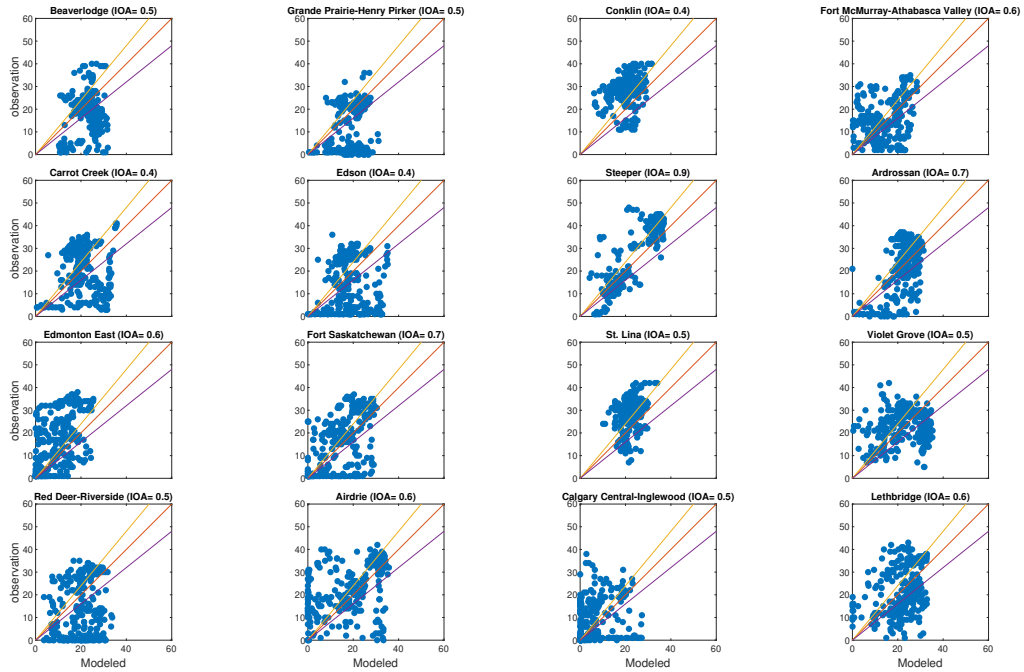

(b) Jan

Figure 3.16: Scatter Plot O_3 for the selected station, comparison of observed and modeled results. The red line shows the identity line (simulation=observation). The yellow and purple lines show ±20% of the line of equality

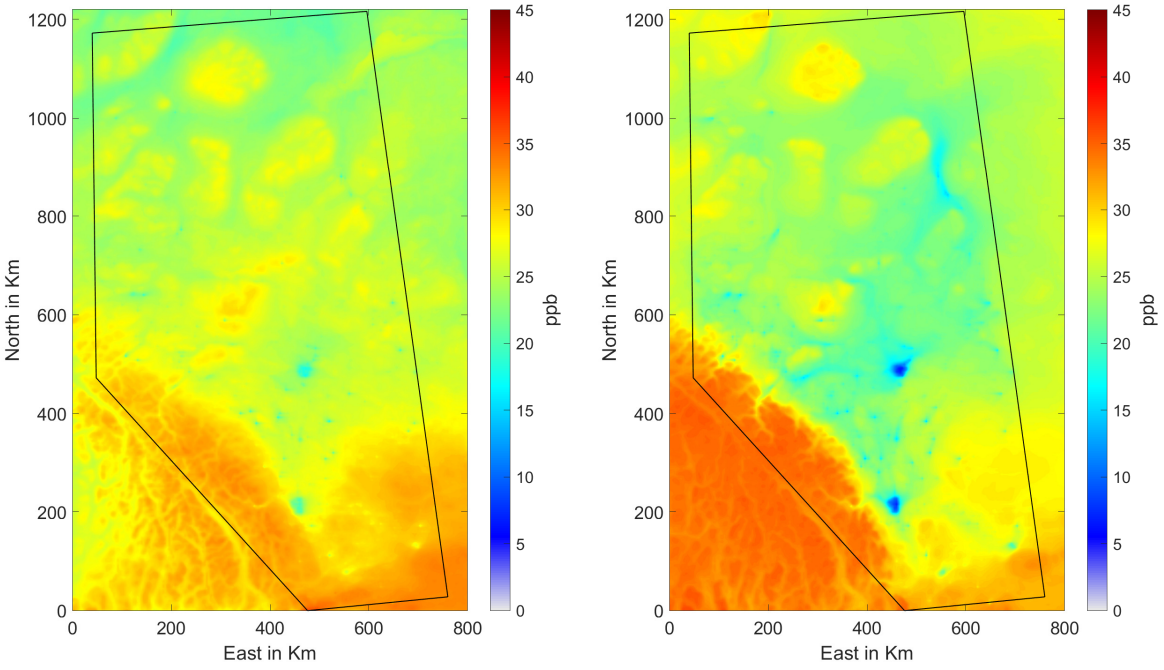

(a) July (b) Jan

Figure 3.17: Average O_3 concentration over the simulation period.

and over the Rocky Mountain, overall Ozone concentration in the summer period is higher than the January period as expected. The minimum level of O_3 concentration is observed in the vicinity of large cities like Edmonton and Calgary for both modeling periods. The reason could be related to the NOx-saturated regime, the null cycle of Ozone and NO_2, and the higher level of NO_2 in that region.

Chapter 4

Results

4.1 Base Case

The model capability to reproduce the historical trend of meteorological and atmospheric data was evaluated in sections 3.7.1 and 3.7.2. Model result biases and the causes for these biases were analyzed. The results of base case scenario that include the emissions from all major sources are reported in this section. The modeling results for the base case scenarios have been summarized in fig. 4.1.

A box shows the interquartile range of the simulation data for one selected station in the left column of fig. 4.1. The right column of fig. 4.1 shows the time series of average value for all monitoring stations. Overall, Alberta experiences significant temperature variation year-round, typical of continental climate. In July, the temperature normally varies between 16 to 30°C with a mean value of around 22°C. For January, it is much colder with the temperature ranging from -5 °C to -50 °with an average value of -15°C[87, 88]. Considering the wind speed, the simulation results indicate that most of the time in both modeling periods, wind speed is less than 10 km/h (≈2.7 m/s). The wind speed variation in the July period is higher. Aside from meteorological parameters, focusing on criteria air contaminants in fig. 4.1, Ozone means value for the July period is slightly higher than that for the January period. In July, Ozone concentration fluctuates around the mean value of approximately 28 ppb. While in the winter period, the Ozone mean concentration is 35% lower and

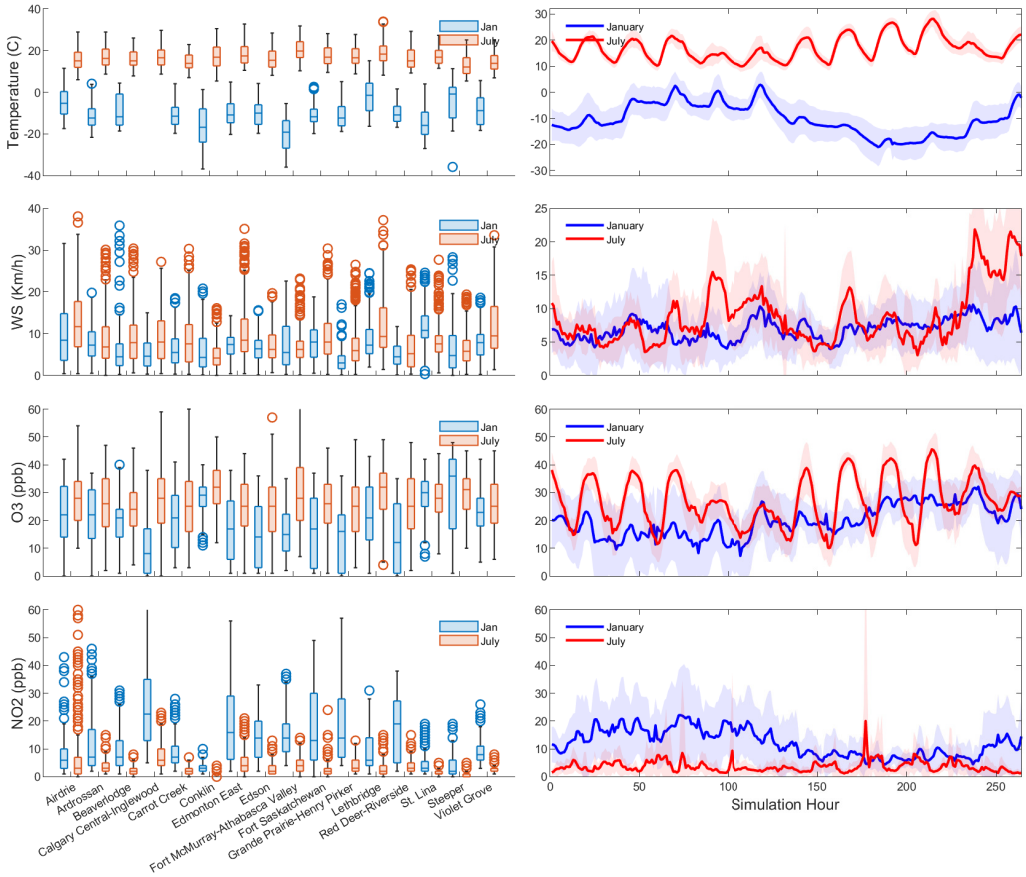

Figure 4.1: Comparing the average of four variables at each station. The left column is a Boxplot showing interquartile data (25th to 75th percentile). Circle points show outrange data. The right column is the average time series of all stations for the respective parameter. The blue color is for January and the red color is for the July period. The Shaded colors show the standard deviation of data.

fluctuates around 18 ppb. The amplitude of Ozone fluctuation is larger in July. The NO_2 trend is almost the opposite of the O_3 behavior. NO_2 concentration in the July period is considerably lower than that of the January period. The average NO_2 concentration in July is less than 5 ppb while in the winter period the mean value of NO_2 is almost two and half times higher with an average of 12 ppb concentration. The standard deviation of the data is depicted using the shaded color, which is higher in winter for all four parameters. Thus the differences between the monitoring station measurements are more pronounced in the January period.

Fig. 4.2 shows atmospheric instability, which is characterized using Monin Obukhov Length (L), averaged over the simulation period. The atmosphere in January is more stable than in July as shown in fig. 4.2. In the January period, some local unstable areas are near populated areas of Alberta in the middle south of the domain. Other unstable areas are near Athabasca Lake and Lake Claire. Other than these local maxima, most of the domain is slightly or extremely stable, which is attributed to the cold temperatures and the temperature inversion phenomena. In contrast, most of the province is slightly unstable in July.

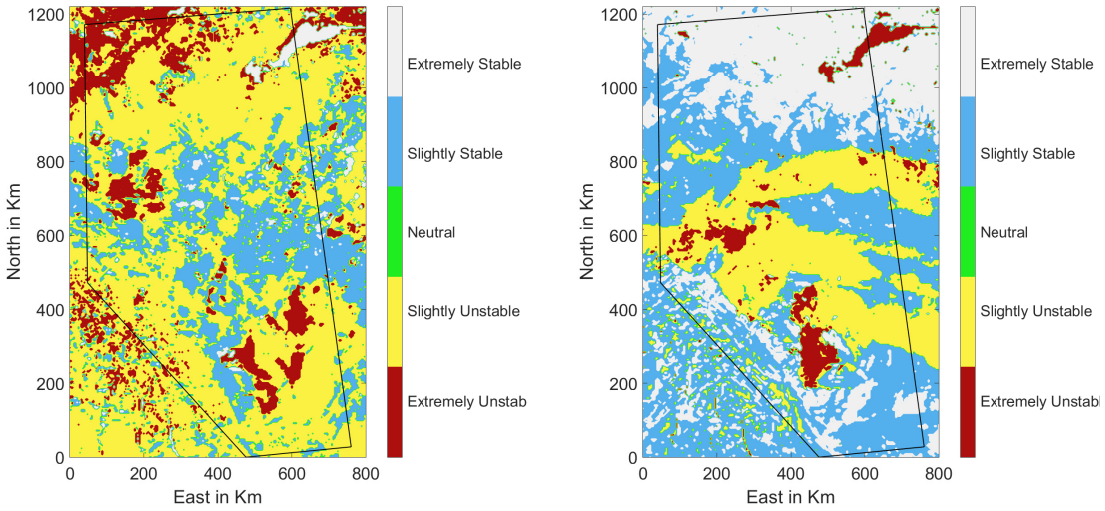

(a) July (b) Jan

Figure 4.2: Average of Monin-Obukhov length over the modeling period

Two stations in the cities of Edmonton and Calgary were chosen to analyze the atmosphere's stability. The time-series comparing the variation of NO_2 and L are presented in fig. 4.3. Comparing the January and July periods for both stations, more positive L or near zero values can be seen in January. The NO_2 concentrations are considerably higher in January than in July.

The occurrence of different classes of Monin Obukhov atmospheric stabilities for each station are provided in histograms in fig. 4.4. Slightly or extremely stable atmosphere occures about 60% of the time for both monitoring stations in the January

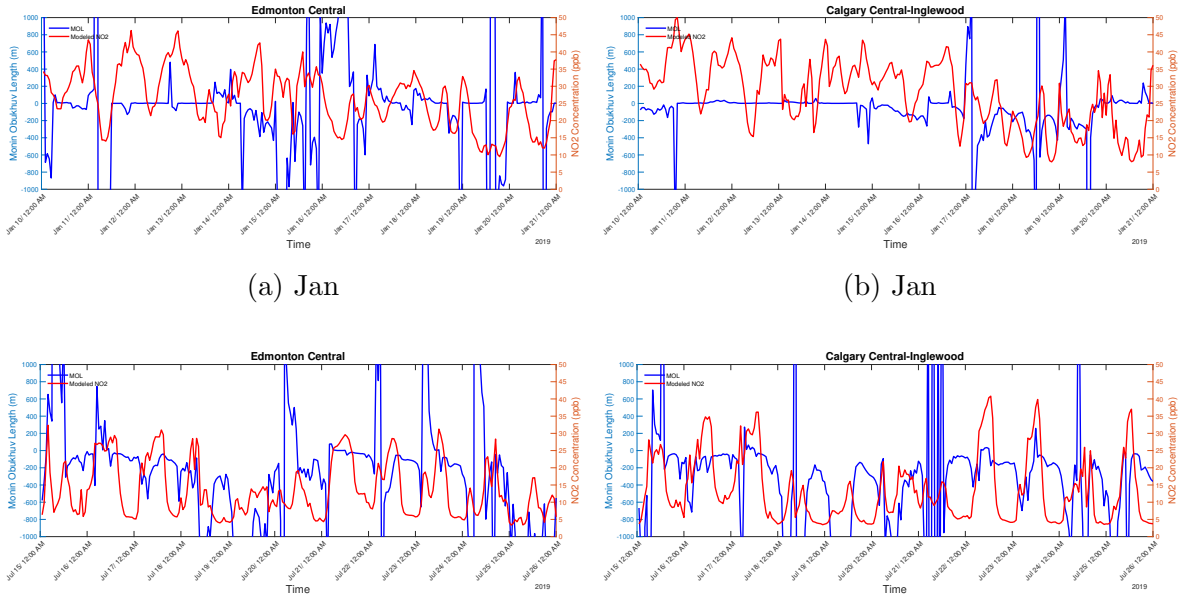

(a) Jan (b) Jan

(c) July (d) July

Figure 4.3: Comparison the Monin-Obukhov Length and NO_2 for the cold (Jan) and warm (July) modeling period. The left column is for Edmonton Central station, while the right column is for Calgary Central Inglewood station.

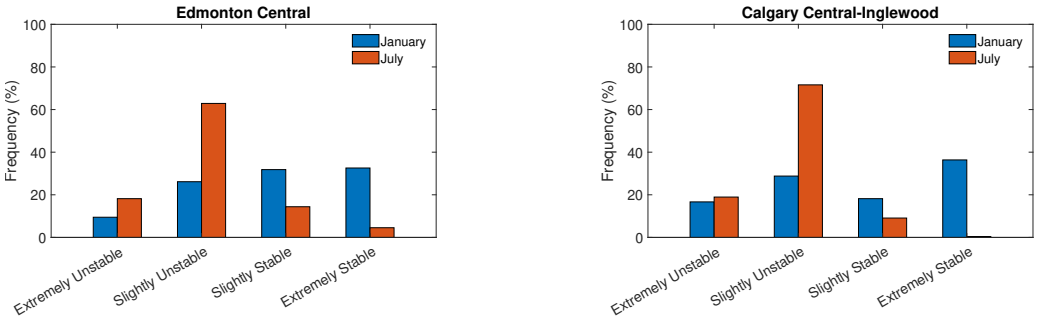

Figure 4.4: The histogram shows the frequency of different classes of Monin Obukhov atmospheric stability in the two modeling periods.

period. For the July period this is less than 20% for both stations. The atmospheric stability in cold temperatures could be one of the main causes for higher ground level NO_2 concentration in the January period.

The spatial distribution of NO_2 and O_3 concentration is shown in fig. 4.5 to better understand the differences between monitoring stations. Since NO_2 is one of the main precursors of O_3, the concentration of these two chemicals are coupled by the null

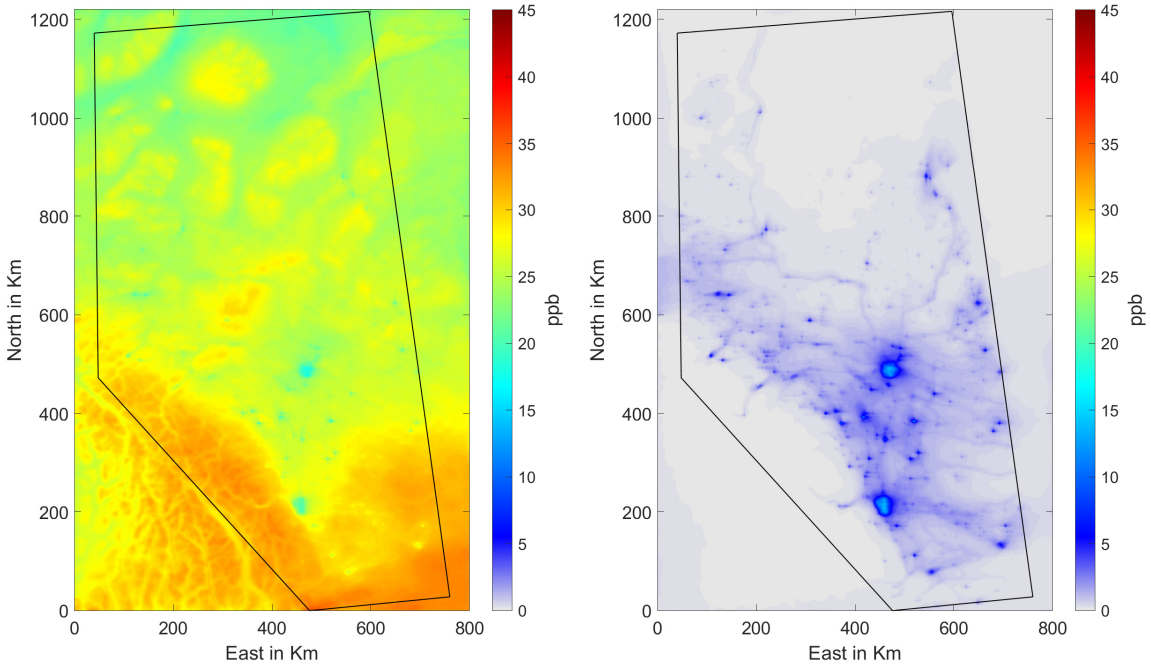

(a) O_3 Concentration-July

(b) NO_2 Concentration-July

(c) O_3 Concentration-Jan

(d) NO_2 Concentration-Jan

Figure 4.5: Simulation: ground level Averaged O_3 and NO_2 concentration. The left column (a),(c) is O_3, while the right column (b),(d) is NO_2. Both January and July periods are shown.

cycle as is evident in fig. 4.5. High level of NO_2 concentration are matched with low areas of O_3 concentration and vice versa. The conversion of NO_2 to O_3 is triggered by sunlight so the difference between the concentration of these two chemicals is observed in the colder season due to the lack of sunlight for activating the process. As expected in the warm season O_3 concentration is higher, especially in rural areas compared to the cold season. However, NO_2 has a completely different behavior. NO_2 concentration in winter is considerably higher in more regions due to a more stable atmosphere and longer NO_2 lifetime in colder temperatures.

4.2 Sensitivity Analysis

Sensitivity analysis (SA) is used to examine the effects of changes (perturbations) in model input on the model output. How the perturbations on an independent variable (input) affect model output is the purpose of SA [89]. For air quality modeling, quantifying the atmospheric response to emissions control scenarios [90][91], determining the uncertainty in the model's response [92], and performing inverse modeling and data assimilation [93][94] are applications of SA.

SA methods, based on the propagation of the perturbations, are divided into two groups [95]:

- **Forward SA**: In this method, the small perturbations are applied to the inputs and then the new model outputs are calculated. The changes are propagated forward through time and space. This method is useful when the effects of a limited number of inputs on all outputs are required. In this approach, the sensitivity coefficients are estimated using the finite difference method or by taking the derivative of the model's equations.

- **Backward SA**: This method is also called adjoint method. In this approach, the small changes in the model's output are propagated backward to determine the change in model inputs. A common application of this approach is improving

the accuracy of the emission inventory files.

Among different sensitivity analysis approaches, there are three common methods in air quality modeling studies: decoupled-direct method (DDM), adjoint (inverse) model, and Brute force (BF) method [96, 97]. The DDM and BF methods are forward SA, while the inverse model is backward SA. In DDM methods, the perturbation directly applied to the scientific equations and sensitivity of concentrations to other chemical compounds or physical parameters like boundary conditions can be calculated using finite-difference [97]. Higher-order sensitivity coefficients are calculated using this method. However, running this model required higher computational resources compares to the other methods [96]. In the BF method, sensitivity coefficients are calculated using the differences between the base case concentration and perturbed-emission scenarios. The BF forward SA method is implemented in this thesis. This approach is source-based and is an efficient approach to analyzing the effect of the perturbations of a limited number of model inputs. In particular, emission sources are perturbed to evaluate their effects on the model outputs [98].

4.2.1 Sensitivity Analysis: Brute Force

Brute-Force SA (BFSA) is widely used in air quality modeling studies [69, 99, 100]. This is a forward SA method, where the sensitivity coefficient is calculated as:

$$S = \frac{C_n - C_b}{\Delta\epsilon} \tag{4.1}$$

BFSA is based on the difference between the model's output to the model's inputs before and after applying perturbation divided by the input perturbation (eq. (4.1)). In this equation, the concentration after applying perturbations is represented by C_n and C_b is the base case concentration. The changes in emission input is defined $\Delta\epsilon$. Clearly in BFSA, a base case that has no perturbation, and a scenario, in which the required perturbation has been applied, are needed. So for analyzing N scenarios N+1 simulations are needed. One of the major benefits of this technique is the

straightforward interpretation of the results. To implement forward SA, appropriate model inputs are modified and the entire simulation is re-run for both modeling periods with a 1-hour time resolution.

4.3 Sensitivity Analysis: Impact of Emission Sources on Nitrogen Dioxide

As mentioned in section 2.3, the NO_2 concentration within large cities is sensitive to the emission from mobile sources and the transportation sector[34]. Conversly, the major NO_2 emission source in Alberta province is UOG industry[13]. To examine how these two sources impact the distribution of NO_2 pollution, a sensitivity study was carried out. Brute Force Sensitivity Analysis was performed to evaluate the variation of NO_2 concentration due to small or large perturbations of the major NO_2 sources (-mobile transportation and UOG). The sensitivity analysis was performed in these two main categories: (1) mobile transportation emission was changed and other emissions held constant; (2) UOG emission was changed, while other emissions held constant. Prior to analyzing the sensitivity results, the base geographical distribution of Mobile and UOG emission sources is plotted.

Major UOG sources are located outside of the urban areas with higher numbers along the Rocky Mountains and in oil sands areas. A concentrated region of UOG emission sources is located in the East of Alberta province near Cold Lake. Major mobile transportation sources are located in the vicinity of major cities and along the Queen Elizabeth Highway (Hwy #2).

4.3.1 Sensitivity Analysis: Zero-out Scenarios

Zero-out sensitivity scenarios are referred to the case in which all the emissions from a specific source are set to be zero. If the impact of the interactions of chemical species of the emission source of interest with different emission sources are neglected, comparing the zero-out scenarios to the base case, provides a comprehensive understanding of

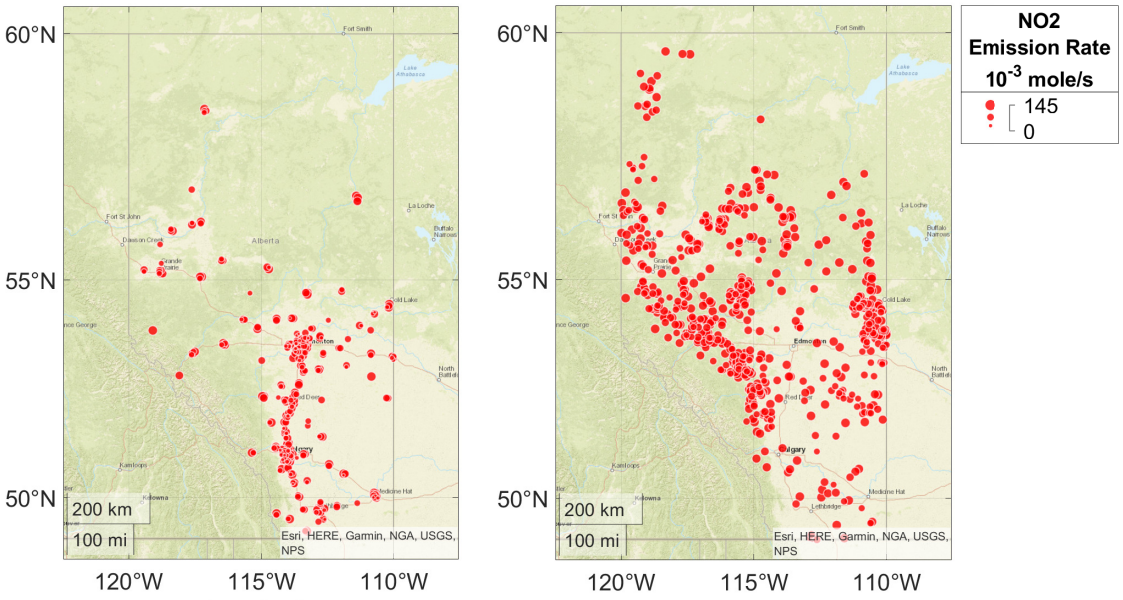

(a) Transportation (b) Upstream Oil & Gas

Figure 4.6: Spatial location and rate of NO_2 emission sources from emission inventory data [13]

that specific source's contribution to the total emission concentration. Colormaps that show average NO_2 reduction over the first 3 days of the simulation periods (after removing the first day to stabilize the effect of BCs and ICs) in July and January due to zeroing out of mobile transportation, 4.7, and UOG sources, 4.8, are shown. Comparing January and July periods, the effect of emission reduction in the July period is more local so the maximum emission reduction is around the location of sources. One of the reasons for such behavior is the short life cycle of NO_2 in warm temperatures. The NO_2 life cycle in the warm temperatures is a few hours (5.9 hours)[101]. In contrast, the NO_2 life cycle in the cold season is almost four times higher and around 21-27 hours[101]. Due to the NO_2 life cycle and atmosphere stability, it can be seen in figs. 4.7a and 4.8a that in the January period, the effect of NO_2 emission reduction is more spread across the province. Mobile transportation sources contribute to more than 50% of NO_2 concentration in the vicinity of major cities in the simulation period. Areas outside of the major cities especially alongside the Rocky Mountains are more affected by UOG sources. As seen when UOG sources

are zeroed out around 60% of NO_2 is reduced in these regions.

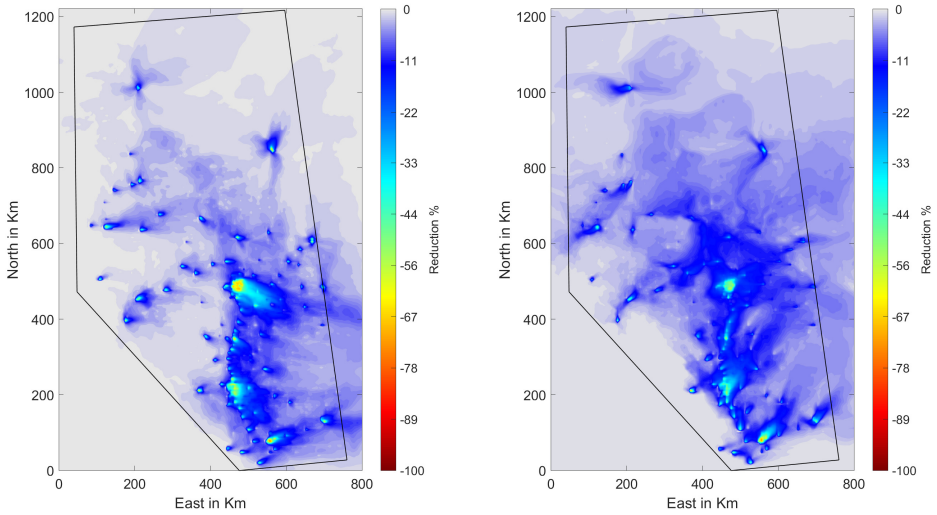

(a) July (b) Jan

Figure 4.7: NO_2 concentration reduction due to zeroing out of Mobile sector emission

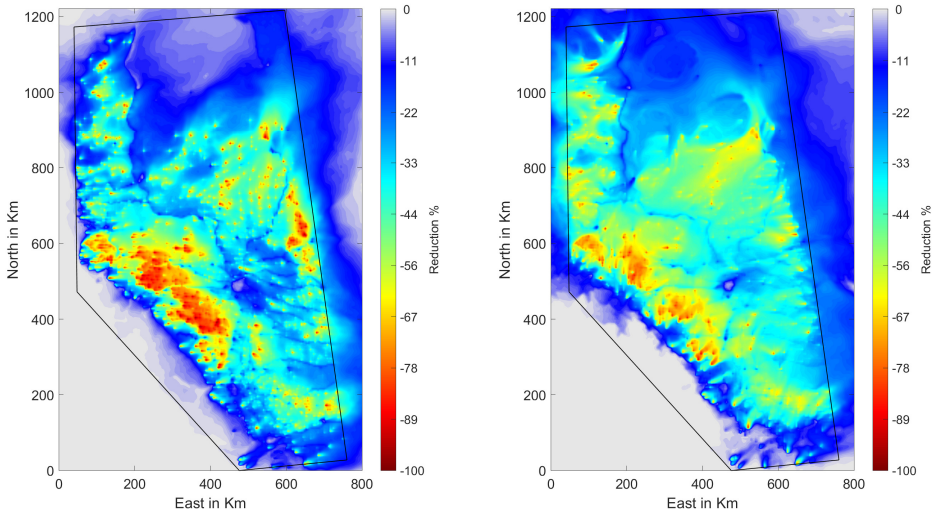

(a) July (b) Jan

Figure 4.8: NO_2 concentration reduction due to zeroing out of UOG sector emission

To provide further insight into the contribution of the different sources on NO_2 concentration, the NO_2 time series at selected stations showing the effect of each source separately are presented in fig. 4.9. Emission sources affect each station differently. For example, at Violet Grove and Carrot Creek UOG sources are dominant. While at Edmonton East and Lethbridge mobile source is the dominant source. Considering

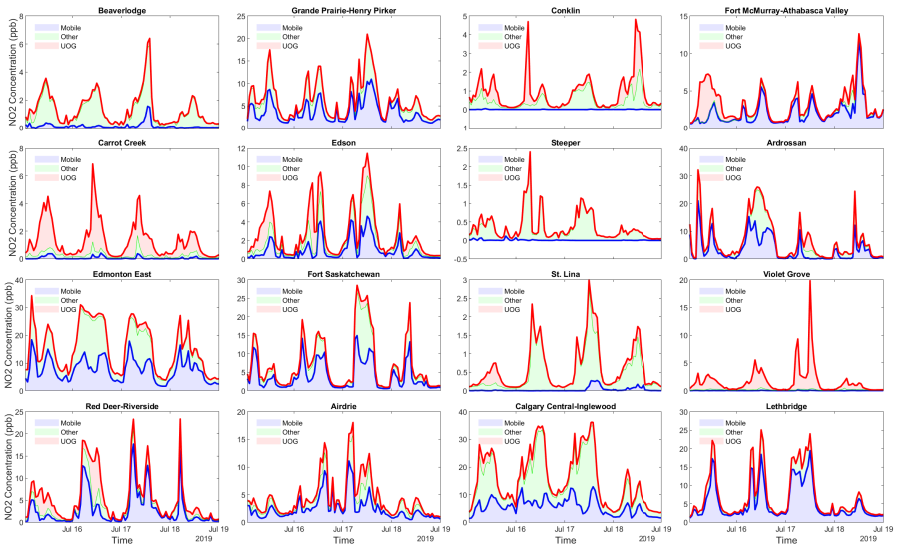

(a) July

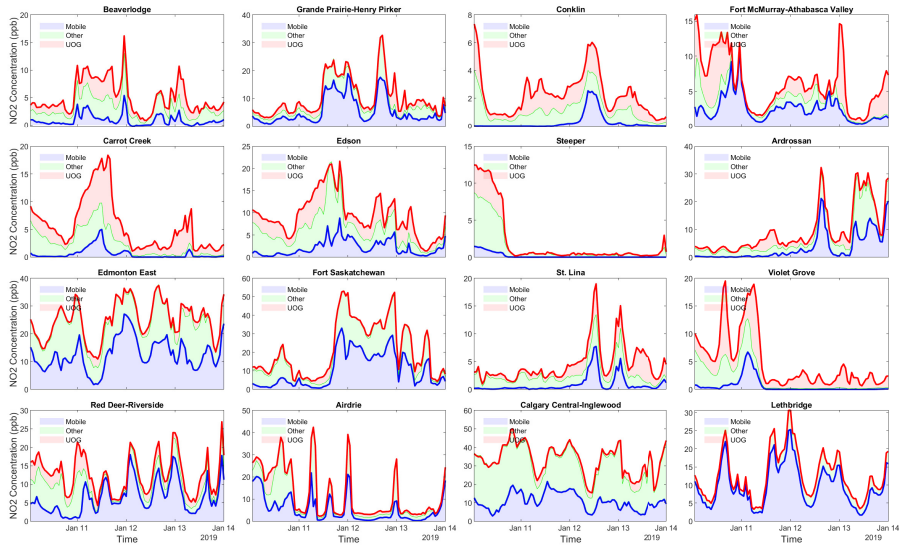

(b) Jan

Figure 4.9: Contribution of UOG (red), Mobile sources(blue), and other sources (green) on forming the time series of NO_2 concentration at selected monitoring stations. At each hour the difference between the lower bound and upper bound of each color shows the contribution of the respective source of that color.

the stations' classification, Violet Grove and Carrot Creek are Regional Backgrounds (RB) stations while Edmonton East and Lethbridge are Population Exposure (PE) stations. Overall, RB stations are more sensitive to UOG effects compared with mo-

bile and other sources. Meanwhile, PE stations are more sensitive to mobile sources. It is also observed in fig. 4.9 that the UOG effect is more pronounced in the January period.

To better understand the impact of two major emission sources, the results of the zeroing-out study were analyzed on the monitoring stations within Alberta's major cities: Edmonton and Calgary. Fig. 4.10 shows the location of these monitoring stations on a map over Edmonton and Calgary. The results of the two periods of three days were considered, one in July and one in January. All five stations shown in this figure are population exposure stations under the NAPS program.

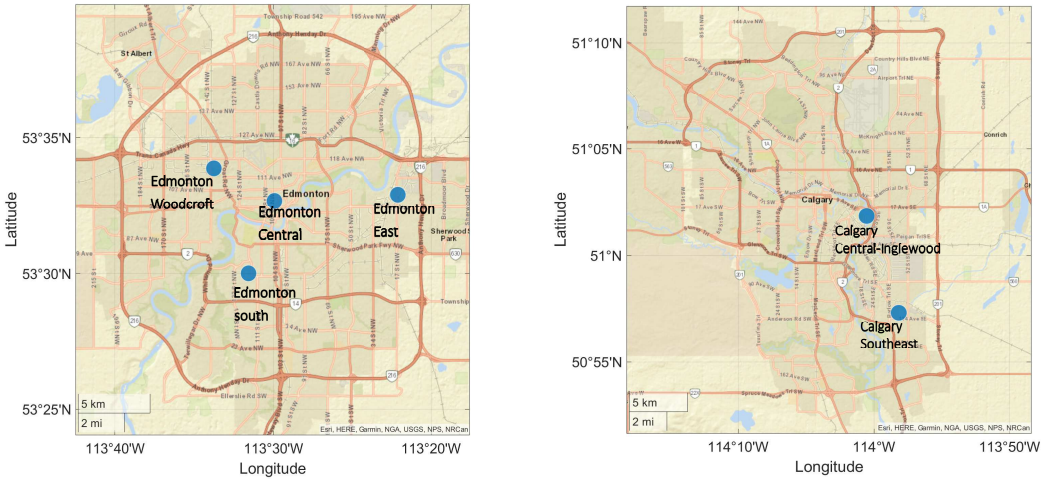

(a) Edmonton (b) Calgary

Figure 4.10: Monitoring stations at major cities

A summary of the zeroing-out results for the major cities monitoring stations is presented in table 4.1. To generate this table, the NO_2 reduction due to the zeroing out of each source was averaged over the three-day of the simulation period. The sensitivity simulations show that the contribution of UOG to NO_2 emission at these stations is almost one-tenth of the impact of mobile sources. For example, averaging the sensitivity simulation results for Edmonton shows that if the mobile sources could be eliminated the NO_2 concentration will reduce by 49% in January and by 60% in

July. The elimination of UOG will only decrease the NO_2 concentration by 5.7% in January and 6% in July for Edmonton. Although the sensitivity of UOG sources is slightly higher for the stations in Calgary compared to Edmonton, the contribution of UOG is still less than 10% for both periods when UOG is zeroed out. Thus the impact of mobile sources is almost four times higher with 40% contribution to the NO_2 concentration in the two major cities. Further, the base NO_2 concentration in January (≈28 ppb) is two times higher than that for July period (≈15 ppb) in both Edmonton and Calgary.

Table 4.1: Comparing the results of zeroing out of Mobile sources and UOG sources

Station Name	Jan			July		
		NO_2 reduction (%) due to			NO_2 reduction (%) due to	
	Base conc. (ppb)	Mobile zero-out	UOG zeroout	Base conc. (ppb)	Mobile zero-out	UOG zeroout
Edmonton Central	30.2	-49.9	-3.9	15.9	-64.3	-5.8
Edmonton East	25.5	-50.1	-7.2	16.2	-49.9	-5.2
Edmonton South	27.5	-48.5	-5.4	15.5	-61.3	-6.0
Edmonton-Woodcroft	25.4	-47.6	-6.3	13.2	-63.2	-6.7
Calgary Central-Inglewood	31.8	-33.8	-9.3	15.9	-36.1	-9.3
Calgary Southeast	23.0	-50.9	-11.9	15.6	-46.6	-8.8

Since each monitoring station is classified with a nearby sources, to further evaluate the sensitivity of NO_2 concentrations to the mobile transportation and UOG emission sources, the site type station category was employed. The site type divides stations into 4 categories: 1. Population Exposure (PE), 2. Point sources (PS), 3. Regional Background (RB), and 4. Traffic (T). The average NO_2 percentage reduction at the monitoring station in 4 different categories are shown for two sensitivity scenarios: (a) Mobile transportation zero-out, fig. 4.11; (b) UOG zero-out scenarios, fig. 4.11. The x-axis shows NO_2 percentage reduction when mobile emissions are set to zero versus the y-axis which shows the NO_2 percentage reduction when UOG emissions are set to zero. The majority of the PE stations (blue points in fig. 4.11) are most sensitive to mobile transportation sources of NO_2. RB stations (red points in fig. 4.11) are most sensitive to UOG sources. For stations in which mobile sources are zeroed out,

a 30% reduction of the NO_2 concentration occurs almost exclusively to the PE and T categories. In contrast, when UOG is zeroed out, many RB stations experience more than 30% NO_2 reduction. For the two PS stations, one is near Fort Mckay oil industries and is more affected by UOG, and the other is in Edmonton and is affected by mobile sources.

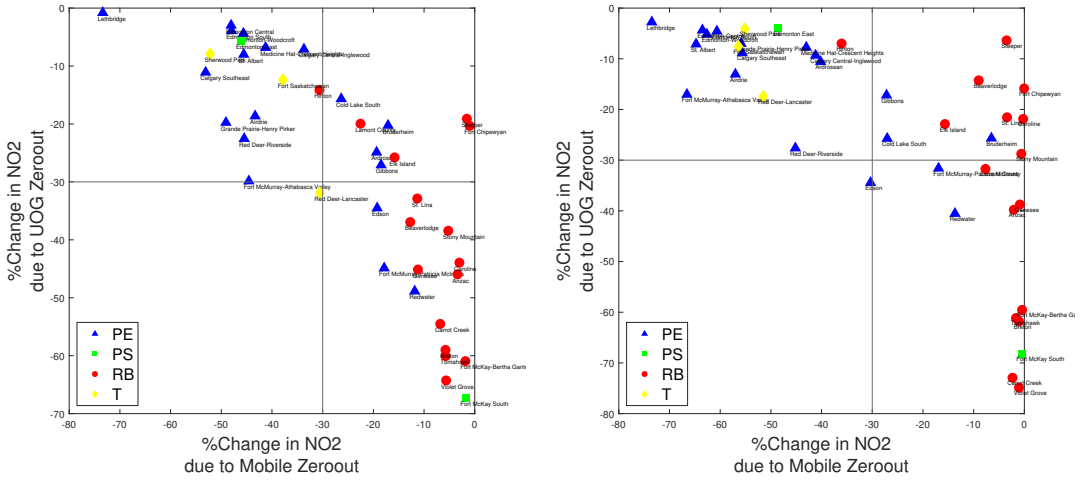

(a) Jan (b) July

Figure 4.11: Comparison the effect of zeroing out of Mobile and UOG sources on the NO_2 concentration for all monitoring stations. Each scatter shows a 3-day averaged NO_2 reduction due to zero-out

The bar chart in fig. 4.12, summarizes these results by site type, giving the percentage reduction and absolute reduction in ppb. Due to zeroing out of mobile sources, PE stations experience 36% (6.5 ppb) and 46% (3.6 ppb) NO_2 reduction in Jan and July periods respectively. However, PE stations, when UOG emission is set to zero, only see 18% (1.7 ppb) and 16%(0.9 ppb) NO_2 reduction in Jan and July period. Traffic stations (T) follow the same trend and results as PE stations. RB site types experience a completely different trend. Zeroing out of UOG in these stations leads to the 40% (2 ppb) and 30% (0.8 ppb) NO_2 reduction in January and July periods respectively. The average effect of mobile source in this type of station is considerably lower (less than 10% (1 ppb) for both simulation periods).

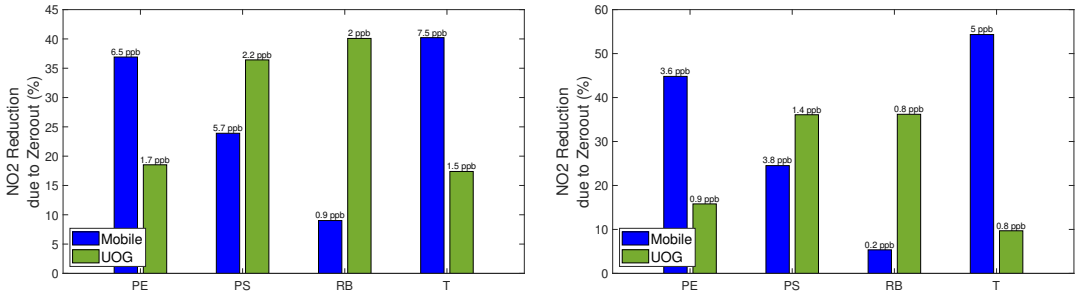

(a) Jan (b) July

Figure 4.12: Sensitivity analysis: impact of zeroing out of Mobile and UOG sources on the NO_2 concentration for different site types. Blue columns show the effect of mobile source zero-out and green columns indicate UOG zero-out impact. The vertical axis shows the absolute percentage change of concentration and the number over each column shows the respective absolute value of concentration change in ppb

4.3.2 Sensitivity Analysis: Emission Perturbation

Rather than a zero out sensitivity analysis, a smaller perturbation is applied in this section. This is to check the linearity of the model to perturbations. Model simulation for the July period with a perturbations of 1%, 5%, 25%, 50%, and 75% emission reduction of mobile and UOG sources were performed. The average of the first three days in the July period are used to find the sensitivity and resulting slope of NO_2 variation due to changes in emission sources. The results of these scenarios are then grouped by site type and averaged over the July period. These results are shown in figs. 4.13 and 4.14. Each data point indicates the average NO_2 reduction over all stations in the respective category due to the emission reduction of either Mobile sources or UOG sources and is shown in fig. 4.13. The same analysis is done for Ozone in fig. 4.14.

The response of the NO_2 concentration to the emission source reduction is almost linear which was not an obvious result considering the complex non-linear model. This is attributed to NO_2 being a source-dependent chemical species, i.e., there is no major atmospheric chemical reaction that leads to the considerable production of NO_2. The behavior of O_3 is non-linear since the most of O_3 concentration in the atmosphere comes from a series of chemical reactions such as reactions 2.3, 2.4, and

2.9.

The approximate slope of the NO_2 reduction due to the emission changes shows the sensitivity. For PE and T site types, the slope of NO_2 reduction due to the perturbation of mobile emission is considerably larger than that for the UOG sources. For RB site type, the perturbation on UOG emission has a larger slope (sensitivity) compared to the Mobile sources. The absolute NO_2 concentration is much lower (averaged near 2 ppb) in RB site types.

This perturbation sensitivity analysis give the (approximate) slope or sensitivity of NO_2 concentration to change in mobile source emissions, which is more pronounced in PE site types. The sensitivity to UOG is highest in non-urban (RB) site types.

The same perturbation analysis is used to look at the sensitivity of O_3 to site types for July period, which is shown in fig. 4.14. Here an emission reduction of Mobile sources leads to an increase of Ozone concentration for all site types in July period. This is attributed to the tropospheric chemistry of these two chemicals through reactions 2.3, 2.4, and 2.5 (null cycle) and the NO_x regime. This behavior usually happens at relatively high levels of NO_2 concentration, which is called the NO_x-saturated regime. In this regime, Ozone concentration varies in the opposite direction of NO_2 variation, which is evident from the left column of fig. 4.14. Therefore, it can be concluded that the Alberta NO_2 regime is NO_x-saturated. Considering the fact that VOCs affect O_3 production (see section 2.4.2), the reason that O_3 response to emission change from mobile sources is different from the response to UOG emission perturbation could be related to the high level of VOC emission from UOG sources.

Using the perturbation method the NO_2 concentration sensitivity to emission changes was analyzed. A linear response of the NO_2 concentration to the perturbation in emission from the Mobile and UOG sources was found at all site type for the July period. This can now be used to estimate how much the emission from the mobile sector should be reduced to meet the 2025 Canadian Ambient Air Quality Standards.

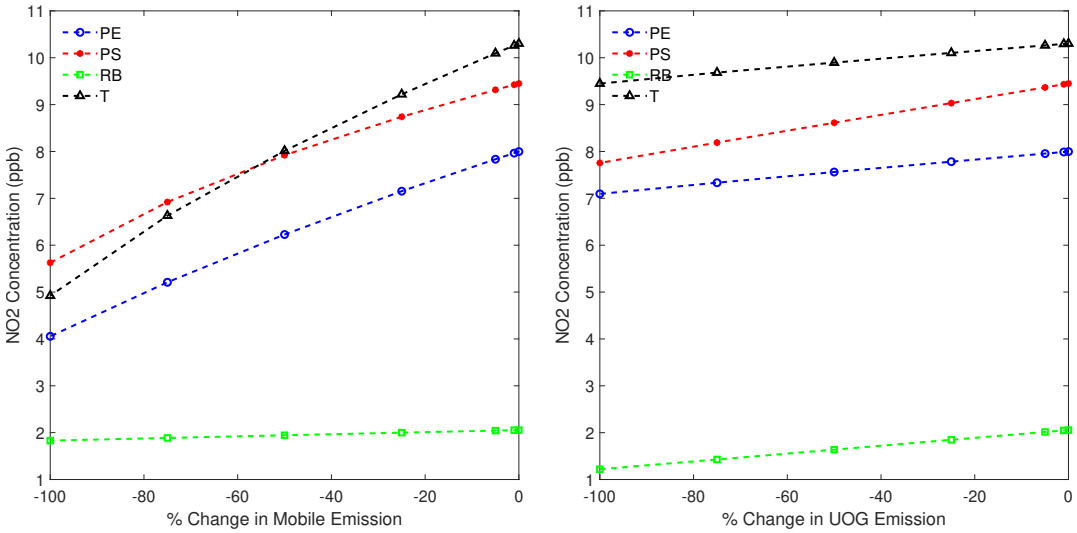

(a) Mobile (b) UOG

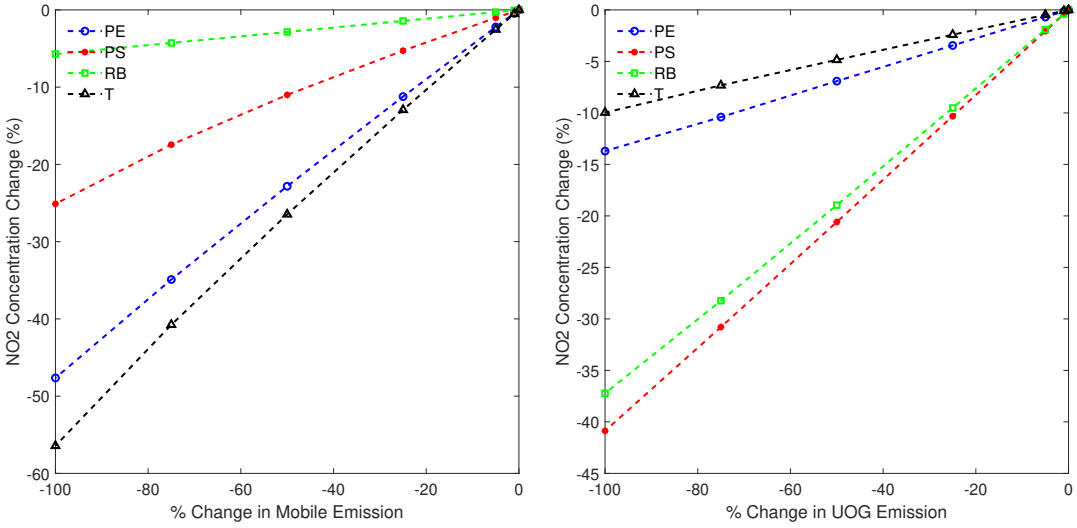

(c) Mobile (d) UOG

Figure 4.13: Comparison the effect of emission perturbation on the NO_2 concentration in July period. The first row shows NO_2 absolute change due to perturbations. The second row shows NO_2 percentage of variation due to perturbations. The left column shows the Mobile sources effect and right colum shows UOG effect.

Since all the stations, which will be in red management level by the year 2025 in table 2.3, are population exposure stations the sensitivity slope can be used to estimate the emission reduction needed. First, assume that the emission will be constant and equal to its value in the year 2019. To reduce the management level from red to yellow for the year 2025, the NO_2 annual average should be less than

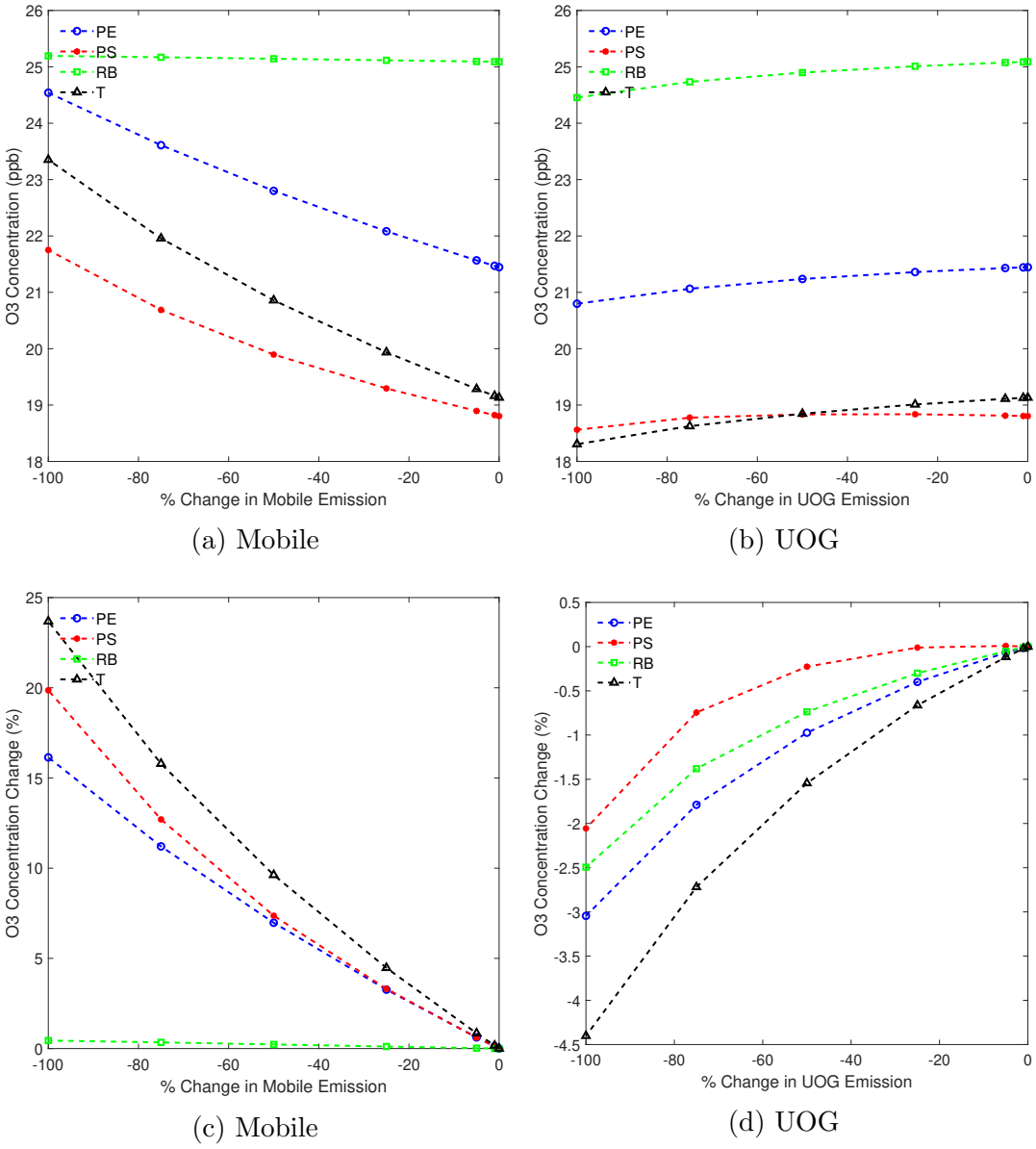

(a) Mobile (b) UOG

(c) Mobile (d) UOG

Figure 4.14: Comparison the effect of emission perturbation on the O_3 concentration in July period. The first row shows O_3 absolute change due to perturbations. The second row shows O_3 percentage of variation due to perturbations. The left column shows the Mobile sources effect and right colum shows UOG effect.

12 ppb. The required concentration reduction needed to achieve this standard is summarized in table 4.2. Then, using the data in fig. 4.13c, a linear curve was fit to the NO_2 concentration change of the PE site type to get the sensitivity (slope).

$$y = 0.4732x + 0.2689 \tag{4.2}$$

This curve fits a straight line with an $R^2 = 0.995$. In eq. (4.2), y represents the NO_2 concentration change (%) and x is the NO_2 emission change (%). It is then simple to calculate the required emission change for achieving the CAAQS 2025 threshold. The results are shown in table 4.2. If the average of the changes is taken for monitoring stations in this table, for an average a minimum of 23% reduction in the emission of mobile sources is needed to have both cities move from red to yellow management level base on the CAAQS for the year 2025.

Table 4.2: Reduction of mobile source emission required for realizing the CAAQS 2025 for Edmonton and Calgary based on sensitivity analysis

	Annual Averaged NO_2	% Concentration Change needed for meeting CAAQS	% Emission Change required
Edmonton Central	14.9	19.5	40.6
Edmonton East	12.1	0.8	1.2
Edmonton-Woodcroft	12.4	3.2	6.2
Calgary Central-Inglewood	15.5	22.6	47.2
Calgary Southeast	13.3	9.8	20.1
Average	13.64	11.2	23.0

4.4 Air Quality Health Index

AQHI is a measure to inform the public about the quality of the surrounding air and the health risk associated with exposure to air pollution. This measure was first introduced by Steib et. al. [14]. AQHI is a value between 1 to 10. To calculate AQHI in Alberta, the ambient concentrations of each $PM_{2.5}$, SO_2, NO_2, O_3, and CO are first compared to specific thresholds defined by the Government of Alberta [102]. These thresholds are 80 $\mu g/cm^3$, 172 ppb, 159 ppb, 76 ppb, and 13 ppm for $PM_{2.5}$, SO_2, NO_2, O_3, and CO respectively. If even one of the pollutants exceeds the thresholds the AQHI will be reported by value 7 (high risk) [102]. If none of them exceeds then the 3-hr moving average of O_3, NO_2, and $PM_{2.5}$ concentration are used to calculate AQHI as:

$$\frac{10}{10.4} * (100 * (e^{0.000871*NO_2} - 1 + e^{0.000537*O_3} - 1 + e^{0.000297*PM_{2.5}} - 1)) \qquad (4.3)$$

Where NO_2 and O_3 are 3-hr moving average in ppb and $PM_{2.5}$ is 3-hr moving average in $\mu g/m^3$. AQHI in rural areas might be affected by industrial activities and there is a possibility of exceeding the thresholds prior to calculating the AQHI based on the eq. (4.3). In this study, the AQHI only calculates for urban areas of Edmonton and Calgary. To calculate AQHI, the simulation results for the base case scenario were used for NO_2 and O_3, and for $PM_{2.5}$ observation data of the respective period were employed for each station. The time variation of AQHI (calculated from the eq. (4.3)) and 3-hour averaged moving concentrations are shown in fig. 4.15. The AQHI values and the respective 3-hr average concentration of three major pollutants are plotted for both January and July periods for 2 stations in Calgary and 3 stations in Edmonton. The AQHI at these five urban stations in the July period did not exceed the AQHI of 3. This indicates that there is a low health risk of exposure to this level of concentration. However, in the January period, a considerable fraction of AQHI is level 4 and even sometimes exceeded the AQHI of 5 and 6 at Calgary Central and Edmonton Central stations. The reason is the higher level of pollution in winter, which is attributed to the atmospheric stabiliy and temperature inversion - see fig. 4.2 and fig. 4.5. This leads to the accumulation of pollution at lower altitudes. The time-series in fig. 4.15 indicate that AQHI is more sensitive to the NO_2 concentration rather than the two other pollutants. For example, the local maximum of AQHI happens at the local maximum of NO_2 in fig. 4.15. Since the AQHI in July did not exceed level 3, the AQHI in the January period will be further examined.

After analyzing the temporal variation of AQHI, the effects of zeroing out of mobile and UOG sources on the improvement of the air quality were examined for the same five stations in Edmonton and Calgary. The zeroing out scenarios simulated for the 3-day period from January 11th to 13th, so in Fig.4.16 the simulated AQHI at

these monitoring stations are shown. Each row represents a specific scenario and each column shows one of the five individual stations. The AQHI is calculated at 1-hour time resolution for each case and shown as a heat map. Comparing the base case, Calgary central station and Edmonton Central station experienced the lowest air quality. In these two stations, the fraction of hours in which the AQHI exceeded level 3 is higher compares to the other station. In Calgary Central, an AQHI of 6 on January 11th, 21:00 (UTC) is achieved.

Next zeroing out scenarios of UOG and Mobile sources is considered. For UOG zeroing out almost no changes on the AQHI is seen for the five stations - look at section 4.4. So if the entire UOG emission were removed the AQHI at the city would not change much. This is as expected and confirms the results of the sensitivity analysis. Next, the mobile sources are zeroed out in fig. 4.16a. This reduces the AQHI at all monitoring stations considerably - compare section 4.4 to fig. 4.16a. All the stations experienced AQHI of 3 or below except Calgary Central-Inglewood station. AQHI at this station is probably affected by other sources rather than UOG and Mobile sources.

It is important to note that the simulation model (CMAQ) is quiet sensitive to the accuracy of the emission files. The discrepancies between real-world emission and model emission files could modify or change the results. A more detailed and accurate emission inventory, particularly Mobile sources (traffic patterns, types of vehicles etc.), are needed to make precise statement in the cities.

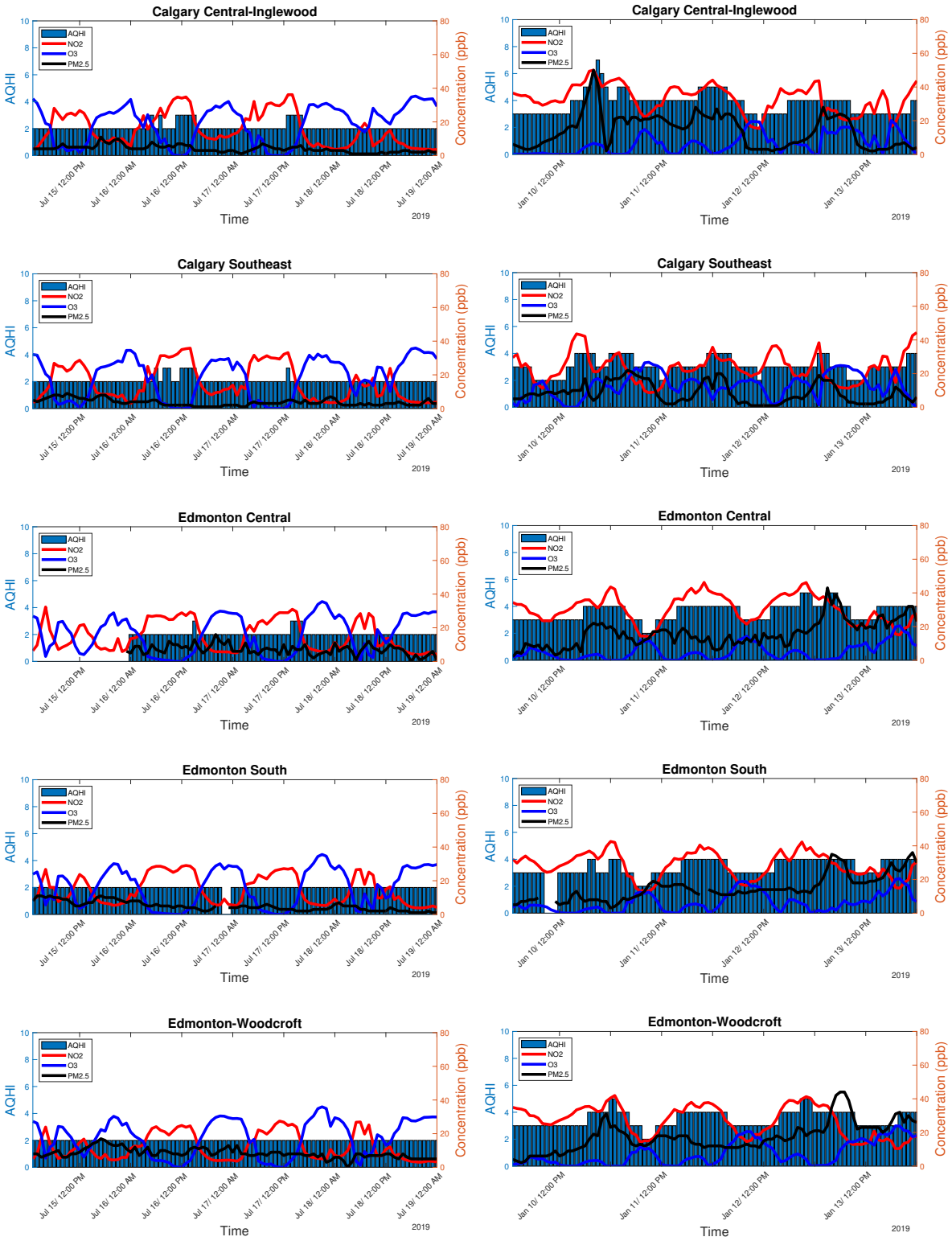

(a) July (b) Jan

Figure 4.15: AQHI (blue box) and pollutant concentration (colored lines) at major cities monitoring stations. AQHI is calculated with eq. (4.3). The left column is July period and the right column is January period

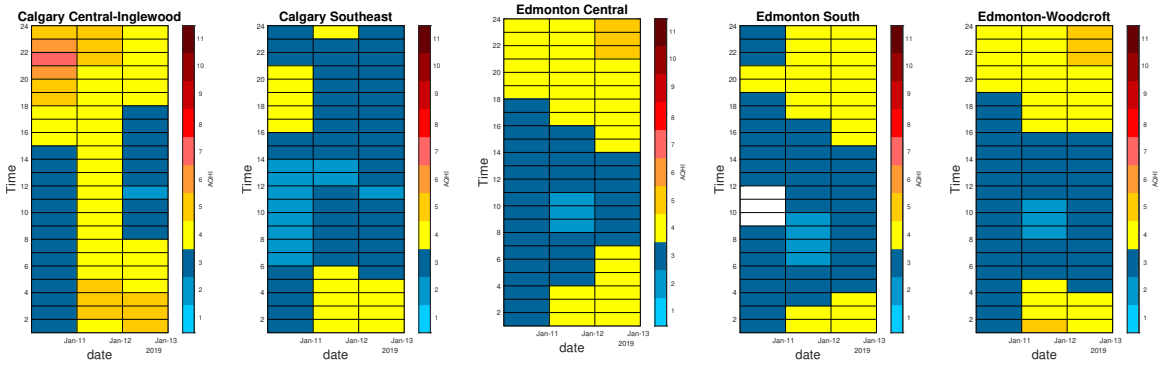

(a) Base

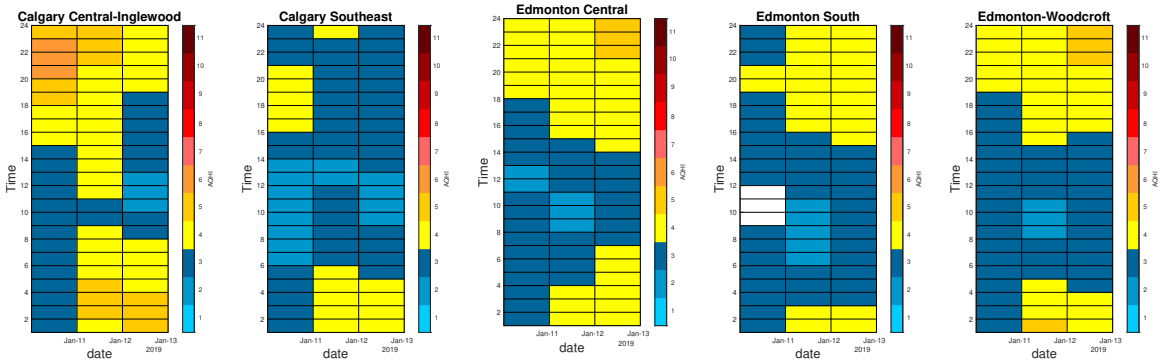

(b) UOG

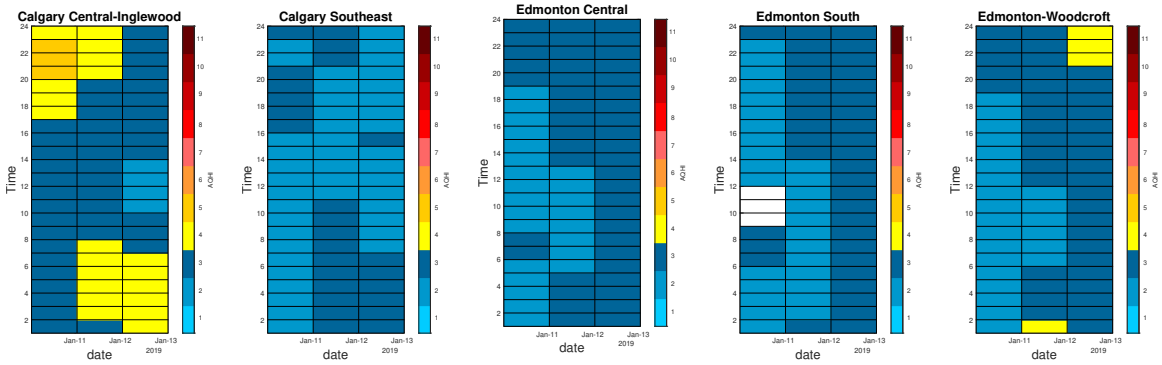

(c) Mobile

Figure 4.16: Zeroing-out scenarios on AQHI for Edmonton and Calgary. (a) Base case January 2019, (b) Zeroing out of UOG, (c) Zeroing out of mobile sources. Each column represents one monitoring station

Chapter 5

Summary, Conclusions and Future Work

An air quality atmospheric model was employed to address the NO_2 exceedance from the 2025 CAAQS in Alberta. The model is a modular platform consisting of three major modules. This model consists of an open-source Weather Research Forecast (WRF) with a nested domain and a resolution of 4km×4km over the province of Alberta. The model has 32 layers in the vertical direction and computes meteorological filed including wind speed and temperature. To add emission inventory data the SMOKE module, which is an open-source emission inventory processing tool, provides a spatiotemporal profile for the emission inventory data. This data was obtained from the government of Alberta. The Community Multiscale Air Quality modeling (CMAQ), an open-source model, analyses the behavior of chemical species of NO_2 and O_3 and is coupled one-way with the WRF model. The results provide valuable insight into the primary sources of NO_2 emission in Alberta and possible emission abatement strategies to meet CAAQS.

Temperature and wind speed from WRF and NO_2 and O_3 concentrations from CMAQ were validated against ground observation at 40 NAPS monitoring stations in Alberta. Validation was done for two periods, one in January 2019 (10th-20th) and one in July 2019 (15th-25th). The meteorological calculation (WRF), when validated, is more accurate for replicating the temperature and wind speed for July compared

to the January time period. However, for both periods the model results satisfy the standard benchmark criteria for model performance in the literature. It was found that WRF modeling results are affected by the grid resolution, the resolution of the land-use model, the proximity to open water, the tendency of the WRF model to overpredict the surface albedo in cold seasons, and the sensitivity of wind speed to elevation.

For the CMAQ module validation results, the model captures the NO_2 and Ozone concentration and their diurnal variations within published uncertainty in the literature. Similar to the WRF module validation results, the CMAQ model is more accurate in July than in January. CMAQ performance is dependent on WRF, and WRF is more accurate in July. For Ozone concentration, the model captures the experimental trends for Ozone levels above 10 ppb with an underestimation for the Ozone values lower than 10 ppb. The model performance for NO_2 is statistically similar for both summer and winter modeling periods and the model satisfies published benchmark criteria for reproducing NO_2 concentration. Sources of discrepancy between CMAQ modeling results and observation data can be linked to the inadequacy of the input data, the bias in the modeled meteorological fields, the incommensurability, the uncertainty in emission inventory, boundary conditions, and initial conditions. The hourly simulation data shows that the average daily NO_2 concentration in winter is $18 \leq NO_2 \leq 24$ ppb in Calgary and Edmonton, three times higher than the average $6 \leq NO_2 \leq 8$ ppb in summer. Industrial areas and oilsands areas also experience the same trend from $3 \leq NO_2 \leq 5$ ppb in the summer to $9 \leq NO_2 \leq 13$ ppb in the winter.

Using the validated model, a sensitivity analysis of NO_2 concentration to primary emission sources, including mobile and UOG sources, is performed. First, a "zero-out" study, where the contribution of each source to the NO_2 concentration is individually set to zero, is conducted. In particular, Mobile sources and UOG sources are examined. Analyzing modeling results for stations based on the site type category

introduced by NAPS revealed that NO_2 concentration at Population Exposure (PE) and Traffic (T) stations are highly affected by emissions from mobile sources. 48% of total NO_x emission in Alberta comes from UOG and 15% comes from mobile sources. The sensitivity of site types PE to UOG are less than 20% and to mobile are 45%, while for site types T they are 10% and 50%, respectively. The sensitivity analysis results at monitoring stations located in the major cities of Edmonton and Calgary show that 54% and 46% of total NO_2 concentration are emitted from mobile sources for January and July modeling periods respectively. However, in these stations, the impact of UOG sources is less than 10% for each modeling period. The UOG sources effect is more pronounced at NAPS Regional Background (RB) site types and outside of urban areas.

To determine the trend of the NO_2 concentration and its response to smaller changes, small perturbations from normal emission (instead of zeroing out) were applied. The modeling results for small perturbations of NO_2 input show that NO_2 concentration varies linearly with the emission changes of mobile sources and UOG sources. However, small perturbations in emissions result in a non-linear response of O_3. The linear response of the NO_2 concentration to the change of mobile emission sources, allows the required emission changes for the realization of 2025 CAAQS in major cities to be calculated. Using the 2019 annual average measured NO_2, the required 2025 CAAQS NO_2, and the linear NO_2 behavior to mobiles sources emission reduction, an average of 23% emission reduction from mobile sources is required for meeting the standards. In the two large Alberta cities, a small perturbation in mobile NO_2 emission sources results in an inverse response with O_3. These results indicate that the Alberta NO_2 regime is NO_x-saturated.

Finally, the impact of criteria air contaminants of NO_2 and O_3 concentration on AQHI were investigated. Analysis of the hourly AQHI over 3 days in each of summer and winter periods indicated that the AQHI is more sensitive to the NO_2 variation compared to the Ozone and $PM_{2.5}$ variation. In the major cities of Edmonton and

Calgary, the impacts of the NO_2 major sources on the AQHI were evaluated, using the results of zero-out scenarios. As expected, in cities, AQHI is more sensitive to Mobile sources compared to UOG sources.

5.1 Future Work

One of the important parameters that affects the model performance is the grid resolution of the chemical transport model [103]. Among common air contaminants, the effect of grid resolution is more pronounced for NO_2 concentration [104]. Generally, the sensitivity of the species to grid resolution depends on the lifetime and transport range of that species [105]. Assessing the impact of grid resolution on NO_2 modeling performance for the province of Alberta is proposed although it will need significant computation. In this study, the horizontal grid resolution of the finer domain was 4km $\times$ 4km. A further study could analyze the finer domain of 1km $\times$ 1km. However, in such a resolution, a more detailed emission inventory file is needed and the presence of traffic data would be necessary. Further a 1km $\times$ 1km grid resolution will require about 16 times higher computational time.

References

[1] J.-P. Rodrigue, *The geography of transport systems the geography of transport systems*, 5th ed. Routledge, 2020.

[2] G. Shaddick, M. L. Thomas, P. Mudu, G. Ruggeri, and S. Gumy, "Half the world's population are exposed to increasing air pollution," *NPJ Climate and Atmospheric Science*, vol. 3, no. 1, Jun. 2020.

[3] H. Magsi, "Industrialization, environment and pollution," *The diplomatic insight*, vol. 7, pp. 24–36, 2014.

[4] "Health Impacts of Air Pollution in Canada: Estimates of premature deaths and nonfatal outcomes," Health Canada, Tech. Rep., 2021.

[5] CASA, "Approaches and Solutions for CAAQS Achievement in Alberta," Sep. 2021, https://www.casahome.org/uploads/source/CASA_Approaches_and_Solutions_for_CAAQS_Achievement_in_Alberta_Project_Charter_Revised_September_2021_final.pdf, Accessed on 01/18/2023.

[6] *Air indicators – Nitrogen dioxide*, https://www.alberta.ca/air-indicators-nitrogen-dioxide.aspx#:~:text=Levels%20of%20NO2%20are,including%20personal%20vehicles%20and%20industry., Accessed on 01/18/2023.

[7] P. Huangfu and R. Atkinson, "Long-term exposure to NO_2 and O_3 and all-cause and respiratory mortality: A systematic review and meta-analysis," *Environment International*, vol. 144, p. 105 998, 2020.

[8] H. Fang and G. Michalski, "Assessing the roles emission sources and atmospheric processes play in simulating δ^{15}N of atmospheric NO_x and NO_3^- using CMAQ (version 5.2.1) and SMOKE (version 4.6)," *Geoscientific Model Development*, vol. 15, no. 10, pp. 4239–4258, 2022.

[9] *Technology innovation and emissions reduction system*, https://www.alberta.ca/technology-innovation-and-emissions-reduction-system.aspx, Accessed on 01/18/2023.

[10] *Air Quality Models*, https://www.epa.gov/scram/air-quality-models, Accessed on 01/18/2023.

[11] J. B. Johnson, "An Introduction to Atmospheric Pollutant Dispersion Modelling," *Environmental Sciences Proceedings*, vol. 19, no. 1, 2022.

[12] "Effects of the spring 2020 COVID-19 public health emergency on urban air quality in Alberta," Government of Alberta, Ministry of Environment and Parks., Tech. Rep., 2022.

[13] U. Nopmongcol *et al.*, "Provincial Air Quality Photochemical Modelling," Alberta Government, Tech. Rep., 2018.

[14] D. M. Stieb, R. T. Burnett, M. Smith-Doiron, O. Brion, H. H. Shin, and V. Economou, "A New Multipollutant, No-Threshold Air Quality Health Index Based on Short-Term Associations Observed in Daily Time-Series Analyses," *Journal of the Air & Waste Management Association*, vol. 58, no. 3, pp. 435–450, Mar. 2008.

[15] "Population exposure to outdoor air pollutants," Environment and Climate Change Canada, Tech. Rep., 2021.

[16] *Environment and Protected Areas*, https://www.alberta.ca/environment-and-protected-areas.aspx, Accessed on 01/18/2023.

[17] *Environmental Protection and Enhancement Act, Revised Statutes of Alberta 2000 Chapter E-12*, https://open.alberta.ca/publications/e12#:~:text=Description,approval%20or%20registration%20is%20required., Accessed on 01/18/2023, 2022.

[18] *Alberta ambient air quality objectives and guidelines summary*, https://open.alberta.ca/publications/9781460134856#summary, Accessed on 10/19/2022, 2019.

[19] *Canadian Ambient Air Quality Standards*, https://ccme.ca/en/air-quality-report Acessed on 01/18/2023.

[20] C. C. of Ministers of the Environment, *Guidance Document on Achievement Determination for Canadian Ambient Air Quality Standards for Nitrogen Dioxide*. Canadian Council of Ministers of the Environment, 2020.

[21] C. C. of Ministers of the Environment, *Guidance Document on Achievement Determination for Canadian Ambient Air Quality Standards for Ozone*. Canadian Council of Ministers of the Environment, 2012.

[22] *Canadian Ambient Air Quality Standards*, https://www.alberta.ca/canadian-ambient-air-quality-standards.aspx, Accessed on 11/9/2022.

[23] P. Thunis *et al.*, "Sensitivity of air quality modeling to different emission inventories: A case study over Europe," *Atmospheric Environment*, vol. 10, p. 100 111, 2021.

[24] X. Li, S. A. Hussain, S. Sobri, and M. S. Md Said, "Overviewing the air quality models on air pollution in Sichuan Basin, China," *Chemosphere*, vol. 271, p. 129 502, 2021.

[25] I. Ribeiro *et al.*, *Air Quality Modelling and Its Applications*, G. Cao and R. Orrù, Eds. Dordrecht: Springer Netherlands, 2014, pp. 45–56.

[26] K. Vijayaraghavan *et al.*, "Photochemical model evaluation of the ground-level ozone impacts on ambient air quality and vegetation health in the Alberta oil sands region: Using present and future emission scenarios," *Atmospheric Environment*, vol. 141, pp. 209–218, 2016.

[27] S. Cho, P. McEachern, R. Morris, T. Shah, J. Johnson, and U. Nopmongcol, "Emission sources sensitivity study for ground-level ozone and $PM_{2.5}$ due to oil sands development using air quality modeling system: Part I- model evaluation for current year base case simulation," *Atmospheric Environment*, vol. 55, pp. 533–541, 2012.

[28] S. Cho, R. Morris, P. McEachern, T. Shah, J. Johnson, and U. Nopmongcol, "Emission sources sensitivity study for ground-level ozone and $PM_{2.5}$ due to oil sands development using air quality modelling system: Part II – Source apportionment modelling," *Atmospheric Environment*, vol. 55, pp. 542–556, 2012.

[29] B. N. Duncan *et al.*, "A space-based, high-resolution view of notable changes in urban NO_x pollution around the world (2005-2014)," *Journal of Geophysical Research: Atmospheres*, vol. 121, no. 2, pp. 976–996, Jan. 2016.

[30] M. Ravina, G. Caramitti, D. Panepinto, and M. Zanetti, "Air quality and photochemical reactions: analysis of NO_x and NO_2 concentrations in the urban area of Turin, Italy," *Air Quality, Atmosphere & Health*, vol. 15, no. 3, pp. 541–558, Feb. 2022.

[31] Y. Shen *et al.*, "Increased diurnal difference of NO_2 concentrations and its impact on recent ozone pollution in eastern China in summer," *Science of The Total Environment*, vol. 858, p. 159 767, 2023.

[32] S. Platikanov, M. Terrado, M. T. Pay, A. Soret, and R. Tauler, "Understanding temporal and spatial changes of O_3 or NO_2 concentrations combining multivariate data analysis methods and air quality transport models," *Science of The Total Environment*, vol. 806, p. 150 923, 2022.

[33] C. Silveira, J. Ferreira, P. Tuccella, G. Curci, and A. I. Miranda, "Combined Effect of High-Resolution Land Cover and Grid Resolution on Surface NO_2 Concentrations," *Climate*, vol. 10, no. 2, 2022.

[34] G. Ghermandi, S. Fabbi, G. Veratti, A. Bigi, and S. Teggi, "Estimate of Secondary NO_2 Levels at Two Urban Traffic Sites Using Observations and Modelling," *Sustainability*, vol. 12, no. 19, p. 7897, Sep. 2020.

[35] I. Oh *et al.*, "Comparison of different hybrid modeling methods to estimate intra-urban NO_2 concentrations," *Atmospheric Environment*, vol. 244, p. 117 907, 2021.

[36] Y. Shen, F. Jiang, S. Feng, Y. Zheng, Z. Cai, and X. Lyu, "Impact of weather and emission changes on NO_2 concentrations in China during 2014–2019," *Environmental Pollution*, vol. 269, p. 116 163, 2021.

[37] N. Zhan, X. Zhang, X. Lu, and J. Qin, "Long-term variations of ground-level NO_2 concentrations along coastal areas in China," *Atmospheric Environment*, vol. 283, p. 119 158, 2022.

[38] S. Zhu, M. M. Kinnon, B. P. Shaffer, G. Samuelsen, J. Brouwer, and D. Dabdub, "An uncertainty for clean air: Air quality modeling implications of underestimating VOC emissions in urban inventories," *Atmospheric Environment*, vol. 211, pp. 256–267, 2019.

[39] *National Pollutant Release Inventory*, https://www.canada.ca/en/services/environment/pollution-waste-management/national-pollutant-release-inventory.html, Accessed on 11/10/2022.

[40] U. E. P. Agency, *Basic Information about Nonpoint Source (NPS) Pollution*, https://www.epa.gov/nps/basic-information-about-nonpoint-source-nps-pollution#:~:text=Nonpoint%20source%20pollution%20can%20include,forest%20lands%2C%20and%20eroding%20streambanks, Accessed on 01/18/2023.

[41] J. Seinfeld and S. Pandis, *Atmospheric Chemistry and Physics: From Air Pollution to Climate Change*. Wiley, 2016.

[42] *Criteria air pollutants*, https://www.epa.gov/criteria-air-pollutants ,Accessed on 10/19/2022.

[43] C. Brown, A. Thi, and G. Wentworth, "Status of Air Quality in Alberta: Air Zones Report 2018-2020," Government of Alberta, Ministry of Environment and Parks., Tech. Rep., 2022.

[44] S. Oesch and M. Faller, "Environmental effects on materials: The effect of the air pollutants SO_2, NO_2, NO and O_3 on the corrosion of copper, zinc and aluminium. A short literature survey and results of laboratory exposures," *Corrosion Science*, vol. 39, no. 9, pp. 1505–1530, 1997.

[45] L. M. David and P. R. Nair, "Tropospheric column O_3 and NO_2 over the Indian region observed by Ozone Monitoring Instrument (OMI): Seasonal changes and long-term trends," *Atmospheric Environment*, vol. 65, pp. 25–39, 2013.

[46] A. J. Cohen *et al.*, "The global burden of disease due to outdoor air pollution," *Journal of Toxicology and Environmental Health, Part A*, vol. 68, no. 13-14, pp. 1301–1307, 2005.

[47] M. Chen *et al.*, "Clinical characteristics and risk factors for fatal outcome in patients with 2019-coronavirus infected disease (COVID-19) in Wuhan, China," 2020.

[48] M. Podrez, "An update to the ambient ratio method for 1-h NO_2 air quality standards dispersion modeling," *Atmospheric Environment*, vol. 103, pp. 163–170, 2015.

[49] J. J. Zhang, Y. Wei, and Z. Fang, "Ozone Pollution: A Major Health Hazard Worldwide," *Frontiers in Immunology*, vol. 10, Oct. 2019.

[50] X. Xu, T. Zhang, and Y. Su, "Temporal variations and trend of ground-level ozone based on long-term measurements in Windsor, Canada," *Atmospheric Chemistry and Physics*, vol. 19, no. 11, pp. 7335–7345, 2019.

[51] J. Gustavo and A. Ugarte, "Use of the CMAQ and WRF-CHEM Models to Investigate Tropospheric Ozone And Particulate Matter in the El Paso-Juarez Airshed," M.S. thesis, 2010.

[52] J. Coates, K. A. Mar, N. Ojha, and T. M. Butler, "The influence of temperature on ozone production under varying NO_x conditions: a modelling study," *Atmospheric Chemistry and Physics*, vol. 16, no. 18, pp. 11 601–11 615, 2016.

[53] Z. Rebello, "Evaluating Surface Concentrations of NO_2 and O_3 in Urban and Rural Regions by Combining Chemistry Transport Modelling with Surface Measurements," M.S. thesis, 2010.

[54] X. Jin, "Observing the distributions and chemistry of major air pollutants (O_3 and $PM_{2.5}$) from space: trends, uncertainties, and health implications," Ph.D. dissertation, 2020.

[55] S. Sillman, "Tropospheric Ozone and Photochemical Smog," *Treatise on Geochemistry*, vol. 9, p. 612, Dec. 2003.

[56] M. Z. Jacobson, *Fundamentals of Atmospheric Modeling*. Cambridge University Press, May 2005.

[57] K. Ashrafi and G. Hoshyaripour, "A Model to Determine Atmospheric Stability and its Correlation with CO Concentration," *World Academy of Science, Engineering and Technology, International Journal of Environmental, Chemical, Ecological, Geological and Geophysical Engineering*, vol. 2, pp. 96–101, 2008.

[58] R. C. Gilliam, C. Hogrefe, and S. Rao, "New methods for evaluating meteorological models used in air quality applications," *Atmospheric Environment*, vol. 40, no. 26, pp. 5073–5086, 2006, Special issue on Model Evaluation: Evaluation of Urban and Regional Eulerian Air Quality Models.

[59] C. Emery, E. Tai, and G. Yarwood, "Enhanced meteorological modeling and performance evaluation for two Texas ozone episodes," *Prepared for the Texas natural resource conservation commission, by ENVIRON International Corporation*, 2001.

[60] D. McNally, "12km MM5 Performance Goals," 2010.

[61] J. Bowden, K. Talgo, and Z. Adelman, "WAQS WRF Meteorological Model – Winter Modeling Application/Evaluation," UNC Institute for the Environment, Chapel Hill, NC, Tech. Rep., 2015.

[62] *Provincial Air Quality Management*, https://www.alberta.ca/provincial-air-quality-management.aspx#:~:text=Alberta's%20Environmental%20Monitoring%20and%20Science,measure%20the%20ambient%20air%20quality., Accessed on 10/21/2022.

[63] *National Air Pollution Surveillance (NAPS) Program*, https://data.ec.gc.ca/data/air/monitor/national-air-pollution-surveillance-naps-program/ProgramInformation-InformationProgramme/?lang=en, Accessed on 10/21/2022.

[64] C. Brown, "Alberta Air Zones Report 2017-2019," Government of Alberta, Ministry of Environment and Parks., Tech. Rep., 2021.

[65] C. C. of Ministers of the Environment, *Ambient Air Monitoring and Quality Assurance/Quality Control Guidelines*. Canadian Council of Ministers of the Environment, 2019.

[66] *SMOKE User Manual v4.8*, https://www.cmascenter.org/help/documentation.cfm?model=smoke&version=4.8, Accessed on 02/09/2023.

[67] *Photochemical Air Quality Modeling, US EPA*, https://www.epa.gov/scram/photochemical-air-quality-modeling, Accessed on 02/09/2023.

[68] *Air Quality Modeling, US EPA*, https://www.epa.gov/air-research/air-quality-modeling, Accessed on 02/09/2023.

[69] T.-F. Chen, K.-H. Chang, and C.-H. Lee, "Simulation and analysis of causes of a haze episode by combining CMAQ-IPR and brute force source sensitivity method," *Atmospheric Environment*, vol. 218, p. 117 006, 2019.

[70] C. G. Nolte, T. L. Spero, J. H. Bowden, M. S. Mallard, and P. D. Dolwick, "The potential effects of climate change on air quality across the conterminous US at 2030 under three Representative Concentration Pathways," *Atmospheric Chemistry and Physics*, vol. 18, no. 20, pp. 15 471–15 489, 2018.

[71] U. E. P. Agency, "Hemispheric CMAQ Model Version 5.3 Output Data – 2017 Monthly daily averaged 108km for Northern Hemisphere,"

[72] R. Dennis *et al.*, "A framework for evaluating regional-scale numerical photochemical modeling systems," *Environmental Fluid Mechanics*, vol. 10, no. 4, pp. 471–489, Mar. 2010.

[73] *CMAQ Model Evaluation Framework*, https://www.epa.gov/cmaq/cmaq-model-evaluation-framework, Accessed on 10/22/2022.

[74] J. C. Chang and S. R. Hanna, "Air quality model performance evaluation," *Meteorology and Atmospheric Physics*, vol. 87, no. 1-3, Jun. 2004.

[75] S. Hanna and J. Chang, "Acceptance criteria for urban dispersion model evaluation," *Meteorology and Atmospheric Physics*, vol. 116, no. 3-4, pp. 133–146, Jan. 2012.

[76] C. Emery, Z. Liu, A. G. Russell, M. T. Odman, G. Yarwood, and N. Kumar, "Recommendations on statistics and benchmarks to assess photochemical model performance," *Journal of the Air & Waste Management Association*, vol. 67, no. 5, pp. 582–598, Mar. 2017.

[77] J. L. Swall and K. M. Foley, "The impact of spatial correlation and incommensurability on model evaluation," *Atmospheric Environment*, vol. 43, no. 6, pp. 1204–1217, 2009.

[78] H. Wan, X. L. Wang, and V. R. Swail, "Homogenization and Trend Analysis of Canadian Near-Surface Wind Speeds," *Journal of Climate*, vol. 23, no. 5, pp. 1209–1225, Mar. 2010.

[79] L. Liu and R. J. A. M. Stevens, "Vertical structure of conventionally neutral atmospheric boundary layers," *Proceedings of the National Academy of Sciences*, vol. 119, no. 22, e2119369119, 2022.

[80] Y. Huang *et al.*, "Numerical simulations for the sources apportionment and control strategies of $PM_{2.5}$ over Pearl River Delta, China, part I: Inventory and $PM_{2.5}$ sources apportionment," *Science of The Total Environment*, vol. 634, pp. 1631–1644, Sep. 2018.

[81] A. A. Wyszogrodzki *et al.*, "Analysis of the surface temperature and wind forecast errors of the NCAR-AirDat operational CONUS 4-km WRF forecasting system," *Meteorology and Atmospheric Physics*, vol. 122, no. 3-4, pp. 125–143, Sep. 2013.

[82] E. Tomasi, L. Giovannini, D. Zardi, and M. de Franceschi, "Optimization of noah and noah_MP WRF land surface schemes in snow-melting conditions over complex terrain," *Monthly Weather Review*, vol. 145, no. 12, pp. 4727–4745, Dec. 2017.

[83] R. Arasa, M. R. Soler, and M. Olid, "Evaluating the Performance of a Regional-Scale Photochemical Modelling System: Part I—Ozone Predictions," *ISRN Meteorology*, vol. 2012, pp. 1–22, Nov. 2012.

[84] A. Russell and R. Dennis, "NARSTO critical review of photochemical models and modeling," *Atmospheric Environment*, vol. 34, no. 12, pp. 2283–2324, 2000.

[85] S. Ortega, M. R. Soler, M. Alarcon, and R. Arasa, "The role of temperature in tropospheric ozone," *International Journal of Environment and Pollution*, vol. 44, no. 1/2/3/4, p. 261, 2011.

[86] G. Schürmann, A. Algieri, I. Hedgecock, G. Manna, N. Pirrone, and F. Sprovieri, "Modelling local and synoptic scale influences on ozone concentrations in a topographically complex region of Southern Italy," *Atmospheric Environment*, vol. 43, no. 29, pp. 4424–4434, 2009.

[87] *Alberta Climate*, https://www.britannica.com/place/Alberta-province/Climate, Accessed on 11/23/2022.

[88] *Weather & Climate Alberta*, https://www.travelalberta.com/ca/plan-your-trip/weather-climate/, Accessed on 11/23/2022.

[89] J. C. Refsgaard, J. P. van der Sluijs, A. L. Højberg, and P. A. Vanrolleghem, "Uncertainty in the environmental modelling process – A framework and guidance," *Environmental Modelling & Software*, vol. 22, no. 11, pp. 1543–1556, 2007.

[90] M. T. Odman, M. Qin, Y. Hu, A. G. Russell, and J. W. Boylan, "Interstate transport of ozone in eastern United States: An analysis of the impact of southeastern states' emissions in 2017," *Atmospheric Environment*, vol. 236, p. 117 628, 2020.

[91] H. Guo *et al.*, "Simulation of summer ozone and its sensitivity to emission changes in China," *Atmospheric Pollution Research*, vol. 10, no. 5, pp. 1543–1552, 2019.

[92] K. Kitayama, Y. Morino, K. Yamaji, and S. Chatani, "Uncertainties in O_3 concentrations simulated by CMAQ over Japan using four chemical mechanisms," *Atmospheric Environment*, vol. 198, pp. 448–462, 2019.

[93] X. Cheng *et al.*, "A New Inverse Modeling Approach for Emission Sources based on the DDM-3D and 3DVAR techniques: an application to air quality forecasts in the Beijing–Tianjin–Hebei Region," Jun. 2021.

[94] M. Wang, S. H. Yim, D. Wong, and K. Ho, "Source contributions of surface ozone in China using an adjoint sensitivity analysis," *Science of The Total Environment*, vol. 662, pp. 385–392, 2019.

[95] A. Hakami *et al.*, "The Adjoint of CMAQ," *Environmental Science & Technology*, vol. 41, no. 22, pp. 7807–7817, Oct. 2007.

[96] *The Decoupled Direct Method*, https://www.epa.gov/cmaq/decoupled-direct-method-three-dimensions-cmaq-ddm-3d#:~:text=CMAQ%2DDDM%2D3D%20is%20a,every%20science%20module%20in%20CMAQ., Accessed on 04/05/2023.

[97] K. Chen, "Source Apportionment of Ozone and Its Health Effects in North China Plain and Southeast U.S.," Ph.D. dissertation, 2020.

[98] A. Hakami, J. H. Seinfeld, T. Chai, Y. Tang, G. R. Carmichael, and A. Sandu, "Adjoint Sensitivity Analysis of Ozone Nonattainment over the Continental United States," *Environmental Science & Technology*, vol. 40, no. 12, pp. 3855–3864, May 2006.

[99] P. Thunis *et al.*, "Source apportionment to support air quality planning: Strengths and weaknesses of existing approaches," *Environment International*, vol. 130, p. 104 825, 2019.

[100] Y. Zhou *et al.*, "Development of a high-resolution emission inventory and its evaluation and application through air quality modeling for Jiangsu Province, China," *Atmospheric Chemistry and Physics*, vol. 17, no. 1, pp. 211–233, 2017.

[101] V. Shah *et al.*, "Effect of changing NO_x lifetime on the seasonality and long-term trends of satellite-observed tropospheric NO_x columns over China," Aug. 2019.

[102] *Air Quality Health Index - Calculation*, https://www.alberta.ca/air-quality-health-index–calculation.aspx, Accessed on 04/05/2023.

[103] M. Fillingham, "The influence of CMAQ model resolution on predicted air quality and associated health impacts," Ph.D. dissertation.

[104] M. Schaap *et al.*, "Performance of European chemistry transport models as function of horizontal resolution," *Atmospheric Environment*, vol. 112, pp. 90–105, 2015.

[105] "Modeling Guidance for Demonstrating Air Quality Goals for Ozone, $PM_{2.5}$, and Regional Haze," U.S. Environmental Protection Agency, Tech. Rep., 2018.

Appendix A: Model Installation

This is a step-by-step explanation of how to install the prerequisites and libraries needed for employing the WRF v4.2.2 model and CMAQ v5.3.3 model on the LINUX UBUNTU 18.04 operating server.

A.1 System Prerequisites

Prior to the WRF model installation, the system is required to be updated, and some preprocessor (m4) commands should be added to the system. Furthermore, two common shell environments named "csh" and "tcsh" are also required. Although most of them are already installed within the operating system, it is essential to make sure they are updated and installed.

```
~$ sudo apt-get update
~$ sudo apt install default-jdk
~$ sudo apt install default-jre
~$ sudo apt install build-essential
~$ sudo apt install csh
~$ sudo apt install tcsh
~$ sudo apt install m4
```

A.1.1 Compilers

The most common compilers used for employing and developing the WRF model are **GNU** and **Intel** compilers. LINUX Ubuntu 18.04 already come up with GNU tools. In this study, the GNU compiler was used to establish the WRF model. Prior to moving to the next step make sure that all the required compiling languages are installed and the GNU compilers are up-to-date. The compiler version in our model is 7.5.0.

```
~$ sudo apt install gfortran
~$ sudo apt install g++
```

A.2 WRF v4.2.2 Model

A.2.1 Libraries

Before installing the required libraries you have to define some environment variables2 which can be set in the terminal or added to .bashrc and .profile files in the home directory. The difference is that when you define variables in the terminal after closing the terminal they vanish. Necessarily, the compiler you are using to install all your libraries should be the same as the ones you will use in WRF.

- `export DIR=/home_dir/Build_WRF/LIBRARIES`
- `export CC=gcc`
- `export CXX=g++`
- `export FC=gfortran`
- `export FCFLAGS=-m64`
- `export F77=gfortran`
- `export F90=gfortran`

- `export FFLAGS=-m64`
- `export JASPERLIB=$DIR/grib2/lib`
- `export JASPERINC=$DIR/grib2/include`
- `export LDFLAGS=-L$DIR/grib2/lib`
- `export CPPFLAGS=-I$DIR/grib2/include`
- `export LD_LIBRARY_PATH=$DIR/netcdf/lib:$LD_LIBRARY_PATH`

The source code and list of required libraries for compiling the WRF model can be found online at https://www2.mmm.ucar.edu/ website. It is recommended to install the following libraries in the given order.

- zlib-1.2.7vc
- libpng-1.2.50
- Jasper-1.900.1
- netcdf-4.1.3
- mpich-3.0.4

After compiling these libraries, their addresses should be added to the PATH environment variable. These addresses can be defined in the .bashrc file or in the terminal.

- `export PATH=$DIR/netcdf/bin:$PATH`
- `export PATH=$DIR/netcdf/lib:$PATH`
- `export NETCDF=$DIR/netcdf`
- `export PATH=$DIR/mpich/bin:$PATH`

After successfully installing all the libraries above, it is recommended to do the library compatibility test which has been provided on the WRF online tutorial website.

A.2.2 Installing WRF

After ensuring that all libraries are compatible and all environment variables are defined correctly, the next step is the WRF and WPS (WRF Pre-processing System) model installation. The source code of the WRF model can be downloaded from the wrf-model repository at GitHub. WPS model also can be downloaded from a subdirectory in the same repository. From user manual provided in that repository make sure that the WRF and WPS are compatible. The WRF model and WPS model used in this study were version 4.2.1 and 4.2 respectively. First, install the WRF model. After untarring the source code of the WRF model run *~$ ./configure* script in the terminal. During the configuration process, choose the "dmpar" option for the GNU compiler (this option is number 34 from the menu appearing in the terminal). Considering the available option for nesting, for convenience choose the basic option (1=basic). After the configuration process from the configure.wrf file created, delete the following line to avoid future errors.

```
-DBUILD_RRTMG_FAST=1/
```

Then the model can be compiled using the em_real option.

```
~$ ./compile_em_real
```

If the process goes well, in the main directory in WRF there will be 4 executable files as follow:

- wrf.exe (model executable)
- real.exe (real data initialization)
- ndown.exe (one-way nesting)

- tc.exe (for tc bogusing–serial only)

A.2.3 Installing WPS

The last step in installing the meteorological module is to compile pre-processing WRF called WPS. First, the directory of the WRF should be added to the environment variables.

- `export WRF_DIR=/base/address/WRFV4.2.2.TAR/WRF`
- `export LD_LIBRARY_PATH=$DIR/grib2/lib:$LD_LIBRARY_PATH`

For simplicity, the WRF file can be copied to the WPS directory. Then *./clean* and *./configure* commands should be executed. Prior to compiling WPS, the configure.wps file should be modified and the following line should be added prior to the WRF_INCLUDE.

- `WRF_DIR=WRF`

Then the *./compile* command should be executed. If the process is successful there will be 3 executable files in the WPS directory.

- geogrid.exe
- ungrid.exe
- metgrid.exe

A list of useful websites that help to build and run the WRF model is provided.

- WRF source code

  https://github.com/wrf-model/WRF/releases

- How to compile WRF (online tutorial)

  https://www2.mmm.ucar.edu/wrf/OnLineTutorial/compilation_tutorial.php

- Download geographical data

  https://www2.mmm.ucar.edu/wrf/users/download/get_sources_wps_geog.html

- Download meteorological data

  https://rda.ucar.edu/datasets/ds083.2/

A.3 CMAQ v5.3.3 Model

A.3.1 Libraries

To run and build the CMAQ model, three main libraries are required to be installed:

- MPI (mpich-3.0.4)
- netCDF-4.1.3
- IOAPI-3.2

The versions of the libraries mentioned are compatible with the previous libraries installed for the WRF model. The order of libraries' installation is important. However, if the required libraries for the WRF model have already been installed, the MPI and netCDF can be employed for building both WRF and CMAQ models. Prior to installing the IOAPI library, add the following environment variables to the ./bashrc file:

- `export INSTALL=$DIR/ioapi-3.2/ioapi`
- `export BIN=Linux2_x86_64gfort_openmpi_4.0.1_gcc_9.1.0`
- `IOAPI=&DIR/ioapi-3.2/ioapi/Linux2_x86_64gfort_openmpi_4.0.1_gcc_9.1.0`

A detailed explanation of how to install these libraries for building CMAQ model can be found at CMAQ GitHub online repository, under the user guide and preparing environment repository:

https://github.com/USEPA/CMAQ/blob/main/DOCS/Users_Guide/CMAQ_UG_ch03_preparing_compute_environment.md

After configuring the libraries, make sure to install m3tools within the IOAPI library. Then add the following variables to the /.bashrc file.

- `export LD_LIBRARY_PATH=$IOAPI:$LD_LAIBRARY_PATH`
- `export LD_LIBRARY_PATH=$DIR/grib2/lib:$LD_LIBRARY_PATH`
- `export LD_LIBRARY_PATH=$DIR/netcdf/lib:$LD_LIBRARY_PATH`
- `export IOAPI_INCL_DIR=$IOAPI`
- `export IOAPI_LIB_DIR=$IOAPI`
- `export NETCDF_LIB_DIR=$DIR/netcdf/lib`
- `export NETCDF_INCL_DIR=$DIR/netcdf/include`
- `export NETCDFF_LIB_DIR=$DIR/netcdf/lib`
- `export NETCDFF_INCL_DIR=$DIR/netcdf/include`
- `export MPI_INCL_DIR=$DIR/mpich/include`
- `export MPI_LIB_DIR=$DIR/mpich/lib`

A.3.2 Installing CMAQ

After configuring the libraries, the detailed and step-by-step explanations, available on CMAQ online GitHub repository, helps you to build the CMAQ model. It is important to note that the CMAQ is built in tcsh shell.

https://github.com/USEPA/CMAQ/blob/main/DOCS/Users_Guide/Tutorials/CMAQ_UG_tutorial_benchmark.md

Appendix B: Emission Preparation

B.1 SMOKE Model

B.1.1 Model installation

The source codes for the SMOKE model are available online at https://cmascenter.org/ website. After creating an account and downloading the model, a directory for SMOKE should be created in the Linux system. It is important to note that tcsh shell is needed for compiling the SMOKE model. Execute the following command on tcsh shell.

- `setenv SMK_HOME <your directory for SMOKE>`
- `mkdir -p $SMK_HOME`
- `source smoke_install.csh`

Then the SMOKE directory sould be added to .cshrc file in the home directory. Add the following line to the end of the file.

- `setenv SMK_HOME <your directory for SMOKE>`

The SMOKE precompiled executables are compatible with INTEL compilers. Therefore, the following steps are needed for configuring new executables compatible with the operating system available. First, the IOAPI library should be downloaded and installed. If the IOAPI has already been installed, a symbolic link to the IOAPI directory should be created in the *$SMK_HOME/subsys/ioapi/ioapi/* directory. Then

a symbolic link to the IOAPI libioapi.a file should be added to the *$SMK_HOME/-subsys/ioapi/Linux2_x86_64gfort/*. Then using the source command, source an appropriate *.assign file. And finally in the directory *$SMKOOT/src/*, the make command is used to build new executables.

A detailed explanation on how to install the model and also new compatible executables can be found in the SMOKE v4.8 user manual. The user manual can be downloaded from cmascenter website:

https://www.cmascenter.org/help/documentation.cfm?model=smoke&version=4.8

B.1.2 Directory Structure

Understanding the structure of data in the SMOKE directory considerably helps to prepare and run the model. Fig. B.1, provide a schematic of all subdirectories and required files to run the SMOKE model. The SMOKE home directory is divided into two general subdirectories. All required data to run the model are in the Data subdirectory and all the executable codes and scripts to edit are in sub sys subdirectory. Running scripts are within the scripts subdirectory and all the options and settings for each run can be determined using the *.assign files in the assign subdirectory.

Furthermore, the details regarding temporal, spatial, and chemical profiles are defined using the files in the ge_dat subdirectory. All the emission inventory data that are readable by SMOKE scripts should be added to the inventory subdirectory. The red files that are shown in fig. B.1 are general files. While these files are necessary for running the model, they are almost constant for each modeling scenario. Only in some cases, minor edits are required. Detailed information about each individual file including its format and structure can be found within the SMOKE user manual addressed earlier.

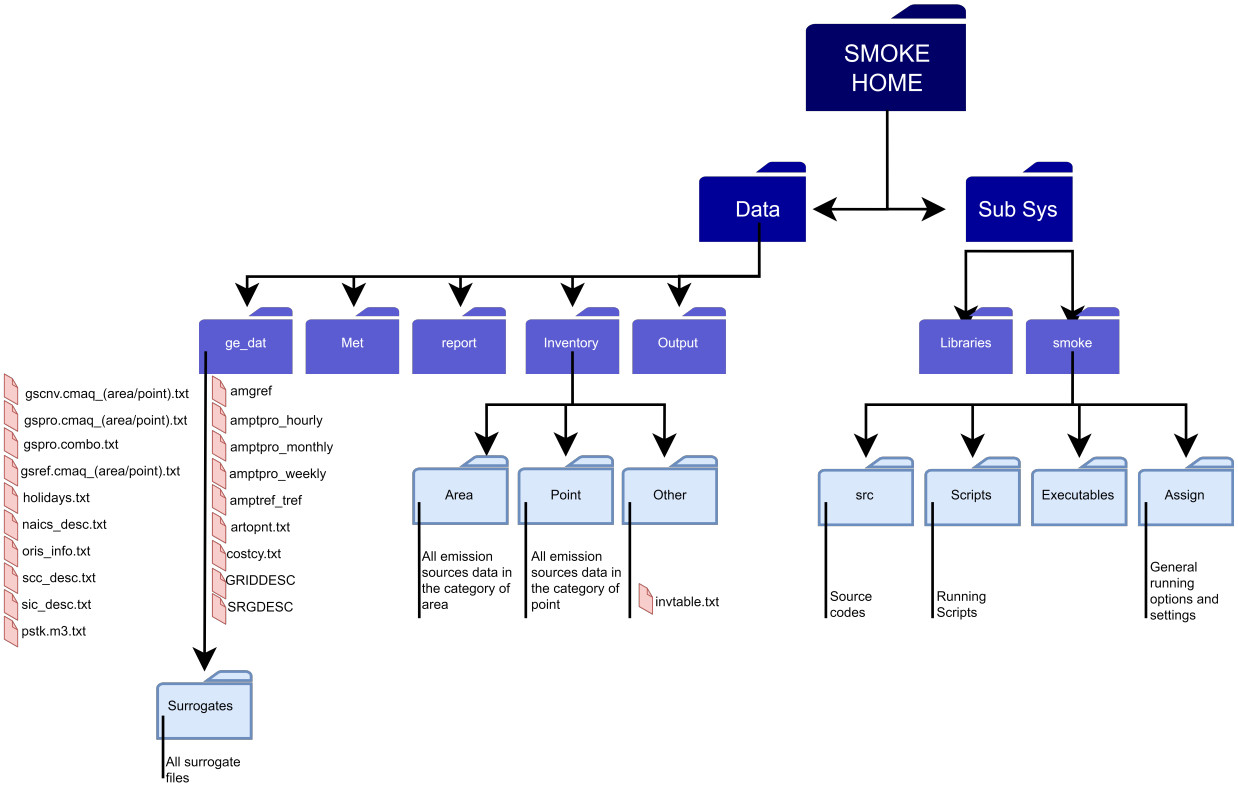

Figure B.1: Structure of SMOKE directories and all necessary files needed to run the model

Appendix C: Running the Model

This appendix is dedicated to the process of setting up and running each module of the atmospheric model. A step-by-step guide on how to run WRF, SMOKE, and CMAQ models is provided.

C.1 WRF Model

In order to run the WRF model, two sets of data are required: static geographical data and gridded meteorological data. The repositories for downloading these two sets of data are introduced in appendix A.2.3. After organizing and putting the downloaded files in the proper directories the following steps should be taken.

In the directory where you build the WRF model, go to WPS directory and open the namelist.wps file. All the options like start date and end date, timestep, the exact location of the computational domain, number of domains and the respective dimension of each domain, location, and resolution of the static geographical data can be modified using the options available within namelist.wps files.

After applying the required modifications to the namelist.wps file, open a terminal in WPS directory and run the geogrid module.

```
~$ ./geogrid.exe
```

This module creates terrestrial data from static geographic data. Then create a link to the gridded meteorological data (fnl/gfs) data that you downloaded.

```
~$ ./link_grib.csh /(directory_of_fnl_data)/fnl
~$ ln -sf ungrib/Variable_Tables/Vtable.GFS Vtable
```

Then, to unpack the fnl data and interpolate them into your modeling domain run the following modules.

```
~$ ./ungrib.exe
~$ ./metgrid.exe
```

Now prior to running the WRF em_real module, create a link from metgrid.exe outputs to the location of the em_real module.

```
~$ cd ../(directory_WRF)/WRF-4.2.2/test/em_real/
~$ ln -sf ../../WPS-4.2/met_em* .
```

In this directory, there is a file named namelist.input. Using these files the duration of the run, timestep, the number of vertical layers, and physical options can be modified for your specific case. After applying the required modifications, run the following commands.

```
~$ ./real.exe
~$ mpirun -np (number_of_CPU_cores) ./wrf.exe
```

The outputs will be created in the same directory.

C.2 SMOKE Model

After compiling the module based on instructions in appendix B.1.1, all the files indicated in the fig. B.1 should be provided for running the model. Some of them are general and there is no need for any change for running different cases and scenarios and some of them should be modified. A detailed explanation of these files is available in the SMOKE User guide. After preparing all the required files and adding the emission files the following steps help you to run the SMOKE model.

In the "assigns" directory, there is a file called "ASSIGNS.nctox.cmaq.cb05_soa.usa12-nc", make a copy of this file and renamed it. Some general options including the location of the emission file and the running time can be modified using scripts within this file. Then execute the following command in the tcsh shell.

```
~$ source (Name_of_the_file_you_generated)
```

Then go to the "run" subdirectory under the "scripts". Then run the following commands. Prior to running these commands, modified the scripts within these files based on your running case.

```
~$ ./smk_area_(yourcase).csh
~$ ./smk_point_(yourcase).csh
~$ ./smk_mrgall_(yourcase).csh
```

The output files will generate in the directory you defined in the ASSIGNS file. To make sure that the run has been successful check all the static log files in the output directory.

C.3 CMAQ Model

The CMAQ model includes four main modules. MCIP module creates CMAQ-ready meteorological data from WRF outputs. ICON and BCON modules create the initial condition and boundary condition. The last module is CCTM which evaluates the physicochemical behavior of chemical species. Make sure that all the module has already been compiled.

The first step is to modify the file called "config_cmaq.csh" in the CMAQ home directory based on your compilers and libraries address. run MCIP module. Then execute the following command tcsh terminal.

```
~$ source config_cmaq.csh gcc
```

In the CMAQ home directory, under the "PREP" and "MCIP" subdirectories, there is a file called run_mcip.csh. Apply the required changes to the scripts. The general information regarding each variable in the scripts can be found in the CMAQ user guide.

```
~$ ./run_mcip.csh
```

Then using hemispheric monthly average or seasonally averaged data from CMAS-center, you can run the ICON and BCON module to generate initial and boundary conditions. ICON and BCON are located under the "PREP" directory in CMAQ's home. Find run_bcon.csh and run_icon.csh and modify them based on your running case. Then execute the following commands.

```
~$ ./run_bcon.csh
~$ ./run_icon.csh
```

Running the CCTM module is the last step. Make sure that the module has already been compiled based on your system configuration. Under "CCTM" and "scripts" subdirectory you will find a file called "run_cctm.csh". All the physical and chemical options of this module can be modified using the options provided within the scripts of this file. Modify the scripts based on your running case and run the module.

```
~$ ./run_cctm.csh
```